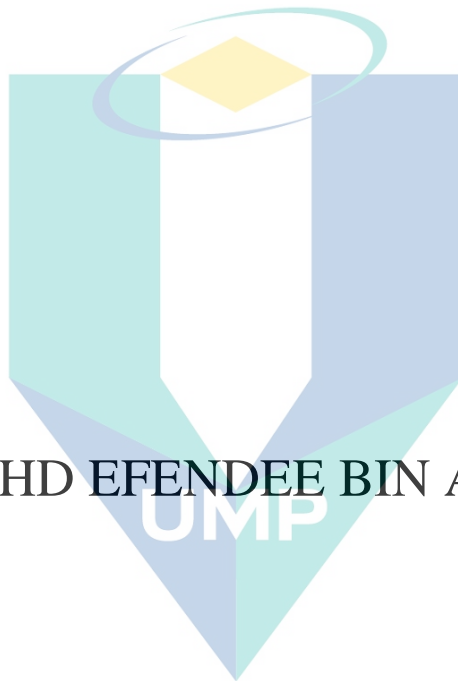


MAGNETIC POLARITY INFLUENCE ON
MACHINING PERFORMANCE OF MAGNETIC
FIELD-ASSISTED EDM



MOHD EFENDEE BIN AWANG

اونيورسيتي مليسيا قهغ

UNIVERSITI MALAYSIA PAHANG

MASTER OF SCIENCE

UNIVERSITI MALAYSIA PAHANG

UNIVERSITI MALAYSIA PAHANG

DECLARATION OF THESIS AND COPYRIGHT

Author's Full Name : MOHD EFENDEE BIN AWANG
Date of Birth : 2 FEBRUARY 1979
Title : MAGNETIC POLARITY INFLUENCE ON
MACHINING PERFORMANCE OF MAGNETIC
FIELD-ASSISTED EDM
Academic Session : SEMESTER 1 2020/21

I declare that this thesis is classified as:

- CONFIDENTIAL (Contains confidential information under the Official Secret Act 1997)*
 RESTRICTED (Contains restricted information as specified by the organization where research was done)*
 OPEN ACCESS I agree that my thesis to be published as online open access (Full Text)

I acknowledge that Universiti Malaysia Pahang reserves the following rights:

1. The Thesis is the Property of Universiti Malaysia Pahang
2. The Library of Universiti Malaysia Pahang has the right to make copies of the thesis for the purpose of research only.
3. The Library has the right to make copies of the thesis for academic exchange.

Certified by:


(Student's Signature)


DR. MOHD AZMIR BIN MOHD AZHARI
DIRECTOR
CENTRE FOR INTERNATIONAL RELATIONS
UNIVERSITI MALAYSIA PAHANG
26300 GAMBANG, KUANTAN
PAHANG DARUL MAKMUR
TEL : +609-549 2819 Fax : +609-549 2729

(Supervisor's Signature)

790202 11 5383
New IC/Passport Number
Date: 27 NOVEMBER 2020

MOHD AZMIR BIN MOHD AZHARI
Name of Supervisor
Date: 27 NOVEMBER 2020

SUPERVISOR'S DECLARATION

I hereby declare that I have checked this thesis and in my opinion, this thesis is adequate in terms of scope and quality for the award of the degree of Master of Science.



DR. MOHD AZMIR BIN MOHD AZHARI
DIRECTOR
CENTRE FOR INTERNATIONAL RELATIONS
UNIVERSITI MALAYSIA PAHANG
26300 GAMBANG, KUANTAN
PAHANG-DARUL MAKMUR
TEL : +609-549 2819 Fax : +609-549 2729

(Supervisor's Signature)

Full Name : Dr. Mohd Azmir Bin Mohd Azhari
Position : Pensyarah Kanan
Date : 27 November 2020



UMP

اونيورسيتي ملايسيا قهغ

UNIVERSITI MALAYSIA PAHANG

STUDENT'S DECLARATION

I hereby declare that the work in this thesis is based on my original work except for quotations and citations which have been duly acknowledged. I also declare that it has not been previously or concurrently submitted for any other degree at Universiti Malaysia Pahang or any other institutions.



(Student's Signature)

Full Name : Mohd Efendee Bin Awang

ID Number : MMF 16004

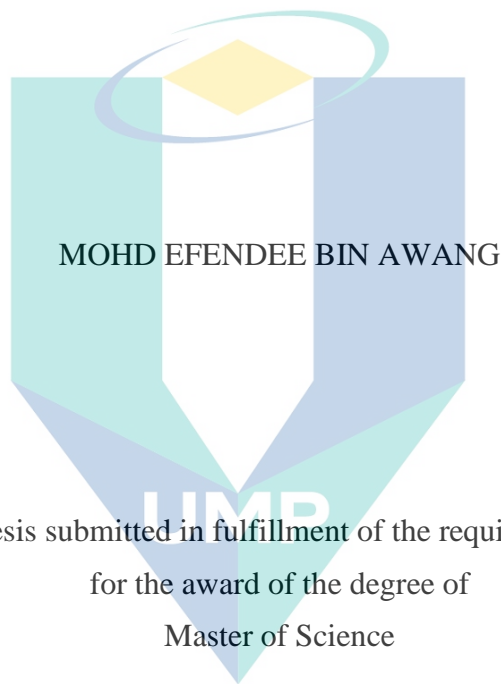
Date : 27 November 2020

UMP

اونيورسيتي ملايسيا قهغ

UNIVERSITI MALAYSIA PAHANG

MAGNETIC POLARITY INFLUENCE ON MACHINING PERFORMANCE
OF MAGNETIC FIELD-ASSISTED EDM



Thesis submitted in fulfillment of the requirements
for the award of the degree of
Master of Science
(Manufacturing Engineering)

اونيورسيتي مليسيا قهغ

UNIVERSITI MALAYSIA PAHANG

Faculty of Manufacturing & Mechatronic Engineering Technology

UNIVERSITI MALAYSIA PAHANG

NOVEMBER 2020

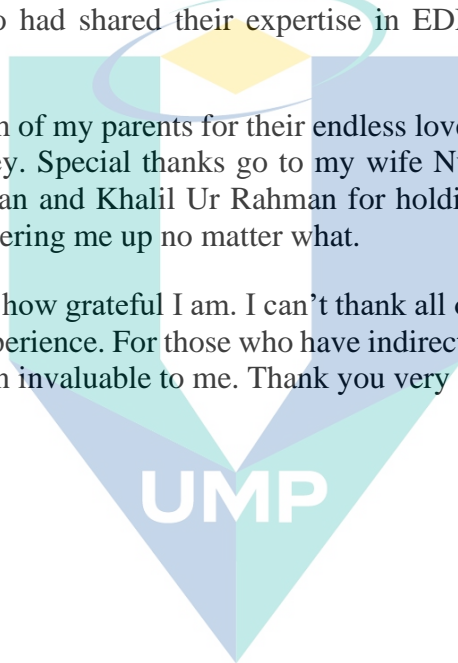
ACKNOWLEDGEMENTS

In the name of Allah, the Most Beneficent and the Most Gracious. All praise to God for the ablation of His strength and grace in completing this thesis. My highest appreciation and thank you to my supervisor Dr. Mohd Azmir Mohd Azhari, for his supervision and significant involvement throughout this thesis. I also would like to thank all UMP staff for their support and help towards my postgraduate affairs, especially to those from the Faculty of Manufacturing and Mechatronic Engineering Technology and IPS for their cooperation.

My deepest gratitude goes to UCTATI for the generosity in partially funding the research via Short Term Grant Scheme and the use of machinery and equipment. In fact, thank you to my colleagues who had shared their expertise in EDM which was essential to the research.

I am so grateful to both of my parents for their endless love and prayers in supporting me throughout this journey. Special thanks go to my wife Nur Hanisah Azmi and beloved sons, Habib Ur Rahman and Khalil Ur Rahman for holding me up throughout ups and downs and always cheering me up no matter what.

Words cannot express how grateful I am. I can't thank all of you enough for encouraging me throughout this experience. For those who have indirectly contributed to this research, your kindness has been invaluable to me. Thank you very much. Alhamdulillah.



اونيورسيتي مليسيا قهغ

UNIVERSITI MALAYSIA PAHANG

ABSTRAK

Pemesinan pelepasan caj elektrik (EDM) adalah salah satu teknik pemesinan bukan tradisional yang biasa digunakan dalam industry pembuatan acuan dan setem logam lembaran. Walaubagaimanapun, masa pemesinan yang panjang ketika proses EDM membawa kepada kadar penyingkiran bahan yang rendah (MRR). Meningkatkan MRR dengan cara meningkatkan nilai arus puncak, ia akan menjejaskan kualiti kekasaran permukaan bahan. Proses EDM menawarkan pelbagai parameter pemesinan dan teknik EDM hybrid yang boleh dimanipulasikan bagi menyelesaikan masalah ini. Kajian ini adalah bertujuan untuk mengkaji kesan polariti magnet terhadap EDM yang dibantu oleh medan magnet (MFAEDM). Selain MRR, kadar haus elektrod dan kekasaran permukaan (R_a) sampel menggambarkan keberkesanan EDM process. Pemasangan bahan magnet di sekitar kawasan pemesinan telah dilaksanakan untuk mengkaji penambahbaikan pada process EDM. Tambahan pula, perihal kesan polariti magnet dalam proses EDM yang dibantu oleh medan magnet (MFAEDM) masih belum diterokai. Dalam eksperimen ini, EDM Charmiles Roboform22 yang menggunakan minyak tanah dan elektrod grafit berbentuk silinder pada ukuran $\varnothing 25$ mm digunakan untuk mencetuskan letusan EDM kedalaman 2 mm pada bahan besi AISI 420. Arus puncak antara 8 A hingga 24 A dan masa nadi 50 μ s hingga 100 μ s telah ditetapkan bersama dengan 0.54 Tesla bagi mencetuskan proses pemesinan untuk polariti Utara-Selatan (N-S) dan Utara-Utara (N-N). Keputusan ujikaji menunjukkan teknik MFAEDM meningkatkan MRR sebanyak 13% berbanding EDM konvensional pada 24 A dan 100 μ s. Kekasaran permukaan yang dihasilkan oleh MFAEDM dikurangkan masing-masing sebanyak 16% dan 20% untuk arus puncak 8 A dan 24 A. Kombinasi polariti N-S menghasilkan penurunan nilai R_a sebanyak 10% untuk arus puncak 8A dan 8% untuk arus puncak 24 A berbanding kombinasi N-N. Ia adalah kerana medan magnet memerah percikan api dan memurnikan proses dengan menarik dan memerangkap habuk besi dengan pantas kepada bahan magnet. Teknik MFAEDM berpotensi untuk menyingkirkan serpihan habuk pemesinan secara lebih cekap dan menambah baik MRR. Dengan demikian ianya turut meningkatkan kualiti kekasaran permukaan untuk memenuhi permintaan aplikasi perindustrian moden.

اونيورسيٲي ملايسيا قهق

UNIVERSITI MALAYSIA PAHANG

ABSTRACT

Electrical discharge machining (EDM) is one of the non-traditional machining techniques where it is commonly used in the mould and die making industry. However, the lengthy machining time in EDM process leads to low material removal rate (MRR). While increasing MRR by increasing peak current value, it affects the quality of surface finish. The EDM process offers a wide-range of machining parameters and hybrid EDM techniques can be manipulated in solving the EDM drawbacks. The present research aims to study the magnetic polarity influence on magnetic field-assisted EDM. In addition to MRR, electrode wear rate and surface roughness (R_a) of the sample illustrate the effectiveness of the EDM process. The installation of magnetic tools in the EDM machining area was implemented to study its improvements in EDM process. Moreover, the description of magnetic polarity impact in magnetic field-assisted EDM (MFAEDM) remains unacquainted. In the experiment, the EDM Charmiles Roboform22 utilized kerosene and cylindrical Ø25 mm graphite electrode to spark 2 mm depth of cut on AISI 420.mod tool steel. Peak current in the range of 8 A to 24 A and 50 μ s to 100 μ s of pulse time were designated along with 0.54 Tesla for both North-South (N-S) and North-North (N-N) polarity. The results show that MFAEDM technique enhanced MRR by 13% as compared to conventional EDM at 24 A and 100 μ s. Surface roughness produced by MFAEDM was reduced by 16% and 20% respectively for peak current of 8 A and 24 A. N-S polarity combination improved R_a value as much as 10% for peak current of 8 A and 8% for 24 A as compared to N-N combination. The reason is the magnetic field squeezes and purifies spark-eroded process by trapping evaporated debris promptly onto the magnetic bar. MFAEDM causes removal of machining debris more efficiently and is able to attain high-efficiency of MRR. Thus, it improves surface finish quality to meet the demands of modern industrial application.

اونيور سیتی ملیسیا قهغ

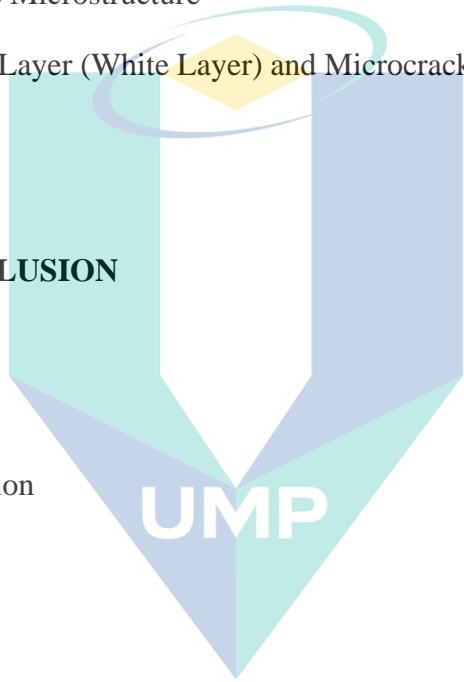
UNIVERSITI MALAYSIA PAHANG

TABLE OF CONTENT

DECLARATION	
TITLE PAGE	
ACKNOWLEDGEMENTS	ii
ABSTRAK	iii
ABSTRACT	iv
TABLE OF CONTENT	v
LIST OF TABLES	viii
LIST OF FIGURES	ix
LIST OF SYMBOLS	xiii
LIST OF ABBREVIATIONS	xiv
CHAPTER 1 INTRODUCTION	1
1.1 Research Background	1
1.2 Problem Statement	2
1.3 Objectives	3
1.4 Scope of The Research	3
1.5 Hypothesis	3
1.6 Thesis Outline	4
CHAPTER 2 LITERATURE REVIEW	5
2.1 Introduction	5
2.2 EDM Overview	5
2.2.1 Basic Principle of EDM Process	5
2.2.2 Spark and Debris	9

2.2.3	EDM Parameters	13
2.2.4	EDM Trend Study	15
2.3	Magnetic Field Assisted EDM	22
2.3.1	Methods in MFAEDM	24
2.3.2	Output of MFAEDM	28
2.3.3	Two-Level Factorial Design	38
2.4	Summary	41
CHAPTER 3 METHODOLOGY		42
3.1	Introduction	42
3.2	Research Process and Equipment	44
3.3	Method of Data Collection	49
3.4	Analysis of Machining Time	53
3.5	Analysis of Material Removal Rate (MRR)	54
3.6	Analysis of Electrode Wear Rate (EWR)	54
3.7	Analysis of Surface Roughness (R_a)	55
3.8	Summary	56
CHAPTER 4 RESULTS AND DISCUSSION		57
4.1	Introduction	57
4.2	Preliminary Experiment of MFAEDM	57
4.3	Comparison between conventional EDM and MFAEDM	62
4.3.1	MRR	63
4.3.2	EWR	66

4.3.3	Surface Roughness	68
4.4	Effect of Magnetic Polarity in MFAEDM	70
4.4.1	MRR	70
4.4.2	EWR	71
4.4.3	Surface Roughness	72
4.5	The Effect of Magnetic Polarity on Surface Microstructure.	74
4.5.1	Surface Microstructure	75
4.5.2	Recast Layer (White Layer) and Microcracks	81
4.6	Summary	83
CHAPTER 5 CONCLUSION		84
5.1	Introduction	84
5.2	Conclusion	84
5.3	Recommendation	86
REFERENCES		87
APPENDICES		95
	APPENDIX A	96
	APPENDIX B	97



اوتنيور سيني مليسيا قهغ

UNIVERSITI MALAYSIA PAHANG

LIST OF TABLES

Table 2.1	Field of recent studies on EDM	17
Table 2.2	Two-level factorial design by Aghdeab and Mohammed (2013)	40
Table 2.3	Two-level factorial design to investigate EDM on beryllium copper from M. Ali et al. (2013) experiment.	40
Table 3.1	Experiment parameters set up	44
Table 3.2	Charmilles Roboform EDM specification	46
Table 3.3	Properties of graphite and copper tungsten electrode	47
Table 3.4	Chemical composition of AISI 420.mod tool steel	47
Table 3.5	Design of MFAEDM experiment	50
Table 4.1	Preliminary experiments of conventional EDM and MFAEDM using graphite electrode	58
Table 4.2	Preliminary experiments of conventional EDM and MFAEDM using copper tungsten electrode	58
Table 4.3	Complete design of experiment table extracted from Design Expert	63
Table 4.4	Element of spectrums from EDX	75

UMP

اونيورسيتي ملايسيا قهغ

UNIVERSITI MALAYSIA PAHANG

LIST OF FIGURES

Figure 2.1	EDM schematic plan	6
Figure 2.2	EDM ionisation discharge process (a) pre-breakdown (b) dielectric breakdown (c) discharge process (d) plasma implosion and (e) post discharge	8
Figure 2.3	Experimental result of two-dimension EDM spark location detection	9
Figure 2.4	The phases of EDM on each spark location; a) ignition phase, b) discharge phase and (c) end of pulse	10
Figure 2.5	Compilation of TEM images single crystal nano-scale of (a) TiC at 5 nm (b) TiC at 0.5 μm (c) Si at 20 nm and (d) Si at 2 μm	11
Figure 2.6	SEM images of (a) Si and (b) TiC debris at 10 μm magnification	11
Figure 2.7	Schematics of gap flow (a) velocity field (b) pressure field and (c) debris flow with normal flushing technique by S. Zhang et al. (2017)	12
Figure 2.8	Result of MRR vs current parameters reported by Arikatla, Mannan, and Krishnaiah (2013)	14
Figure 2.9	Result of MRR vs pulse on time from Arikatla et al. (2013)	14
Figure 2.10	Current research trend in EDM	15
Figure 2.11	Schematic of the experimental setup demonstrates (a) magnetic field acting perpendicular to an electrode and (b) actual experiment set up of Singh Bains et al. (2016)	16
Figure 2.12	Lines of a magnetic field	22
Figure 2.13	Various combinations of poles and iron fillings (a) unlike poles – attract, (b) iron filling pattern of N-S (c) like poles – repel and (d) iron filling pattern of N-N	23
Figure 2.14	Resultant magnetic field pattern and neutral spot of (a) N-S combination, (b) N-N combination	24
Figure 2.15	The set-up for discharge pulse parameters sensing	25
Figure 2.16	Illustration magnet force assisted EDM configuration by Lin and Lee (2008)	26
Figure 2.17	Discharge waveforms of (a) conventional EDM and (b) MFAEDM	26
Figure 2.18	The experimental layout with external magnetic field by Khan, Ndaliman et. al (2013)	27

Figure 2.19	Experiment set up for MFAEDM by Gholipoor, Baseri et al. (2016)	27
Figure 2.20	MRR for conventional EDM and MFAEDM by Lin and Lee (2008)	28
Figure 2.21	MRR from Gholipoor, Baseri et al. (2016) experiment; (a) tool rotational speed, (b) water flow rate (c) gas pressure (Pa) and (d) discharge energy (KJ)	29
Figure 2.22	Graph of EWR result from Gholipoor, Baseri et al. (2016) MFAEDM experiment; (a) tool rotational speed (rpm), (b) water flow rate (ml/min) (c) gas pressure (KPa) and (d) discharge energy (KJ)	30
Figure 2.23	Trend of EWR using graphite electrode obtained by Lin and Lee (2008)	31
Figure 2.24	Result of surface roughness measurement by Lin and Lee (2008)	32
Figure 2.25	Comparison of R_a behavior at $I_p = 2.5$ A	32
Figure 2.26	Surface roughness outcomes for MFAEDM and conventional EDM for different processing parameters, a) tool rotational speed, b) water flow rate, c) gas pressure and d) discharge energy discovered by Gholipoor, Baseri et al. (2016)	33
Figure 2.27	Interaction of pulse duration and surface roughness examined by Arikatla et al. (2013)	34
Figure 2.28	Cross-section SEM image of a metal zone in EDM revealed by Efendee et al. (2018)	34
Figure 2.29	SEM observation of a) splatter, b) recast layer lap and c) craters and folds reported by Khan et al. (2013)	35
Figure 2.30	Microcracks obtained by (a) conventional EDM and (b) MFAEDM	36
Figure 2.31	(a) Cross sectional view and (b) close up of microcracks on EDM surface	37
Figure 2.32	SEM photographs of (a) D2 white layer and (b) H13 white layer courtesy of Lee and Tai (2003)	38
Figure 2.33	(a) One variable at a time (OVAT) versus (b) two-level factorial design	39
Figure 3.1	Overall research outline to achieve research objectives	43
Figure 3.2	Flow chart of experiment methodology	45
Figure 3.3	Charmilles Roboform EDM	46
Figure 3.4	a) Graphite electrode and b) copper tungsten electrode	46

Figure 3.5	Stavax ESR specimens	48
Figure 3.6	Permanent magnet (0.54 Tesla)	48
Figure 3.7	Fixture used for clamping specimen and magnetic bars	49
Figure 3.8	Illustration of magnetic field-assisted EDM arrangement	51
Figure 3.9	AISI 420.mod tool steel sample after EDM machining	51
Figure 3.10	Electronic balance device used to weigh the electrode and samples	52
Figure 3.11	Surface roughness measurement in progress	52
Figure 3.12	Sectioned and polished samples of AISI 420.mod	53
Figure 3.13	(a) Optical microscope and (b) scanning electron microscope	53
Figure 3.14	Surface roughness measurement methods	55
Figure 4.1	Comparison of MRR between conventional EDM and MFAEDM using graphite electrode	59
Figure 4.2	Comparison of MRR between conventional EDM and MFAEDM using copper tungsten electrode	59
Figure 4.3	Illustration of SR between conventional EDM and MFAEDM at different peak current using graphite electrode	60
Figure 4.4	Illustration of SR between conventional EDM and MFAEDM at different peak current using copper tungsten electrode	61
Figure 4.5	Effect of different polarity in MFAEDM on MRR	61
Figure 4.6	Comparison of MRR between conventional EDM and MFAEDM at 50 μ s	65
Figure 4.7	Effect of MRR between conventional EDM and MFAEDM at 100 μ s pulse time	65
Figure 4.8	Comparison graph of EWR for conventional EDM and MFAEDM at 50 μ s	67
Figure 4.9	Comparison graph of EWR for conventional EDM and MFAEDM at 100 μ s	67
Figure 4.10	Surface roughness comparison of conventional EDM and MFAEDM at 50 μ s	69
Figure 4.11	Surface roughness comparison of conventional EDM and MFAEDM at 100 μ s	69
Figure 4.12	Effect of magnetic polarity in MFAEDM on MRR at 50 μ s pulse time	71
Figure 4.13	Effect of magnetic polarity in MFAEDM on surface roughness by using graphite electrode	73

Figure 4.14	Surface microstructure of (a) conventional EDM, (b) N-N MFAEDM and (c) N-S MFAEDM at 200× magnification of optical microscope (24 A, 50 μs)	73
Figure 4.15	EDM surface layers (N-S MFAEDM, 24 A, 100 μs)	74
Figure 4.16	Spectrum spot on EDM sample surface (N-S MFAEDM, 24 A, 100 μs)	74
Figure 4.17	Surface of conventional EDM and MFAEDM at 8 A, 50 μs (200×)	76
Figure 4.18	Surface of conventional EDM and MFAEDM at 8 A, 100 μs (200×)	76
Figure 4.19	Surface of conventional EDM and MFAEDM at 24 A, 50 μs (200×)	76
Figure 4.20	a) SEM (100×) and b) 3D surface texture (5×) of N-N MFAEDM at 24 A, 100 μs	78
Figure 4.21	a) SEM (100×) and b) 3D surface texture (5×) of N-S MFAEDM at 24 A, 100 μs	79
Figure 4.22	Crater surface comparison of (a) conventional EDM and (b) N-N MFAEDM (c) N-S MFAEDM at 24 A, 100 μs (SEM 500×)	80
Figure 4.23	Microcracks on EDM surface at 8 A, 100 μs (SEM 1000×)	81
Figure 4.24	Cross sectional view of recast layer for conventional EDM (24 A, 100 μs, SEM 2000×)	82
Figure 4.25	Cross sectional view of recast layer for N-S MFAEDM (24 A, 100 μs, SEM 2000×)	82

اونيورسيتي ملايسيا قهغ

UNIVERSITI MALAYSIA PAHANG

LIST OF SYMBOLS

A	Ampere
\emptyset	Diameter
g/min	Gram per minute
I_p	Peak current
kg	Kilogram
g	Gram
mm	Millimetres
τ_p	Pulse time
t_{on}	Pulse time on
t_{off}	Pulse time off
T	Tesla
μs	Micro-second
μm	Micro-meter
R_a	Arithmetic average of absolute height profile value
V	Voltage

UMP

اونيورسيتي ملايسيا قهغ

UNIVERSITI MALAYSIA PAHANG

LIST OF ABBREVIATIONS

3D	Three dimensional
ANOVA	Analysis of variance
BeCu	Berylium copper
C	Carbon
Cr	Chromium
DOE	Design of experiment
EDM	Electric discharge machining
EDX	Energy-dispersive X-ray spectroscopy
EWR	Electrode wear rate
Fe	Ferum
HAZ	Heat affected zone
MFAEDM	Magnetic field assisted EDM
Mn	Manganese
MRR	Material removal rate
N-N	North to north
N-S	North to south
SEM	Scanning electron microscope
SR	Surface roughness
TEM	Transmission electron microscope
V	Vanadium

اونیورسیتی ملیسیا قہق

UNIVERSITI MALAYSIA PAHANG

CHAPTER 1

INTRODUCTION

1.1 Research Background

This thesis presents a research about electrical discharge machining process under a condition whereby magnetic field is presented around the spark gap. The electrical discharge machining (EDM) is a well-known material removal process for conductive materials of which repetitive spark discharges are produced between the tool and workpiece. In EDM machining system, electrode tool (cathode) and workpiece (anode) are separated by diminutive distance about 0.01 mm - 0.50 mm known as the spark gap. This spark gap is either flooded or immersed inside the dielectric fluid. Quality of spark discharge is controlled by machining parameters such as pulsing time and direct peak current between sample workpiece and electrode tool. At the same time, dielectric fluid in the machining area is ionized; thus, enabling the spark discharge to pass between the tool and workpiece. Each spark produces intense heat in the range of 8,000 °C to 12,000 °C to melt and immediately vaporise a small volume of workpiece material repeatedly. Crater on its surface is created from outburst energy contained in each spark. Excellent combination of EDM machining parameters would result in reasonable material removal rate, surface finish and machining tolerance.

Amongst important EDM machining parameters usually used in this study area were machining polarity (P), peak current (I_p), pulse duration (t_p), high-voltage auxiliary current (I_H), no-load voltage (V) and servo reference voltage (S_v). EDM machining outputs such as material removal rate (MRR), surface roughness (R_a) and electrode wear rate (EWR) depend on the combination of EDM machining parameters which may affect material machinability. The main idea of this study is to find appropriate magnetic polarity combination to produce better EDM output and to explore the influence of magnetic field on the spark.

The magnetic field flux line surrounds the machining area when two or more magnetic bars are brought together. At the presence of a magnetic field, the spark has the ability to enhance surface finish and machining time. The significant focus in this research emphasizes the effects of magnetic polarity on magnetic field-assisted EDM machining. The investigations of magnetic polarity effects under selected conditions were studied accordingly. Currently, there is a lack of study in magnetic polarity on the EDM process which offers a research gap and an exciting topic to explore. The result of this research will encourage severe adjustment for EDM technology improvement.

1.2 Problem Statement

Electrical Discharge Machining (EDM) is operated to create precise and intricate geometry shapes; but in the meantime, it has issues pertaining to material removal rate and surface quality. According to Lee and Tai (2003); Lin and Lee (2008), the EDM machining speed is not only defined by generator settings but also by flushing system and debris density in the gap. EDM Flushing is needed to circulate dielectric fluid between electrodes and the workpiece to remove eroded particles from the spark gap. If the eroded particles remain in the spark gap, it definitely falters the next spark. Meanwhile, too high fluid pressure from the flushing nozzle could turn the spark out arcing. The migration of unnecessary carbon particle during the process may also form pyrolytic carbon layer onto the electrode surface as described by L. Li, Zhao, Li, Feng, and Bai (2017). Hence, effective flushing system provides efficient debris extraction to increase the material removal process and to avoid pyrolytic carbon formation.

Magnetic field-assisted EDM technique offers a promising alternative to supports EDM flushing and to solve the aforementioned problems. A variation of magnetic applications in EDM machining were previously studied by Luo and Chen (1990), Yeo, Murali, and Cheah (2004), Lin and Lee (2008); Singh Bains, Sidhu, and Payal (2016) and Ming et al., (2020) to enhance MRR and surface quality. However, the setup has its limitation as the method is applicable only for ferromagnetic materials. From those literature review, it was found that none of those focus on magnetic polarity effects on MFAEDM process. As far as this research gap is concerned, north-south (N-S) and north-north (N-N) polarity combinations are applied in MFAEDM.

1.3 Objectives

There are three (3) key objectives for this study.

1. To compare the output of conventional EDM and Magnetic Field-assisted EDM (MFAEDM) machining by using graphite electrode on AISI 420.mod tool steel.
2. To study the result of EDM machining by different combinations of magnetic polarity (north-south and north-north) on MFAEDM.
3. To analyse the surface microstructure of magnetic polarity during MFAEDM process.

1.4 Scope of The Research

This research is based on EDM spark progression adjustment using a magnetic field add-on the conventional discharge process. Graphite material was selected as the tool for the study because of its high tool wear resistance and to observe possible formation of pyrolytic carbon onto the electrode surface. Meanwhile, AISI 420.mod tool steel was selected as the sample material because it is common used in tool and dies fabrication. The coverage of this study is to analyse both machining outcomes from conventional EDM and MFAEDM within 8 A to 24 A of peak currents. The selection of this peak current range is discovered from literature evaluation and works well to avoid lengthy machining time and overburnt on sample surface. This study is limited to magnetic field intensity of 0.54 T because of the limitation to have various permanent magnets strengths. The EDM outcomes considered for observation include machining time (t), material removed rate (MRR), electrode wear rate (EWR), and surface roughness (SR).

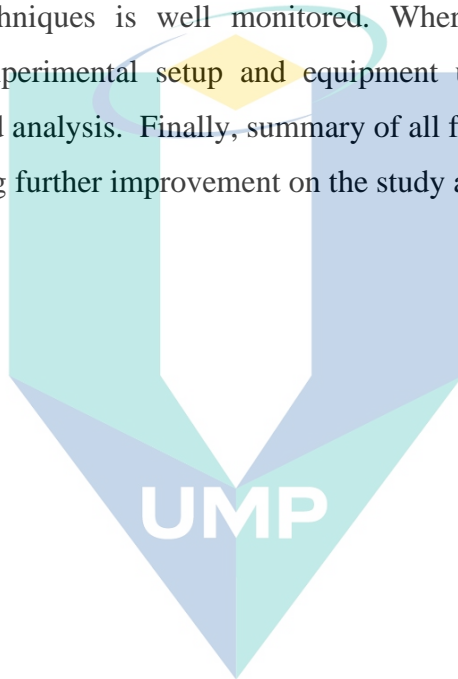
1.5 Hypothesis

If magnetic field is applied to EDM process, evaporated debris is attracted into the magnetic material; thus, enhancing the effectiveness of EDM flushing scheme. The environment can ease the next spark-eroded process so that the condition produces shorter machining time; consequently improves material removed rate (MRR). The altered spark under the magnetic influence provides finer surface finish than conventional EDM

process. The combination of north-south or north-north polarity shows positive impact on magnetic field-assisted EDM.

1.6 Thesis Outline

The thesis consists of five (5) chapters, where Chapter 1 discusses its general information such as introduction of the dissertation, problem analysis, objectives, scope of the project and research hypothesis. While in Chapter 2, literature review of EDM from journals, publication papers and textbook are conferred accordingly so that the overview of EDM current techniques is well monitored. Whereas, Chapter 3 presents the description of the experimental setup and equipment used; Chapter 4 describes the research outcomes and analysis. Finally, summary of all findings and suggestion of new development including further improvement on the study are elaborated in Chapter 5.



اونيورسيتي ملايسيا قهغ

UNIVERSITI MALAYSIA PAHANG

CHAPTER 2

LITERATURE REVIEW

2.1 Introduction

This second chapter discusses existing investigations of EDM to gain theoretical understanding and recent findings. Firstly, it reviews EDM fundamental machining concepts including spark production process. Next, its main machining parameters are presented as these factors greatly influence the machining result. Then, the effects of electrode type selection are discussed as they affect EDM machining quality and tool wear. Finally, the subject of MFAEDM focuses on getting extensive information to provide comprehensive overview of the study. This topic also explores various experimental designs utilized by other scholars as reference and guide to this experiment.

2.2 EDM Overview

2.2.1 Basic Principle of EDM Process

Electrical discharge machine (EDM) is a non-traditional material removal practice which is widely used in mould, tool and die industries. The first primary finding of EDM process was formally reported by an English chemist, Joseph Priestly in 1770 (De Wolf, Cardon, & Balic, 2010). Then, EDM machining technique was introduced to engineering industry in late 1940s when the method was implemented by two Soviet scientists, B.R. and N. I. Lazarenko (Ho & Newman, 2003). The technique was identified as a material removal process by successing repetitive electrical discharges to melt metalwork using electrode in dielectric fluid (Puertas and Luis 2003).

EDM is a cost-effective production method when high accuracy is required. Usually, this technique is used when certain features are no longer possible to be made by conventional or other machining techniques. Diagram plan of EDM system construction, as shown in Figure 2.1 consists of several elements such as power supply, pump,

dielectric, electrode and workpiece. The system is powered by DC power supply to create potential differences between the workpiece and electrode to initiate the spark for discharging process. A piece of work is melted in phases and occurs in dielectric fluid that is non-conductor electrical. The servo motor controls electrode movement toward the workpiece at constant opening to maintain spark gap in the machining area for ionisation process (Bojorquez, Marloth, & Es-Said, 2002). This material is partially eroded due to continuous discharge process but in short pulse by the electrode (Marafona & Chousal, 2006).

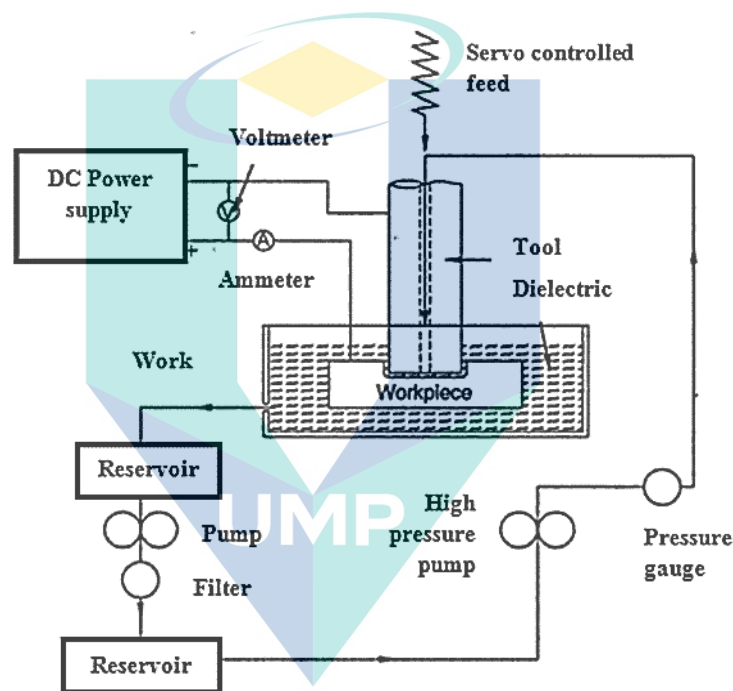


Figure 2.1 EDM schematic plan
Source: Rao (2013)

The conversion of electrical energy to thermal energy generated between tool and material in plasma channels could reach temperatures ranging from 8000 °C to 12,000 °C to melt the workpiece and wearing the electrode. The ionisation process starts when there is an electrical current flow between the electrode and the workpiece causing explosive spark in short time, as illustrated in Figure 2.2. Dielectric in the spark gap separates the open gap voltage between the electrode (anode) and workpiece (cathode). Figure 2.2(a) shows the dielectric-breakdown begins with the increment of electric field concentration until it is sufficient for dielectric breakdown to occur; subsequently, conductive plasma

channels are formed in the gap (Figure 2.2(b)). During discharge, the plasma channel continues to expand within the gap to provide thermal energy needed to melt and partially evaporate the working material. When pulse time (t_{on}) is complete, voltage between the electrode and material is turned off automatically. The current drops rapidly and the plasma can no longer be maintained due to lack of electricity. Eventually, plasma explosion occurs resulting in removal of dissolved material into small debris particles as shown in Figure 2.2(d). The debris in molten material state re-solidifies and are flushed away from the discharge location (Figure 2.2(e)) by dielectric fluid flow which also provides new dielectric medium.

EDM machinability towards any electrically conductive material, regardless of its hardness, into complicated shapes with high accuracy becomes a unique advantage. In fact, EDM has no problem with mechanical stress, chatter and vibration during machining as there is no direct physical contact (Ramasawmy & Blunt, 2004). As there is no collision with the workpiece and electrode in this process, small-scale machining can be conducted up to 0.1 mm with this process (Ho & Newman, 2003). Therefore, this capability is applied to EDM micromachining; whereby micro-hole drilling and three-dimensional micro-cavity as small as 5 μm can be formed (Rajurkar & Yu, 2000). Apart of those capabilities and benefits of electrical discharge machine for material removal machining, the EDM process has several limitations such as creating micro-cracks, alterations in metal surface area, heat-affected zone (HAZ), and recast layer formation on machined surfaces (Saxena, Agarwal, & Khare, 2016; Seyedzavvar & Shabgard, 2012).

اونيور سيني مليسيا فھق

UNIVERSITI MALAYSIA PAHANG

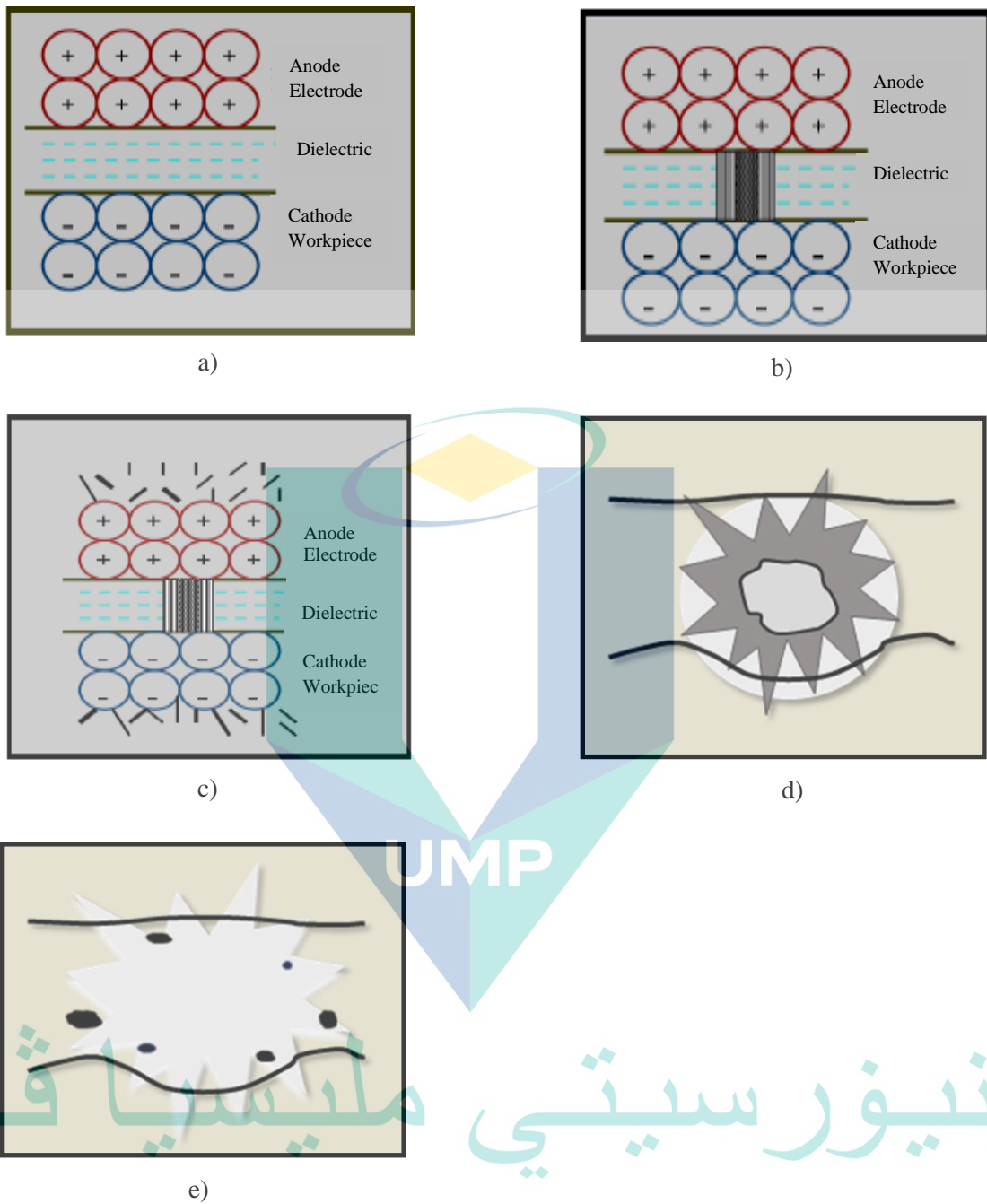


Figure 2.2 EDM ionisation discharge process (a) pre-breakdown (b) dielectric breakdown (c) discharge process (d) plasma implosion and (e) post discharge

Source: S. K. Choudhary and Jadoun (2014)

2.2.2 Spark and Debris

Research on the maintenance of spark discharge in EDM was investigated by Fan et al. (2016). The authors discovered that the generation of sparks and their continuity depend on the size of gap voltage and is associated with the structure of pulse power circuit. Another important requirement in EDM is distance of the resulting spark gap. The value of gap depends on the state of machining technology, generator parameters and penetration speed into the material. In practice, the gap can change from 5 mm to 1/100 mm depending on the operation performed and the settings employed (Sommer & Sommer, 2005).

A study on the detection of two-dimensional ignition locations by electromagnetic detection method in EDM was conducted by Qiang, Yong, and Wansheng (2002). The method used is based energy emission from the sparks transformed into electromagnetic waves around the workpiece. Sensor systems consist of high precision linear components and cubic ferrite were used to detect magnetic field intensity. The relationship between sensor system output and two-dimensional splitter under the speculated electrode was introduced, and the curve diagram was taken. The information obtained by locating the spark and triggering phase is depicted in Figure 2.3. In addition, discharge process phase at each spark was described by Konig and Klocke (1997) as shown in Figure 2.4.

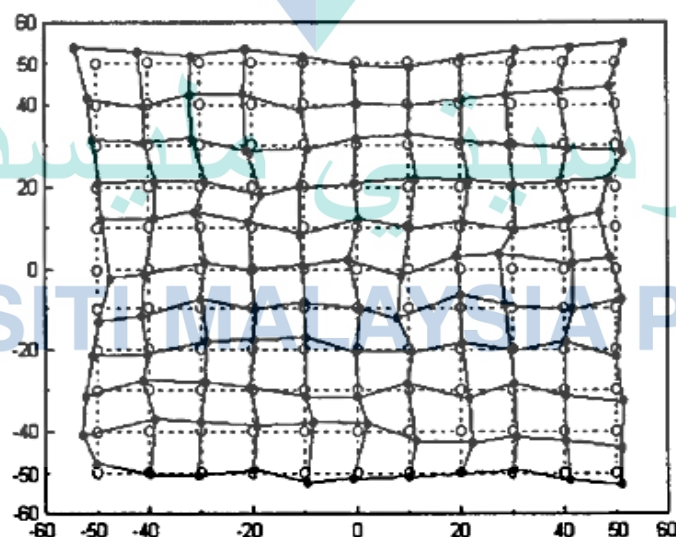


Figure 2.3 Experimental result of two-dimension EDM spark location detection
Source: Qiang et al. (2002)

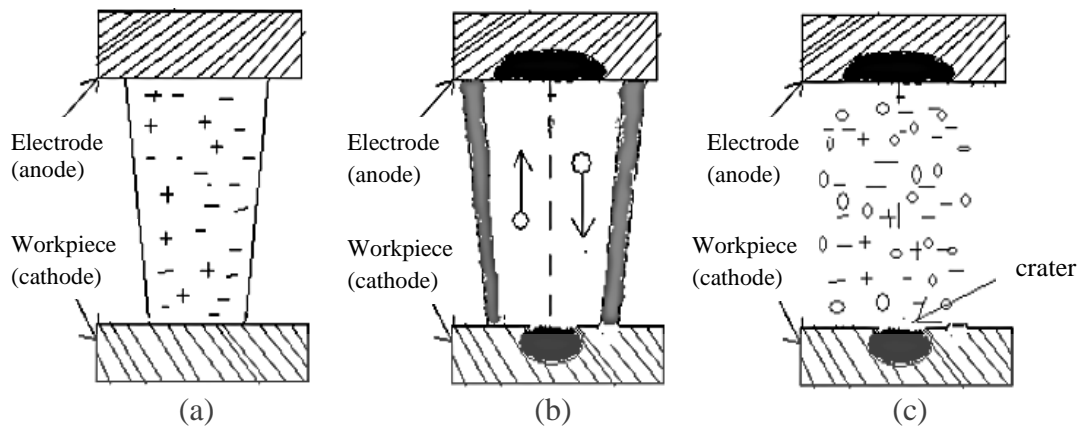


Figure 2.4 The phases of EDM on each spark location; a) ignition phase, b) discharge phase and (c) end of pulse

Source: König and Klocke (1997)

Machining debris from the EDM process is difficult to remove from the machining area due to small spark gap between the electrode and workpiece (Rajurkar & Pandit, 1988; S. Zhang et al., 2017). The excess debris is found scattered in dielectric fluids, especially those accumulated in the machining gap tend to cause abnormal electrical discharges. Therefore, the stability of EDM advances are impaired. The debris should be removed from the gap correctly as it greatly influences the machining efficiency and accuracy particularly for deep hole machining process. If the debris can be effectively and completely removed, the EDM process has the potential to produce high efficiency and high-quality surface finish as well as high accuracy machining. Researchers have introduced magnetic field applications in EDM to remove debris from the gap and improve debris circulation to achieve this purpose (Shabgard, Gholipoor, & Baseri, 2016).

Debris properties of EDM machining have been studied in detailed by Murray, Sun, Patil, Wood, and Clare (2016). The authors analysed the length of the debris. Images from SEM and TEM in Figure 2.5 show that the size of these debris particles are between 1nm or less and up to 10 μm . Morphological observation by TEM indicates that the debris particles are mostly spherical as shown in Figure 2.6. It was discovered debris from electrode particles was present in all sample regions. This is evident that debris plays an important role in the electrical state of discharge gap.

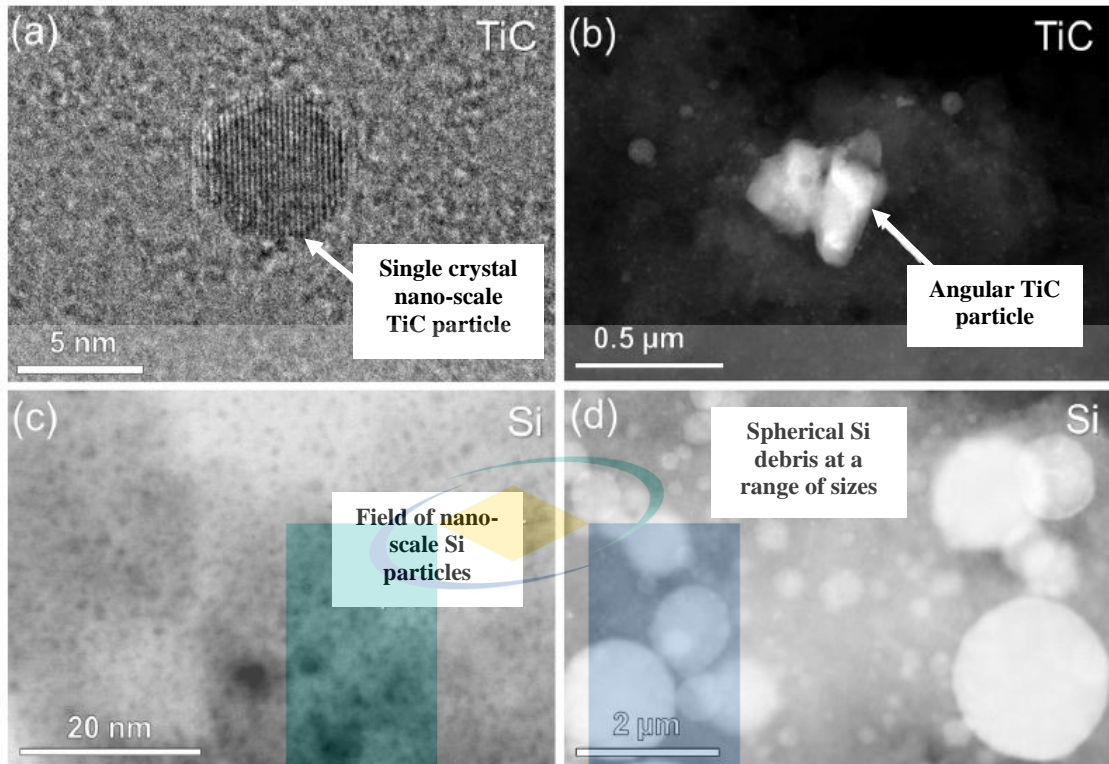


Figure 2.5 Compilation of TEM images single crystal nano-scale of (a) TiC at 5 nm (b) TiC at 0.5 μm (c) Si at 20 nm and (d) Si at 2 μm

Source: (Murray et al., 2016)

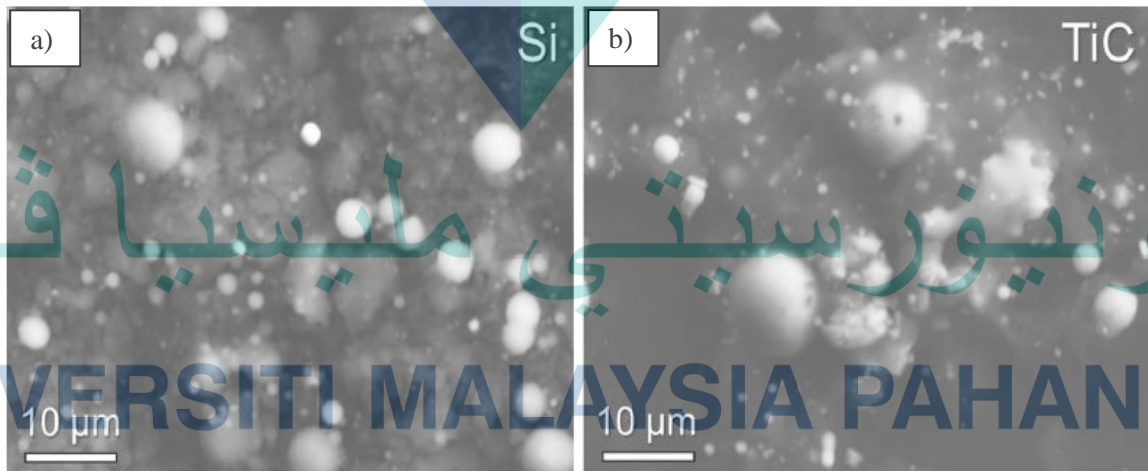


Figure 2.6 SEM images of (a) Si and (b) TiC debris at 10 μm magnification

Source: (Murray et al., 2016)

Another study on debris was conducted by S. Zhang et al. (2017) who studied debris movement and its removal processes. A simulation study of 3D debris flow in the gap was developed as shown in Figure 2.7. The authors considered debris increment against EDM release cycles and the obstruction generated by self-adjusting tool in the gap flow movement. Statistical analysis and analysis of debris distribution under different machining conditions were performed for different depths, containment velocities (Figure 2.7(a)), pressure (Figure 2.7(b)) and debris gap flow (Figure 2.7(c)) to prove the findings.

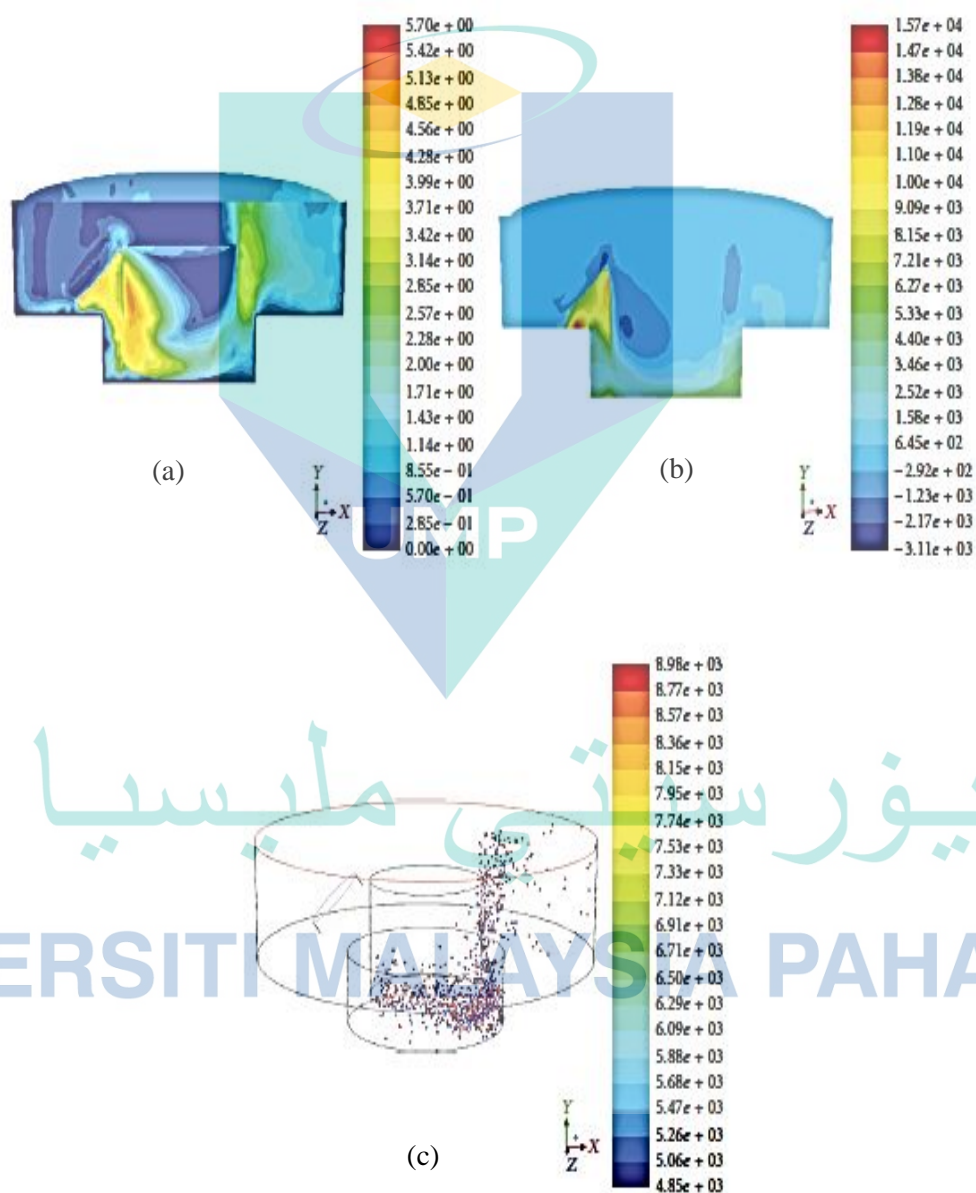


Figure 2.7 Schematics of gap flow (a) velocity field (b) pressure field and (c) debris flow with normal flushing technique by S. Zhang et al. (2017)

2.2.3 EDM Parameters

An important aspect to consider before performing electrical machining is the selection of machining parameters. EDM machinability on certain materials depends on the suitability of tool and parameters selected. These factors determine machining output such as surface roughness, electrode wear and material removal rate. Current flows into the system and voltage continues to rise until it creates an ionisation path in the dielectric. As the current surges, the voltage drops at certain point to stabilise the gap. The selected voltage value determines the width of spark gap between the electrode and the workpiece (Mahendran, Devarajan, Nagarajan, & Majdi, 2010). If high voltage value is applied, wider spark gap is produced. Wider spark gap helps flushing cycle, reduces heat and stabilises the cut. However, high voltage affects EDM material cutting results; consequently, speeds up tool wear rate and coarse surface roughness.

Peak current (I_p) is another significant parameter in EDM machining and it is measured in amperage (A). To obtain high removal rate, higher current voltage is usually applied; but, resulting in poor surface finish and high tool wear. Graphite electrodes were reported to function at high current without much damage (Ho & Newman, 2003). Puertas and Luis (2003) observed that the most influential factor on material removal rate is peak current; followed by duty cycle factor, pulse time factor and the interaction effect of the first two. The material removal rate increases as logically expected when current intensity and duty cycle are increased. Meanwhile, an increase in pulse time decreases MRR as illustrated in Figure 2.8 and Figure 2.9.

Based on other observations made by Kiyak and Cakır (2007) the result shows pulse time parameter is a factor in surface roughness and material removal rate. It has been noted that excellent machined surface quality can be obtained by setting machining parameters at low pulse and short pulse time. Whilst, the combination results in low material removal rates; it also results in high machining time and cost. On the other hand, if high removal rates are required, high pulse and pulse times should be selected. However, this selection produces poor surface roughness due to deeper and wider crater on the machine surface. High temperature from high pulse time speeds up the removal rate and yields in material properties lost.

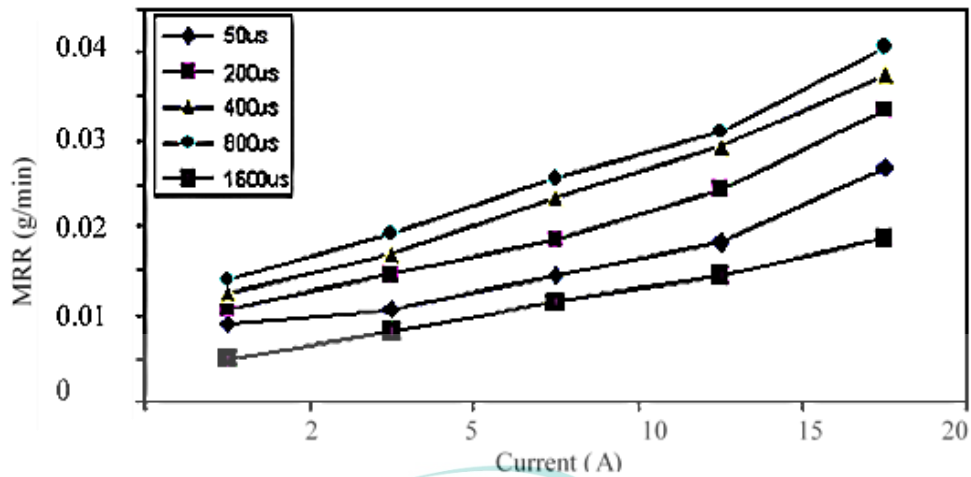


Figure 2.8 Result of MRR vs current parameters reported by Arikatla, Mannan, and Krishnaiah (2013)

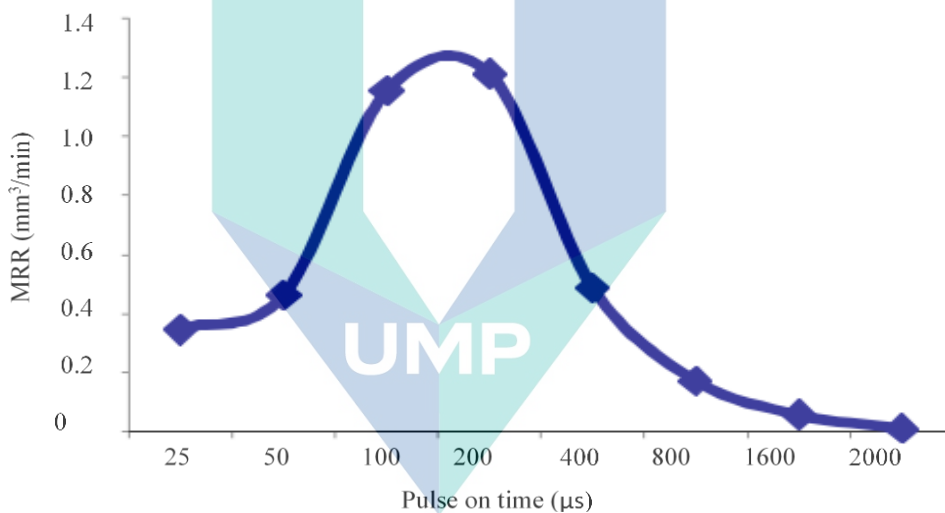


Figure 2.9 Result of MRR vs pulse on time from Arikatla et al. (2013)

Tool wear and material removal rates are also affected by the type of dielectric and flushing method employed. Good dielectric fluid should possess basic characteristics such as high thermal conductivity, low viscosity coefficient and high flowing rate. The function of dielectric fluid is to flush gaseous and solid debris during machining and keep the temperature below flashpoint. In EDM die sinking process, kerosene is popular as dielectric fluid. However, distilled water is preferred in micro EDM because its temperature is not affected by long working time (Chen, Yan, & Huang, 1999; Mahendran et al., 2010). Recent researchers also used kerosene with certain additives to obtain high material removal rate and improve surface roughness. According to Jeavudeen, Jailani,

and Murugan (2020); Wu, Yan, Huang, and Chen (2005), application of additives in dielectric fluid can improve workpiece surface quality, increase material removal rate (MRR) and decrease tool wear rate especially in mid-finish and finish machining.

2.2.4 EDM Trend Study

Several EDM hybrid techniques have been introduced to improve EDM machining performance. Those include dielectric-powder based EDM, dry EDM, ultrasonic vibration-assisted EDM and magnetic field-assisted EDM. The main purpose is to solve EDM limitations. Studies to improve metal debris removal in the spark gap area using various techniques have been tested including dynamic jet flushing, effect of height electrode jump (Okada, 2004), ultra-sonic vibration of electrode (Q. Zhang, Zhang, Deng, Qin, & Niu, 2002) and different types of dielectric fluid to maximise metal waste collection and maintain stability of machining progress. Research progress on cryogenic EDM (CEDM) was well reported by Abbas, Solomon, and Bahari (2007). It was popularly invented by 2009 onwards. Figure 2.10 shows the main area of EDM which is becoming a trend in EDM. Research reviews on EDM advance techniques by Abbas et al. (2007); S. K. Choudhary and Jadoun (2014); Pandey and Singh (2010); Shabgard et al. (2016) have discussed most of EDM advance techniques but do not have any description on cryogenic EDM studies examined by Abdulkareem, Khan, and Konneh (2009); Sundaram, Yildiz, and Rajurkar (2009).

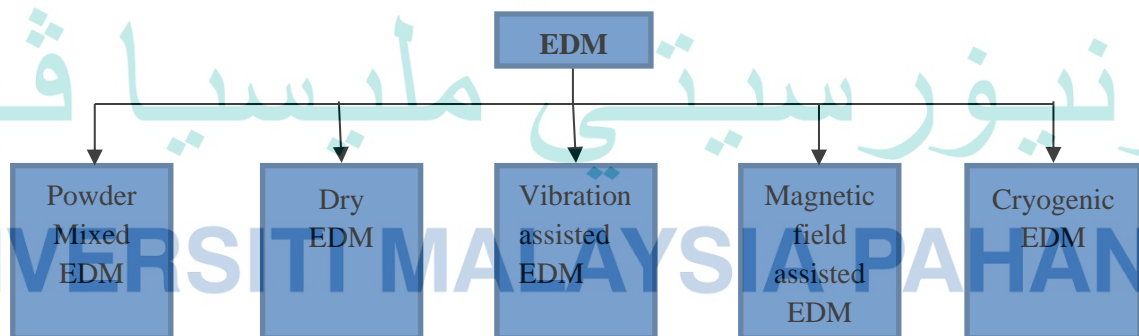


Figure 2.10 Current research trend in EDM

The use of magnetic fields in EDM machining was also introduced to facilitate the removal of machined iron dust from machining areas. Perfect flushing circulation provides an excellent medium for the next spark process, which means that MRR

increases as there is no delay in spark processing. The first study using this magnetic apparatus was performed by De Bruijn in 1978 (Abbas et al., 2007; Shabgard et al., 2016). Among other scholars who have innovated the use of magnets in EDM are (Efendee, Saifuldin, Gebremariam, & Azhari, 2018; Gholipoor, Baseri, Shakeri, & Shabgard, 2016; Gholipoor, Shabgard, Mohammadpourfard, & Abbasi, 2020; Khan et al., 2013; Lin & Lee, 2008; Luo & Chen, 1990; Ming et al., 2020; Rouniyar & Shandilya, 2020; Singh Bains et al., 2016; Teimouri & Baseri, 2012; Tomura & Kunieda, 2009; Yeo et al., 2004; X. Zhang & Uchiyama, 2017). A review from Shabgard et al. (2016) mentions that magnetic field acts as perpendicular to the electrode spark and the magnetic field is efficient in transporting debris out of the machining area as shown in Figure 2.11. The findings show the use of magnetic fields can improve spark gaps cleaning because ferromagnetic material is extracted and sticks to the magnetic material rapidly. Another MFAEDM experiment in pulsating magnetic field for near dry EDM was examined by Joshi, Govindan, Malshe, and Rajurkar (2011) and Gholipoor et al. (2016) to characterize EDM hybrid performance. Both studies demonstrate that the pressure from tangential magnetic field is able to increase electrons movement and ionizations activities in the plasma channel. With corresponding machine parameters, the approach increases machining productivity by 130% compared to conventional near dry EDM. Table 2.1 shows several fields of EDM which is being a research trend for 2018 to 2020.

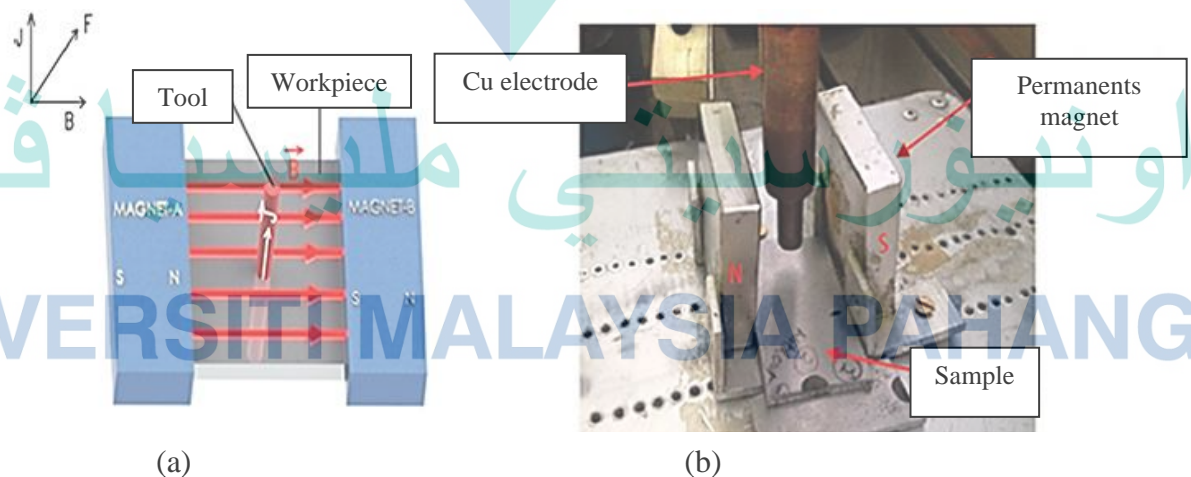


Figure 2.11 Schematic of the experimental setup demonstrates (a) magnetic field acting perpendicular to an electrode and (b) actual experiment set up of Singh Bains et al. (2016)

Table 2.1 Field of recent studies on EDM

EDM Field of Studies	Year	Researcher contribution
Powder Mixed EDM	2018	(A. Kumar, Mandal, Dixit, & Mandal, 2018); Investigation of powder mixed EDM process parameters for machining Inconel alloy using response surface methodology
		(F Modica et al, 2018); The influence of powder mixed water-based fluid on micro-EDM process
		(AK Rouniyar et al., 2018); Multi-Objective Optimization using Taguchi and Grey Relational Analysis on Machining of Ti-6Al-4V Alloy by Powder Mixed EDM Process
		(M Bhaumik & K Maity, 2018); Effect of deep cryotreated tungsten carbide electrode and SiC powder on EDM performance of AISI 304
	2019	(NABJ Hosni & MAB Lajis, 2018); Modelling and optimization of chromium powder mixed EDM by response surface methodology approach
		(AP Tiwary & BB Pradhan, 2019); Influence of various metal powder mixed dielectric on micro-EDM characteristics of Ti-6Al-4V
		(P Sivaprakasam et al., 2019); Experimental investigations on nano powder mixed Micro-Wire EDM process of inconel-718 alloy
		(M Hourmand et al., 2019); Microstructure characterization and maximization of the material removal rate in nano-powder mixed EDM of Al-Mg2Si metal matrix composite—ANFIS and RSM
		(M Kolli & A Kumar, 2019); Assessing the Influence of Surfactant and B4C Powder Mixed in Dielectric Fluid on EDM of Titanium Alloy
		(TD Nguyen et al., 2019); Die steel surface layer quality improvement in titanium μ -powder mixed die sinking electrical discharge machining
2020	(Sahu & Mandal, 2020); Critical analysis of surface integrity parameters and dimensional accuracy in powder-mixed EDM	
	(A. Kumar, Mandal, Dixit, & Mandal, 2020); Quantitative analysis of bubble size and electrodes gap at different dielectric conditions in powder mixed EDM process	
	(Jeavudeen et al., 2020); Powder additives influence on dielectric strength of EDM fluid and material removal	
	(George, Chandan, Manu, & Mathew, 2020); Experimental Investigation of Silicon Powder Mixed EDM Using Graphene and CNT Nano Particle Coated Electrodes	
		(Chakraborty, Mitra, & Bose, 2020); Experimental investigation on enhancing die corner accuracy during powder mixed wire EDM of Ti6Al4V

Table 2.1 Continued

EDM Field of Studies	Year	Researcher contribution
Dry EDM	2018	(NS Khundrakpam, GS Brar & D Deepak, 2018); Grey-Taguchi optimization of near dry EDM process parameters on the surface roughness
		(NS Khundrakpam & GS Brar, 2018); Genetic algorithm approach for optimizing surface roughness of near dry EDM
		(FTB Macedo, 2018); Fundamental Investigation of Dry EDM Plasmas (A Żyra, W Bizoń & S Skoczypiec, 2018); Primary research on dry electrodischarge machining with additional workpiece cooling
		(M Wiessner et al., 2018); Fundamental investigation of EDM plasmas, part I: a comparison between electric discharges in gaseous and liquid dielectric media
		(VK Yadav, P Kumar & A Dvivedi, 2019); Effect of tool rotation in near-dry EDM process on machining characteristics of HSS
		(VS Ganachari, UN Chate & LY Waghmode, 2019); A comparative performance study of dry and near dry EDM processes in machining of spring steel material
	2019	(P Nagarajan, PK Murugesan & E Natarajan, 2019); Optimum Control Parameters During Machining of LM13 Aluminum Alloy Under Dry Electrical Discharge Machining (EDM) With A Modified Tool Design
		(VK Yadav, P Kumar & A Dvivedi, 2019); Performance enhancement of rotary tool near-dry EDM of HSS by supplying oxygen gas in the dielectric medium
		(Baseri, 2019); Multi-response Optimization of Dry EDM with Different Mediums Using the Taguchi Based Grey Relational Analysis
		(Yadav, Kumar, & Dvivedi, 2020); Investigation on the Effect of Input Parameters on Surface Quality During Rotary Tool Near-Dry EDM
		(Sundriyal, Yadav, Walia, & Kumar, 2020); Thermophysical-Based Modeling of Material Removal in Powder Mixed Near-Dry EDM
		(Rajkumar, Giridharan, Oyyaravelu, & Balan, 2020); Investigation on Magnetic Field-assisted Near-dry Electrical Discharge Machining of Inconel 600
2020	(Banu, Ali, Rahman, & Konneh, 2020); Stability of micro dry wire EDM: OFAT and DOE method	
	(M. Y. Ali, Banu, Rahman, Al Hazza, & Chowdhury, 2020); Micro Dry Wire EDM: Kerf Investigation using Response Surface Methodology	
	(Rajabinasab, Abedini, Hadad, & Hajjighorbani, 2020); Experimental investigation of the effect of tool material on the performance of AISI 4140 steel in the rotary near dry electrical discharge machining	

Table 2.1 Continued

EDM Field of Studies	Year	Researcher contribution
Vibration assisted EDM	2018	(AWJ Hsue, TJ Hab & TM Lin, 2018); Pulse efficiency and gap status of rotary ultrasonic assisted electrical discharge machining and EDM milling
		(Y Liu et al., 2018); A simulation study of debris removal process in ultrasonic vibration assisted electrical discharge machining (EDM) of deep holes
		(S Kumar, S Grover & RS Walia, 2018); Analyzing and modeling the performance index of ultrasonic vibration assisted EDM using graph theory and matrix approach
		(H Ni et al., 2018); A comparative investigation on hybrid EDM for drilling small deep holes
	2019	(P Singh, V Yadava & A Narayan, 2019); Micro-EDM performance of Inconel 718 superalloy with and without ultrasonic vibration
		(K Mishra, BR Sarkar & B Bhattacharyya, 2019); Vibration-Assisted Micro-EDM Process
		(KP Maity & M Choubey, 2019); A review on vibration-assisted EDM, micro-EDM and WEDM
		(RB Azhiri, AS Bideskan & F Javidpour, 2019); Study on material removal rate, surface quality, and residual stress of AISI D2 tool steel in electrical discharge machining in presence of ultrasonic vibration effect
		(Q Han, H Wan & D Han, 2019); EDM-drilling Characteristics with the Rotation Motion of SS304
		(Xu, Wu, Gao, Liu, & Song, 2020); Error modeling and accuracy optimization of rotating ultrasonic vibration assisted EDM machine tool
2020	(Choubey, Maity, & Sharma, 2020); Finite element modeling of material removal rate in micro-EDM process with and without ultrasonic vibration	
	(G. Singh, Satsangi, & Prajapati, 2020); Effect of Rotating Magnetic Field and Ultrasonic Vibration on Micro-EDM Process	
	(Mao, Yang, Zhang, Zhu, & Huo, 2020); Development of Multi Micro Holes Synchronous Rotating and Vibration EDM Machine Tool	
(Shitara, Fujita, & Yan, 2020); Direct observation of discharging phenomena in vibration-assisted micro-electrical discharge machining		

Table 2.1 Continued

EDM Field of Studies	Year	Researcher contribution
Cryogenic EDM	2018	(R Manivannan, M Pradeep Kumar, 2018); Improving the machining performance characteristics of the μ EDM drilling process by the online cryogenic cooling approach
		(N Singh, N Panpalia & MM Singh,2018); Comparison of machining characteristics of Inconel 601 with normal and cryogenic cooled electrode in EDM using RSM
		(N Singh, BC Routara & RK Nayak,2018); Study of machining characteristics of Inconel 601 with cryogenic cooled electrode in EDM using RSM
		(CP Mohanty et al., 2018); Optimization of cryo-treated EDM variables using TOPSIS-based TLBO algorithm
	2019	(W Tahir, M Jahanzaib & A Raza, 2019); Effect of process parameters on cutting speed of wire EDM process in machining HSLA steel with cryogenic treated brass wire
		(GS Grewal & DP Dhiman, 2019); Effect of deep cryogenic treatment on copper electrode for non-traditional electric discharge machining (EDM)
		(Prakash, Tariq, Davis, Singh, & Debnath, 2020); Influence of cryogenic treatment on the performance of micro-EDM tool electrode in machining of magnesium alloy AZ31B
	2020	(Satynarayana, Rajkiran, & Chakradhar, 2020); A Role of cryogenic in Wire cut EDM process
		(J. Singh, Singh, & Pandey, 2020); Electric discharge machining using rapid manufactured complex shape copper electrode with cryogenic cooling channel
		(R. Choudhary et al., 2020); Analysis of cryogenic tool wear during electrical discharge machining of titanium alloy grade 5
(Y. Li, Cui, Lin, & Li, 2020); Machining Characteristics of IN718 by EDM with Cooled Electrode and Vibration of the Workpiece		
(Goyal, Rohilla, Kumar, Goyal, & Mittal, 2020); Selection of range of pulse duration during cryogenically assisted electric discharge machining		

Table 2.1 Continued

EDM Field of Studies	Year	Researcher contribution
Magnetic field-assisted EDM	2018	(P Singh Bains, SS Sidhu & HS Payal, 2018); Investigation of magnetic field-assisted EDM of composites
		(H Beravala & PM Pandey, 2018); Experimental investigations to evaluate the effect of magnetic field on the performance of air and argon gas assisted EDM processes
		(A Gholipoor & M Mohammadpourfard, 2018); Study of the effect of tools ultrasonic vibrations and external magnetic field on machined surface integrity at EDM process
		(AM Efendee et al., 2018); Effect of magnetic polarity on surface roughness during magnetic field assisted EDM of tool steel
	2019	(Y Feng et al., 2019); Investigation on machining performance of micro-holes EDM in ZrB ₂ -SiC ceramics using a magnetic suspension spindle system
		(NS Chityal, A Bhandare & UA Dabade, 2019); Experimental investigation on a shield and magnetic assisted EDM of EN24 steel
		(S Bhowmik & D Zindani, 2019); Magnetic Field Assisted Micro-EDM
		(AK Rouniyar & P Shandilya, 2019); Improvement in Machined Surface with the use of Powder and Magnetic Field Assisted on Machining Aluminium 6061 Alloy with EDM
		(MR Shabgard & A Gholipoor, 2019); Investigating the effects of external magnetic field on machining characteristics of electrical discharge machining process, numerically and experimentally
		(Ming et al., 2020); A comparative investigation on magnetic field-assisted EDM of magnetic and non-magnetic materials
		(Renjith & Paul, 2020); Machining characteristics of micro-magnetic field assisted EDM (μ -MFAEDM)
		(Rouniyar & Shandilya, 2020); Optimization of process parameters in magnetic field assisted powder mixed EDM of aluminium 6061 alloy
2020	(G. Singh et al., 2020); Effect of Rotating Magnetic Field and Ultrasonic Vibration on Micro-EDM Process	
	(Sushil Kumar, Goud, & Suri, 2020); An Investigation of Magnetic-field-assisted EDM by Silicon and Boron Based Dielectric of Inconel 706	
	(S. Kumar et al., 2020); Multi-response optimization of magnetic field assisted EDM through desirability function using response surface methodology	
	(Sivaprakasam, Hariharan, & Elias, 2020); Experimental investigations on magnetic field-assisted micro-electric discharge machining of inconel alloy	
(Y. Zhang, Zhang, Zhang, & Li, 2020); Reduction of energy consumption and thermal deformation in WEDM by magnetic field assisted technology		

2.3 Magnetic Field Assisted EDM

Any magnetic object has a magnetic field that attracts ferrous components such as iron, steel, nickel and cobalt. Lines of magnetic fields surround a magnet as pattern space, as shown in Figure 2.12 below. The direction of magnetic flux flow noticeably leaves the north pole out, heading to the south pole as a circulated closed-loop line pattern. The intensity of magnetic field is high at the pole area because the flux lines are more concentrated or closely spaced. However, this magnetic flux does not move as the flow direction of magnetic lines; and it is in a static state around the magnet (Giancoli, 2013).

The magnetic field line pattern creates a new line pattern when two or more magnets are joined together. If two magnets with the same poles are placed next to each other in adjacent manner and brought close together, the resultant interaction of the magnetic fields causes repulsive force. In other words, it repels each other. When two different poles of magnets are arranged to face each other either in (N-S) or (S-N) combination, the resulting magnetic field has attractive force. The effect of the magnetic polarity combination on magnetic field lines can be visualized using iron fillings as illustrated in Figure 2.13.

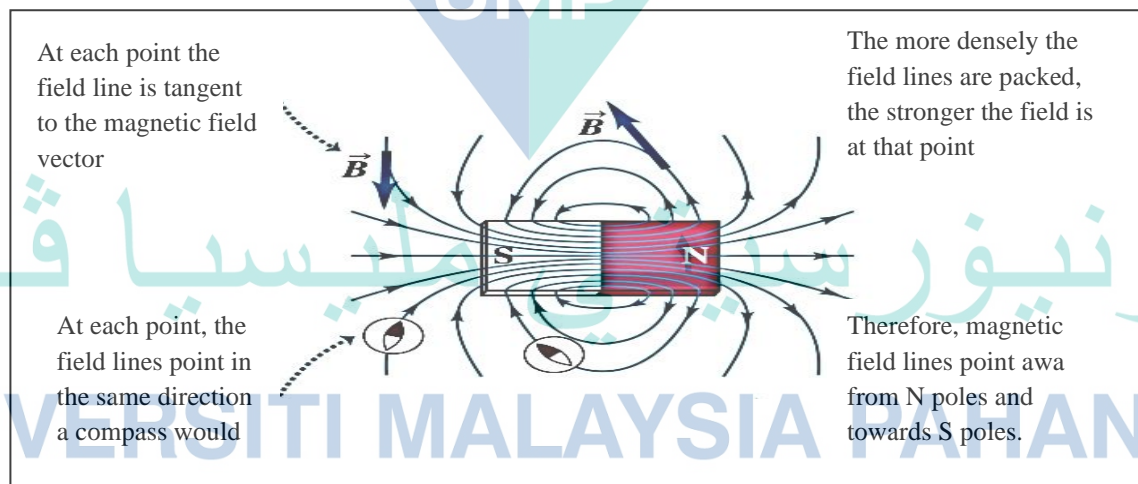


Figure 2.12 Lines of a magnetic field

Source: Giancoli (2013)

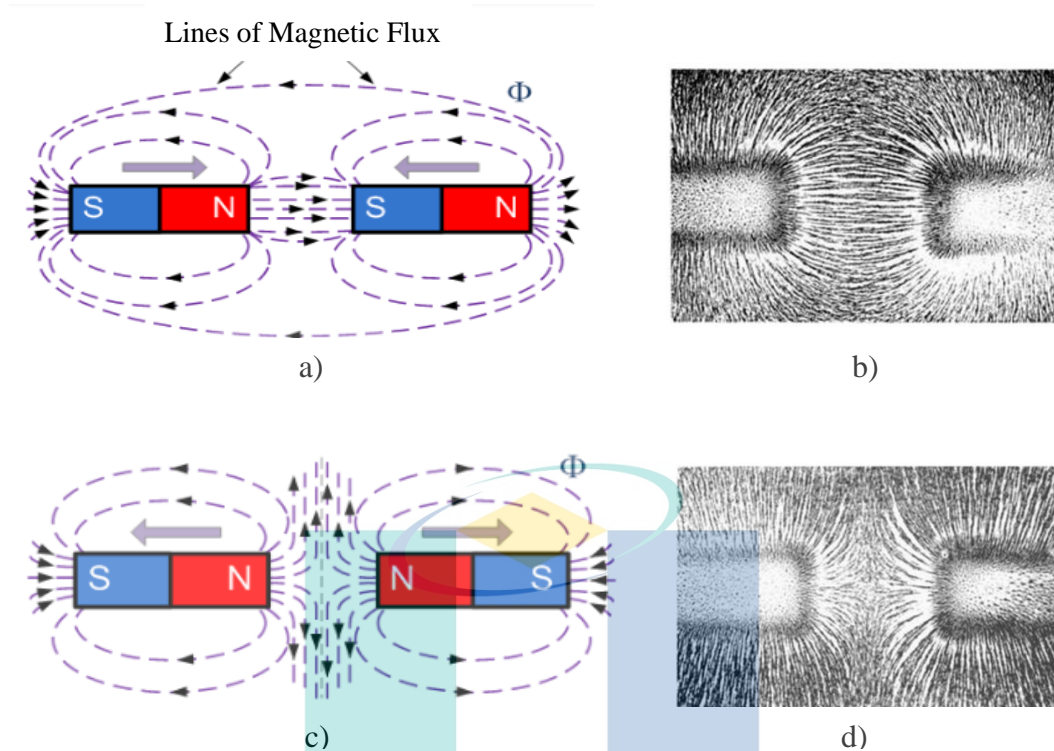


Figure 2.13 Various combinations of poles and iron filings (a) unlike poles – attract, (b) iron filling pattern of N-S (c) like poles – repel and (d) iron filling pattern of N-N

Source: Revision World Networks Limited (2018, January) *Magnetic fields*. Retrieved from <https://revisionworld.com/>

Figure 2.14 shows the magnetic field lines and the resultant magnetic field patterns for N-N and N-S permanent magnets combination. Combination of two magnetic fields from different polarities (N-S or S-N) produces neutral spot but the spot located outside of the desired magnetic fields as illustrated in Figure 2.14(a). Meanwhile for (N-N or S-S) combination a neutral spot is created in the middle of magnetic flux line. This neutral spot can be seen as in Figure 2.14(b). At this neutral point, the resulting magnetic field is zero (Serway & Jewett, 2013).

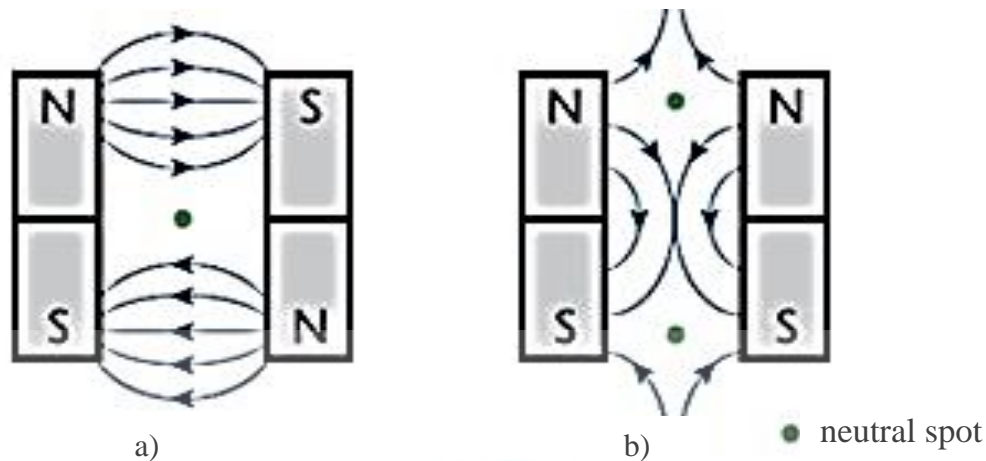


Figure 2.14 Resultant magnetic field pattern and neutral spot of (a) N-S combination, (b) N-N combination

Source: Revision World Networks Limited (2018, January) *Magnetic fields*. Retrieved from <https://revisionworld.com/>

2.3.1 Methods in MFAEDM

MFAEDM was conducted where the EDM instrument was coupled with magnetic field to overcome EDM disadvantages. In the investigation, constant magnetic field was proposed and applied perpendicularly to the discharge channel. The experiment used discharge current and pulse duration as the main machining parameters to study its effect on surface roughness and MRR. Report by Sunil Kumar, Srivastava, and Kumar (2015); Ming et al. (2020); Yeo et al. (2004) suggest that MFAEDM is suitable for machining of ferromagnetic and non-ferromagnetic materials because of its advantages such as easy application, facilitating flushing system, economically competence and environmentally friendly.

Figure 2.15 shows the experiment set up for studying electromagnetic field effect in super-finishing EDM conducted by Luo and Chen (1990). The arrangement was developed to sense micro-thermal energy and discharge pulse in investigating surface roughness of superfinishing EDM. However, the outcome is not satisfying because the difficulty in stabilising current pulse at small electric parameters of the pulse generator. Pulse distortion and pulse fluctuation occur during transmission process which makes it difficult to attain the desired pulse parameters. Anyhow, the experiment manages to demonstrate that smooth surface can be achieved but only by short pulse.

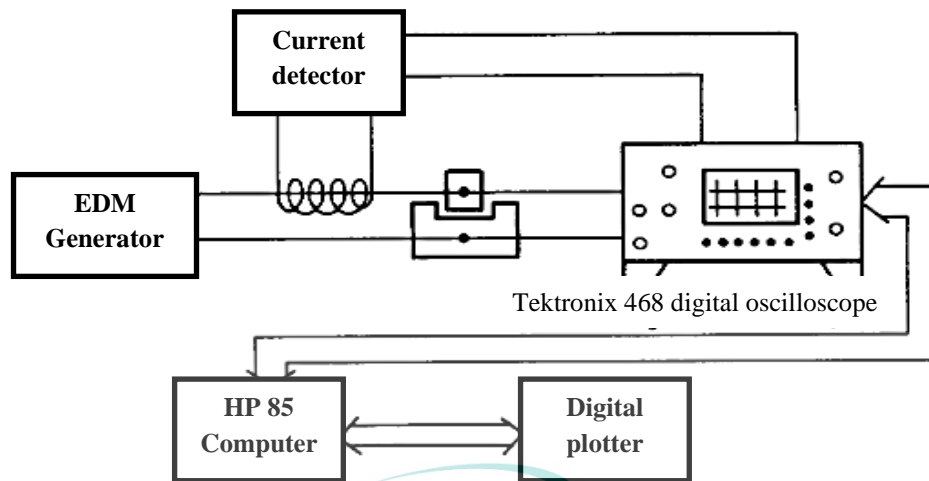


Figure 2.15 The set-up for discharge pulse parameters sensing
 Source: Luo and Chen (1990)

Lin and Lee (2008) proposed a novel method to purify the spark gap by adding magnetic force to conventional EDM system. The gap condition affects EDM machining stability so metal debris should be expelled immediately after each spark process. In the experiment, peak current and pulse duration were chosen as the main parameters to study the output characteristics. A rotational disc with a couple of magnetic devices were placed under the machining zone to eject metal debris from the spark gap. Then, EDM process stability was compared using an oscilloscope to detect discharge waveform. The experiment set up was arranged as shown in Figure 2.16. Lin and Lee (2008) also configured the differences of discharge wave form to verify the stability of MFAEDM compared to conventional EDM. Figure 2.17 shows the waveform progress trends for both methods. The waveform indicates MFAEDM sparking growth is much stable (Figure 2.17(b)) compared to conventional EDM as arcing or abnormal discharge are presence (Figure 2.17(a)). This abnormal discharge is caused by the accumulated machining debris in the machining zone. Subsequently, MFAEDM has better machining stability because the metal debris is expelled efficiently by the magnetic field; hence, reducing the abnormal discharge. The same experiment method was repeated by Lin, Chen, Wang, and Lee (2009) who discovered the optimisation of the above. It is MFAEDM research based on Taguchi method and variance analysis (ANOVA). Experiments based on this method have been conducted by the author to validate the optimization findings.

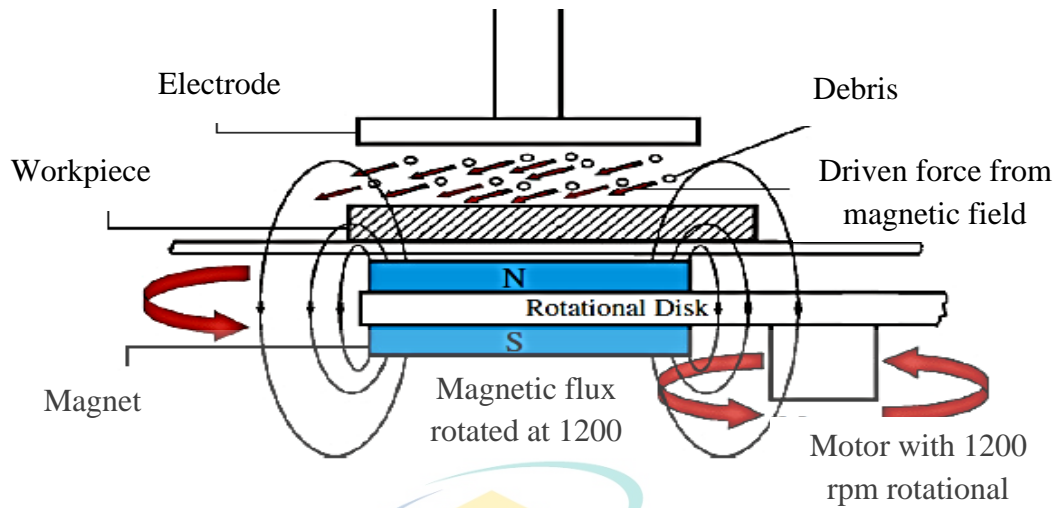


Figure 2.16 Illustration magnet force assisted EDM configuration by Lin and Lee (2008)

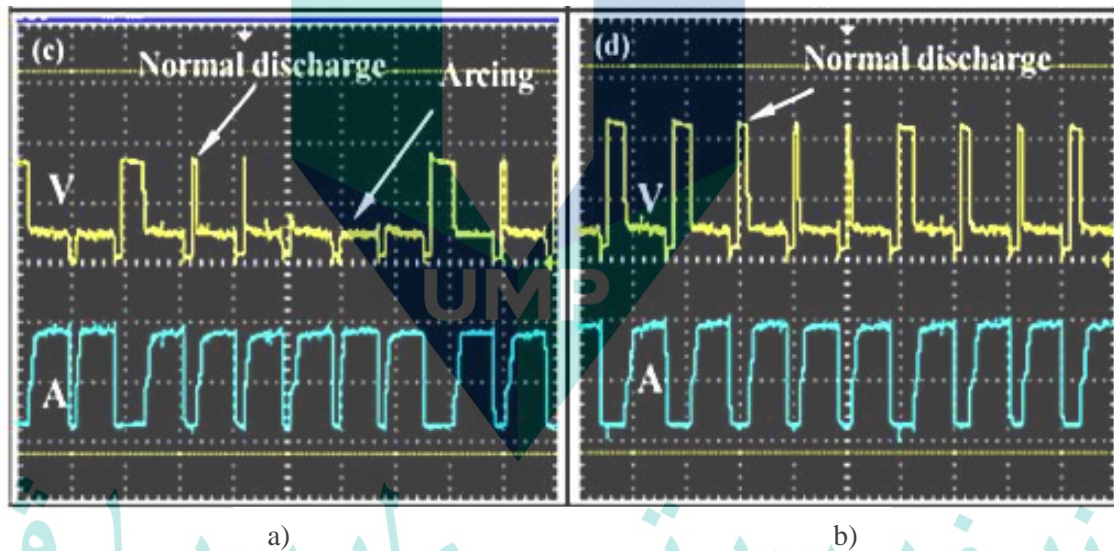


Figure 2.17 Discharge waveforms of (a) conventional EDM and (b) MFAEDM
Source: Lin and Lee (2008)

Figure 2.18 shows the experimental layout for EDM with six (6) external magnetic fields around the machining area by Khan et al. (2013). The magnets were placed on the north pole facing the aluminium electrode. The experimentation employed peak current in the range of 2.5 A to 6.5 A and 7.0 μ s to 10.5 μ s of pulse time to observe surface roughness of MRR and EWR. In Gholipour et al. (2016) study, a pair of magnets was mounted onto rotary tool to develop MFAEDM mechanism in near dry EDM case as

illustrated in Figure 2.19. An electric motor powered the rotary motion which was attached to the electrode and speed level was controlled by LS600 inverter. Two different strength intensities (0.38 T and 1.2 T) were applied to the system to improve debris removal process; thus, minimising the probability of abnormal discharge process. An optical micrograph was used to analyse sample surface integrity. Meanwhile, waveform analysis was utilized to study magnetic field effects in near dry MFAEDM.

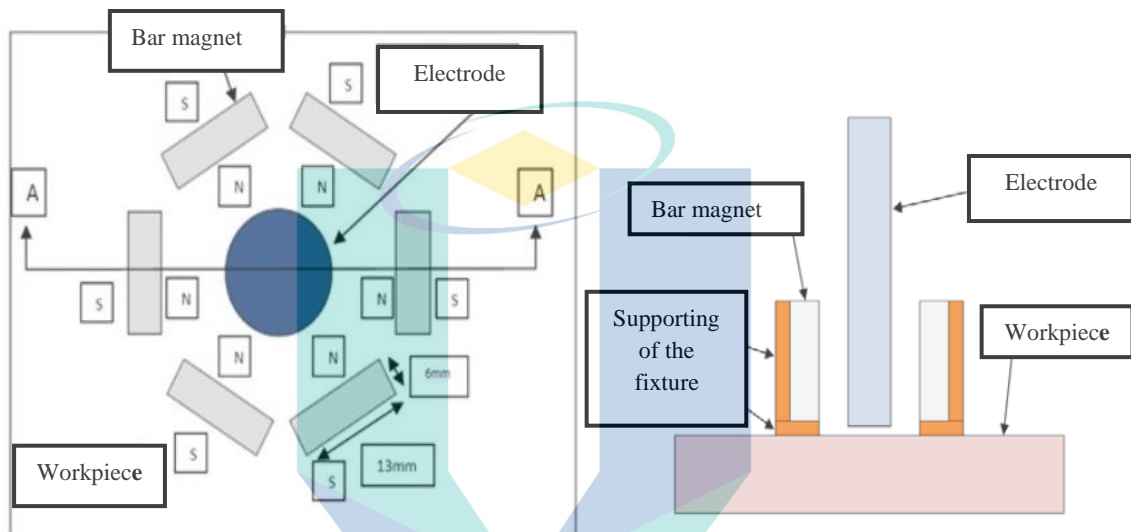


Figure 2.18 The experimental layout with external magnetic field by Khan, Ndaliman et. al (2013)

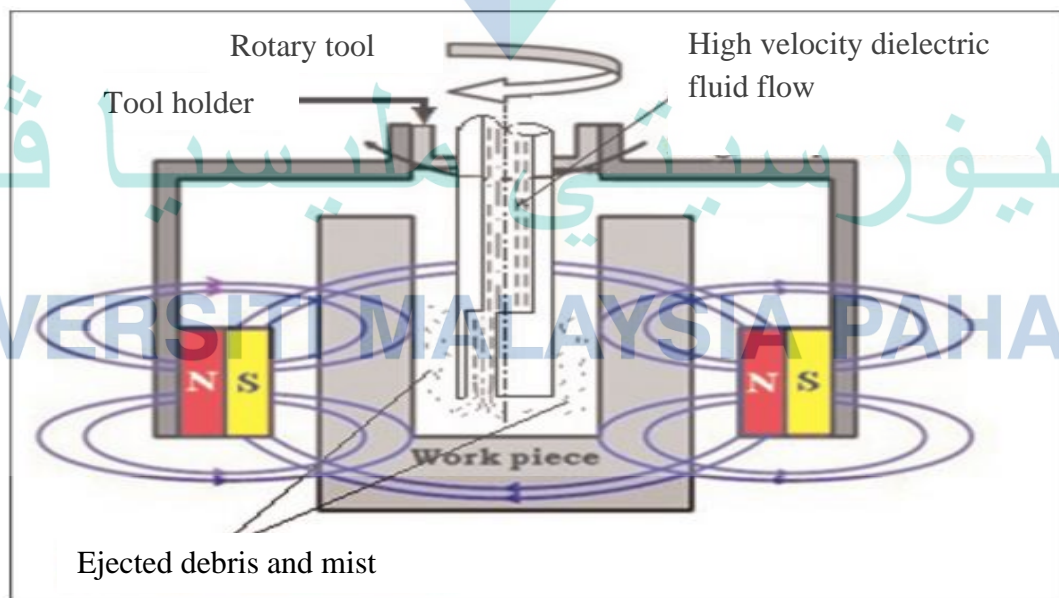


Figure 2.19 Experiment set up for MFAEDM by Gholipoor, Baseri et al. (2016)

2.3.2 Output of MFAEDM

Machining parameters are the factors that significantly influence the results of machining output. There are a few machining outputs are commonly inspected to study the effectiveness of EDM machining. The first benchmark for determining machining result efficacy is through material removal rate (MRR) comparison. Theoretically, when a magnetic innovation was developed in EDM machining area, this device reduces the probability of abnormal electrical discharge (Khan et al., 2013; Ming et al., 2020). As a result, smooth continuation of the discharge process is carried out properly and it speeds up the machining process as well as increases EDM productivity. Machining efficiency could be proved if MRR value derived from this method is higher than the conventional process. Figure 2.20 shows the research result from Lin and Lee (2008) study to support the claim that using MRR application in MFAEDM can be enhanced due to better EDM process stability. From the graph, MRR revenue from MFAEDM increases almost threefold compared to conventional EDM. On the other hand, the results of Gholipoor et al. (2016) study shown in Figure 2.21 indicates that EDM assisted by magnetic field can increase MRR value within the range of 30% to 60% compared to similar experiment without magnetic field.

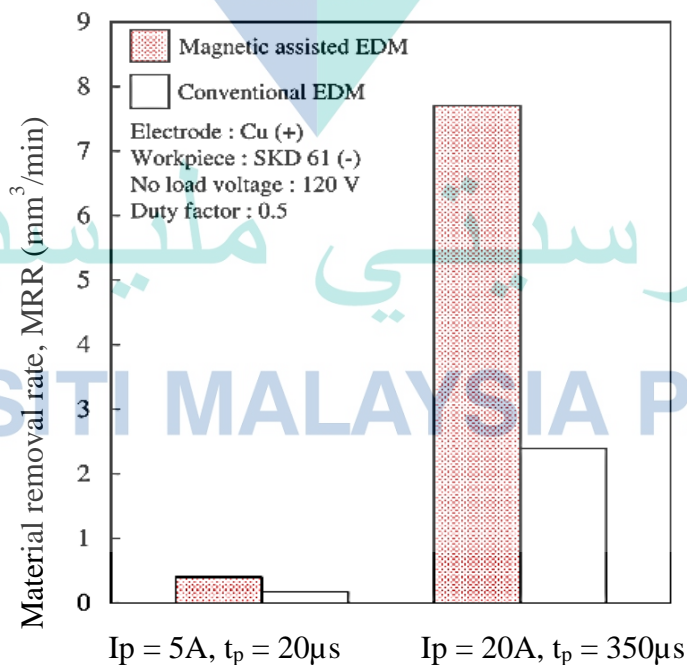


Figure 2.20 MRR for conventional EDM and MFAEDM by Lin and Lee (2008)

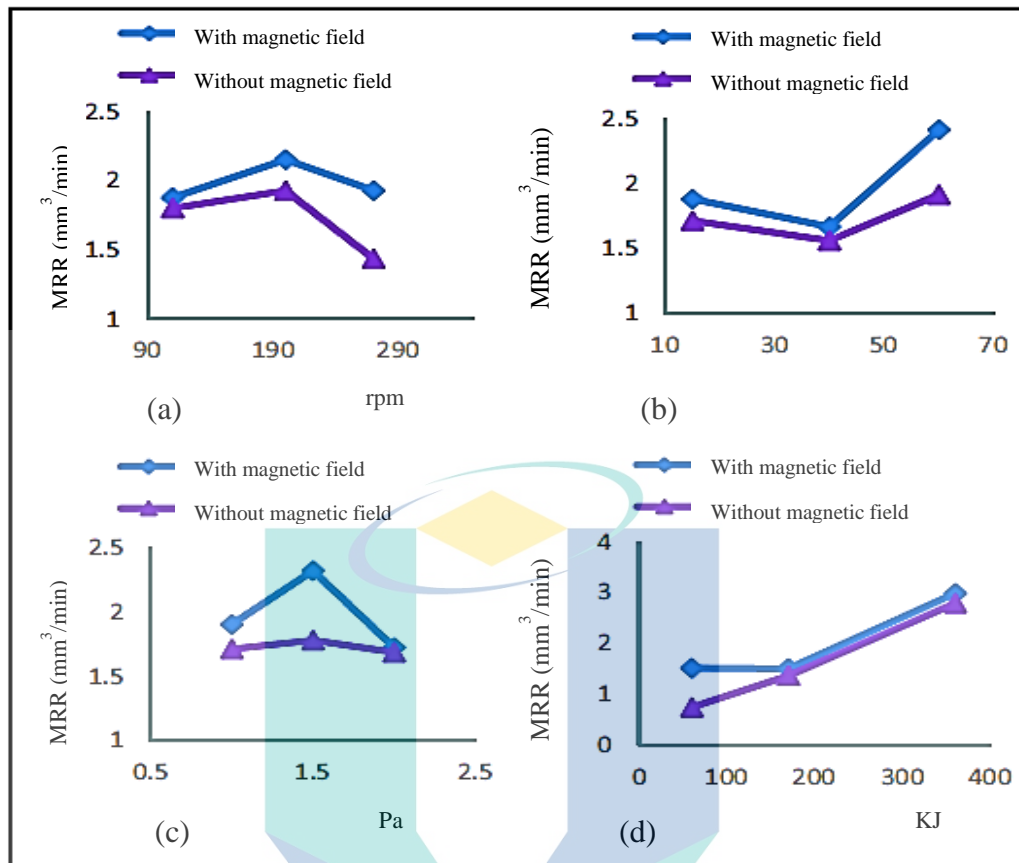


Figure 2.21 MRR from Gholipoor, Baseri et al. (2016) experiment; (a) tool rotational speed, (b) water flow rate (c) gas pressure (Pa) and (d) discharge energy (KJ)

The second most frequently discussed factor in determining EDM machining performance is electrode wear rate (EWR). Apart from the selected parameters, the wear rate is also subjected to the type of electrode used. The results from Haron, Ghani, Burhanuddin, Seong, and Swee (2008); Lin et al. (2009) show that the MRR is higher and the EWR is lower with copper electrode than graphite electrode. However, graphite is increasingly becoming the material of choice as an electrode especially for roughing process (Haron et al., 2008; Klocke, Schwade, Klink, & Veselovac, 2013). The recorded EWR values for copper base electrode were slightly higher than conventional EDM. Figure 2.22 displays that EWR obtained by MFAEDM is higher than that obtained by non-magnetic EDM process. The EWR is enhanced in the case of magnetic MFAEDM because effective ionisation improves discharge progression so the machining process can be completed in shorter time. MFAEDM mechanism is also effective in removing electrode debris in the machining zone and corroding electrode material as it erodes

specimens material. Meanwhile, the graph trend is quite different for EWR obtained using graphite for the electrode, because its value is negative as shown in Figure 2.23. This phenomenon occurs because of the added mass at the electrode. The mass is a result of the ionization process and the formation of pyrolytic carbon on the electrode surface. Thus, making it heavier than before the machining process begins.

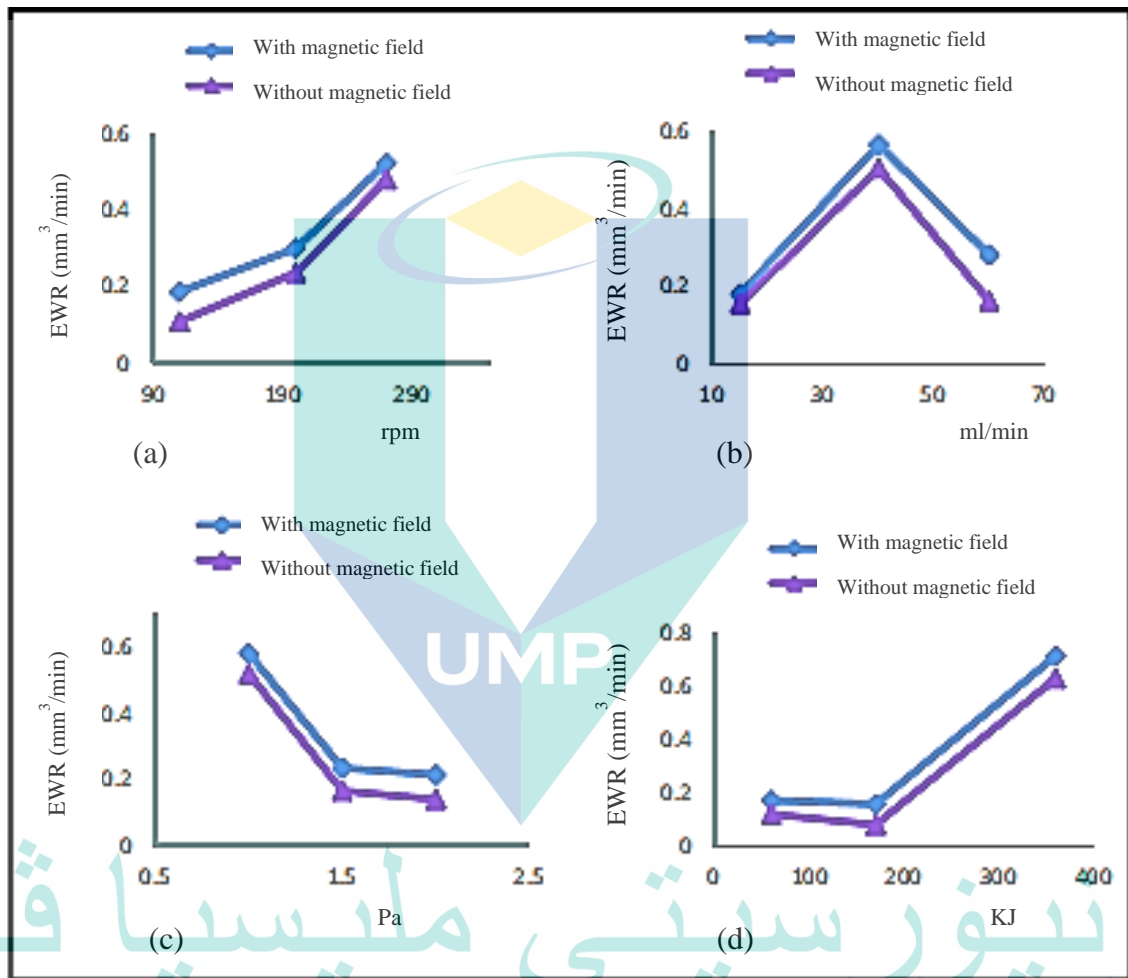


Figure 2.22 Graph of EWR result from Gholipoor, Baseri et al. (2016) MFAEDM experiment; (a) tool rotational speed (rpm), (b) water flow rate (ml/min) (c) gas pressure (KPa) and (d) discharge energy (KJ)

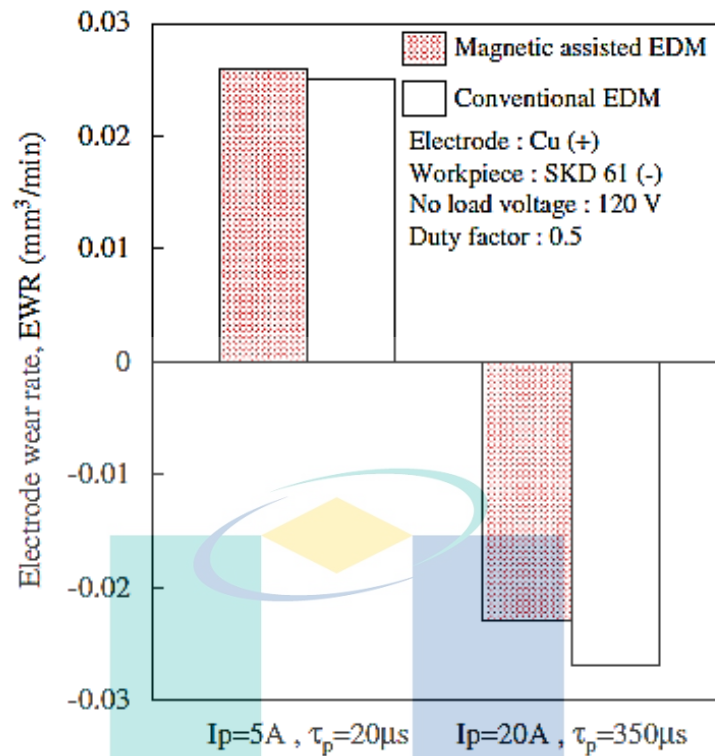


Figure 2.23 Trend of EWR using graphite electrode obtained by Lin and Lee (2008)

Another output that can be compared to determine the effectiveness of EDM is through specimen surface roughness. Figure 2.24, Figure 2.25 and Figure 2.26 show the results of surface roughness measurement for MFAEDM experiments. The figures exhibit that MFAEDM offers a clear advantage over surface roughness compared to conventional EDM. The surface roughness of MFAEDM is less than that of conventional EDM; where the average value of surface roughness are reduced from R_a 3.15 μm to 3.04 μm (Lin et al., 2009). This trend is generally due to the possibility of melting metal fragments to adhere to specimen surface. It decreases with the presence of external magnetic field. Hence, the magnetic field refines the quality of discharge spark.

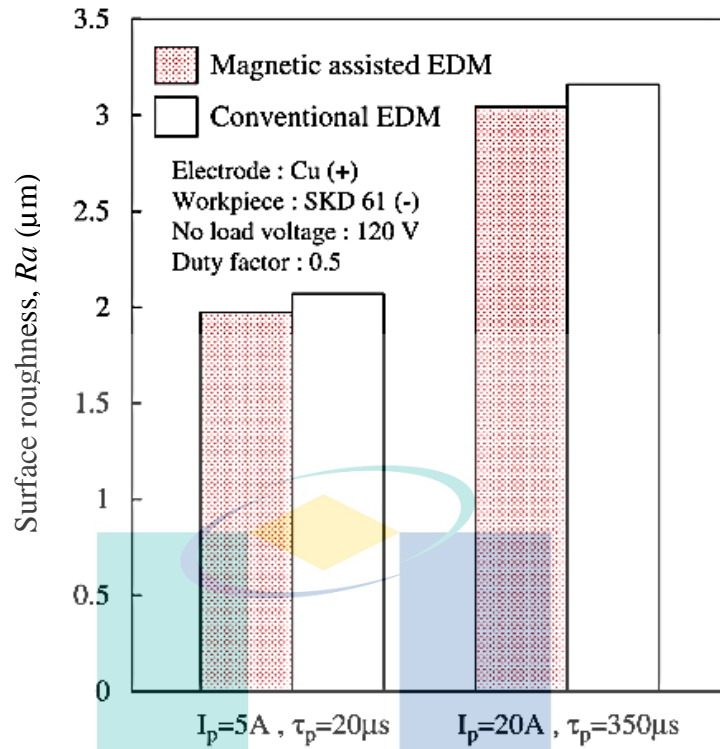


Figure 2.24 Result of surface roughness measurement by Lin and Lee (2008)

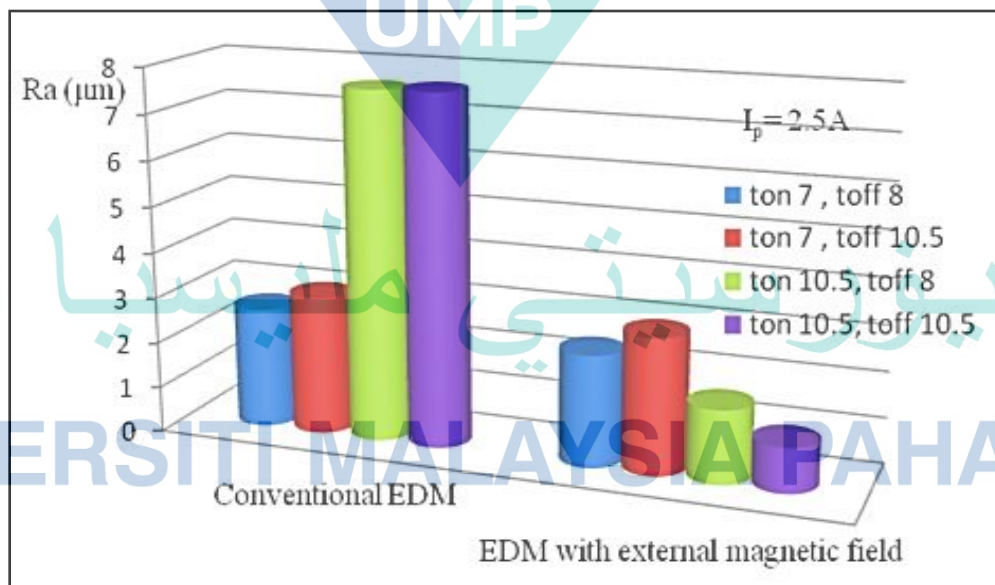


Figure 2.25 Comparison of R_a behavior at $I_p = 2.5 \text{ A}$

Source: Khan et al. (2013)

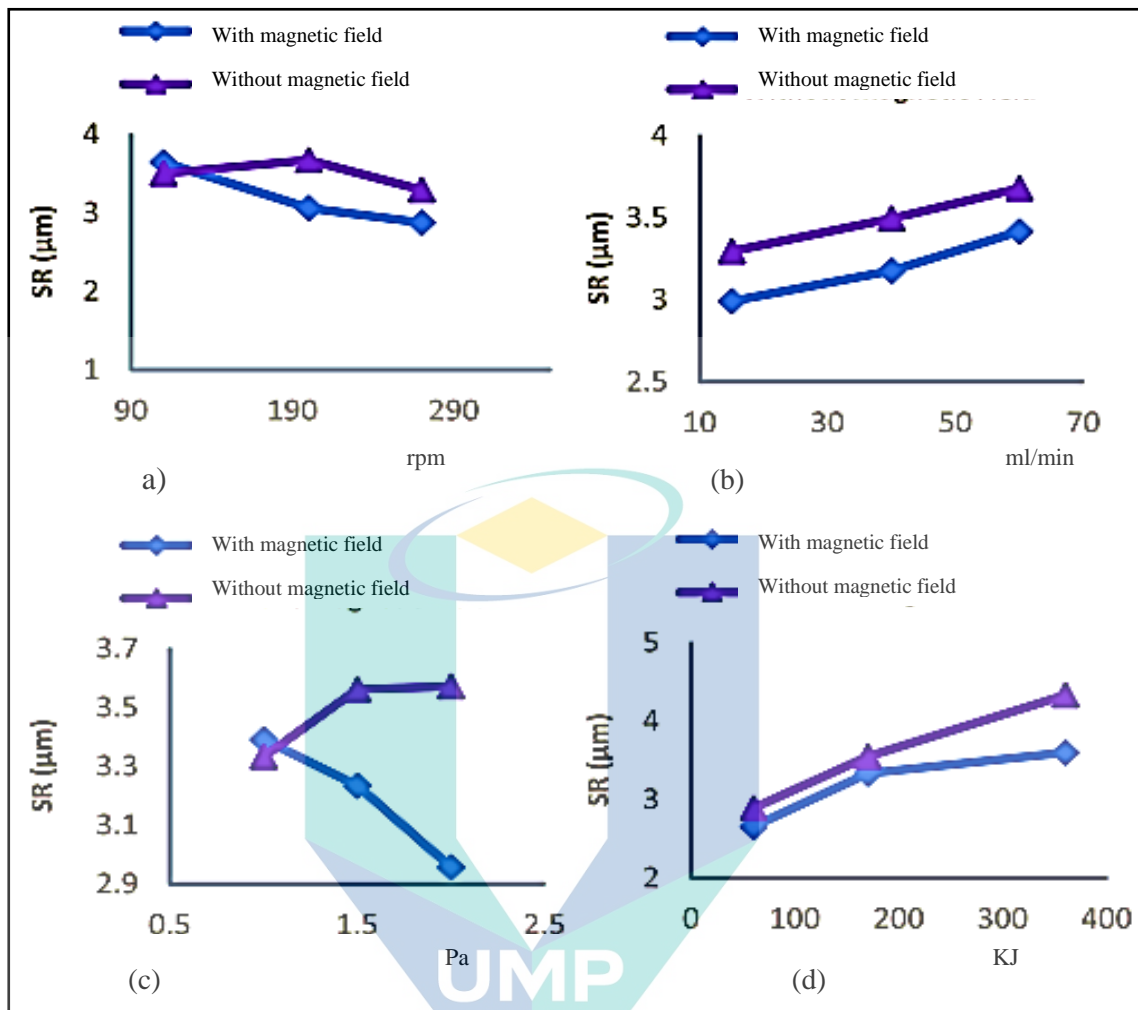


Figure 2.26 Surface roughness outcomes for MFAEDM and conventional EDM for different processing parameters, a) tool rotational speed, b) water flow rate, c) gas pressure and d) discharge energy discovered by Gholipour, Baseri et al. (2016)

The relationship of surface roughness and the peak current is evident as they are directly proportional to each other until it reaches the machining limit where the specimen surface burns out. Surface roughness is also associated with pulse time factor. Figure 2.27 shows the relationship between surface roughness and pulse time. Although surface roughness increases with rising pulse time, once it reaches its maximum value, surface roughness decreases with increasing pulse duration. When pulse duration is too long, energy density in the discharge area decreases. The eroded specimen material decreases for one pulse (t_{on}) and surface topography becomes more uniform. Therefore, surface roughness tends to decrease with longer pulse duration.

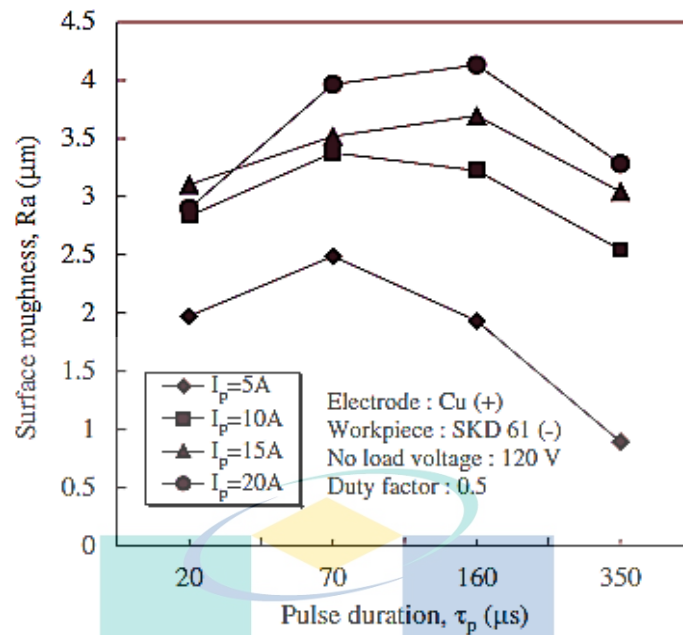


Figure 2.27 Interaction of pulse duration and surface roughness examined by Arikatla et al. (2013)

Another important topic to review on MFAEDM output is micro-crack and white layer. The layers from EDM machining can be observed in Figure 2.28 which are composed of recast layer, heat-affected zone and base metal. The severely affected layers are formed on recast layer surface from rapid heating and cooling effects caused by the discharge process based on peak current values and pulse time duration.

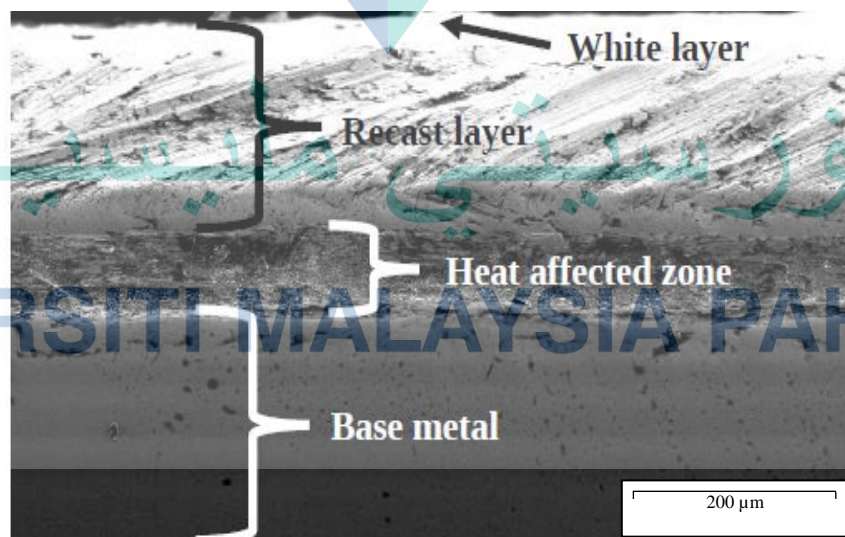


Figure 2.28 Cross-section SEM image of a metal zone in EDM revealed by Efendee et al. (2018)

The attributes of recast layer can be examined in Figure 2.9 whereby conventional EDM has more prominent and deeper craters than those by MFAEDM. Among features that can be observed on the surface of the EDM sample are splatters (Figure 2.29 (a)), long continuous lap of recast layer (Figure 2.29(b)), craters and folds as in Figure 2.29(c). Meanwhile, the second layer is heat-affected layer that makes chemical composition and carbon content of the material are different from the base material. The benefit of this process is the abrasion enhancement and erosion resistance. However, some defects could not be avoided such as micro-cracks and induced stresses. The fracture defects on these surfaces are the main concern as they lead to reduced material resistance to fatigue and corrosion (Lim, Lee, Wong, & Lu, 1991; Wong, Lim, & Lee, 1995).

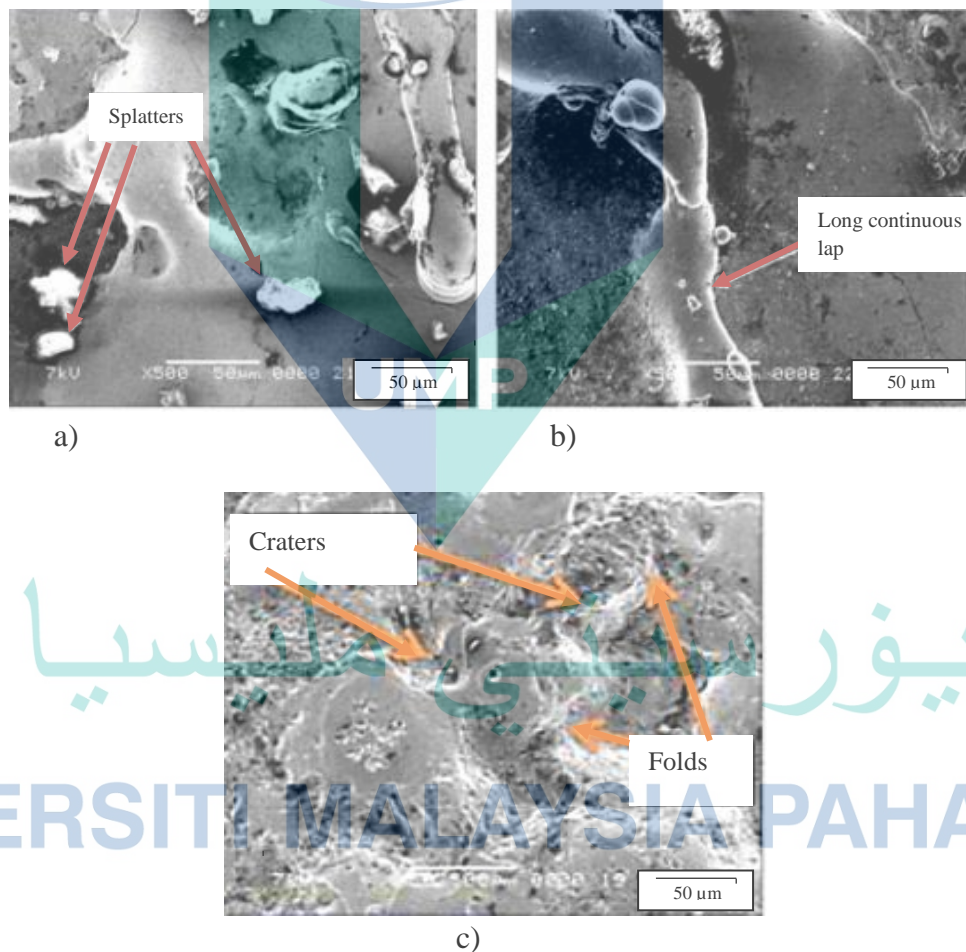


Figure 2.29 SEM observation of a) splatter, b) recast layer lap and c) craters and folds reported by Khan et al. (2013)

A study on the relationship between EDM parameters, surface cracks and white layer was investigated by Lee and Tai (2003). The study analyses MFAEDM machining characteristic on material surface of D2 and H13 tool steels. The formation of microcracks is due to carbon infiltration and more contraction in molten material than the parent material during cooling process. When surface pressure exceeds ultimate tensile strength; then, the formation of microcracking occurs (Thomson, 1989). The effect of thermal conductivity is considered as the most significant influence because the material with higher thermal conductivity has better ability to sink heat away from the heating region; thus, reducing the tendency of surface cracking. Figure 2.30 shows conventional EDM surface finish exhibits more microcracking than MFAEDM. While Figure 2.31 shows surface cracking phenomena from cross sectional view.

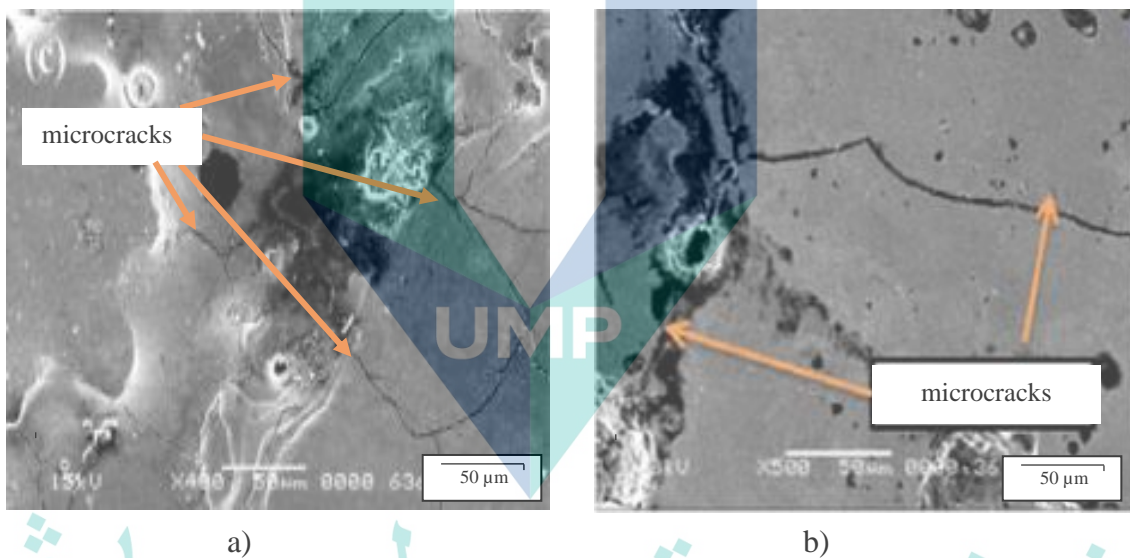


Figure 2.30 — Microcracks obtained by (a) conventional EDM and (b) MFAEDM

Source: Lin and Lee (2008)

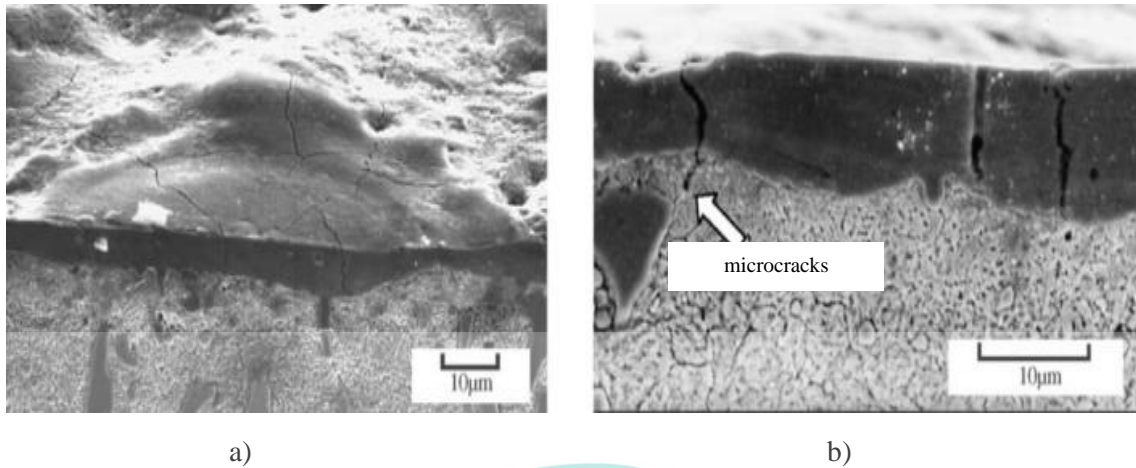


Figure 2.31 (a) Cross sectional view and (b) close up of microcracks on EDM surface
Source: Lee and Tai (2003)

Another feature formed on specimen surface after EDM machining is the white layer. This white coating is formed by molten metal that cannot be disposed by dielectric. It can be seen that pulse on duration mainly influences the white layer thickness where it increases as the pulse on duration increases (Eubank, Patel, Barruffet, & Bozkurt, 1993). As more heat is transferred into the sample, the pulse on duration also increases. Hence, the dielectric is increasingly unable to clear away the molten material so it builds up upon the sample surface. During cooling time or pulse time off, the accumulated solvent forms white coating. Its depth depends on the amount of molten material left on the sample surface during machining. Lee and Tai (2003) also indicates that the variation of white layer thickness depends on peak current value. At higher peak currents, the material removal rate is higher and formation rate of the white layer increases. Figure 2.32 shows the sample of white layers observation and this white layer is also reported to have high hardness and is difficult to etching (Lee & Tai, 2003). The formed white layer contains martensite and austenite with some dissolved carbides (Newton, Melkote, Watkins, Trejo, & Reister, 2009). The addition of carbon elements to the composition makes the white layer poses elevated hardness (Mamalis, Vosniakos, Vaxevanidis, & Prohaszka, 1987; Zinelis, 2007).

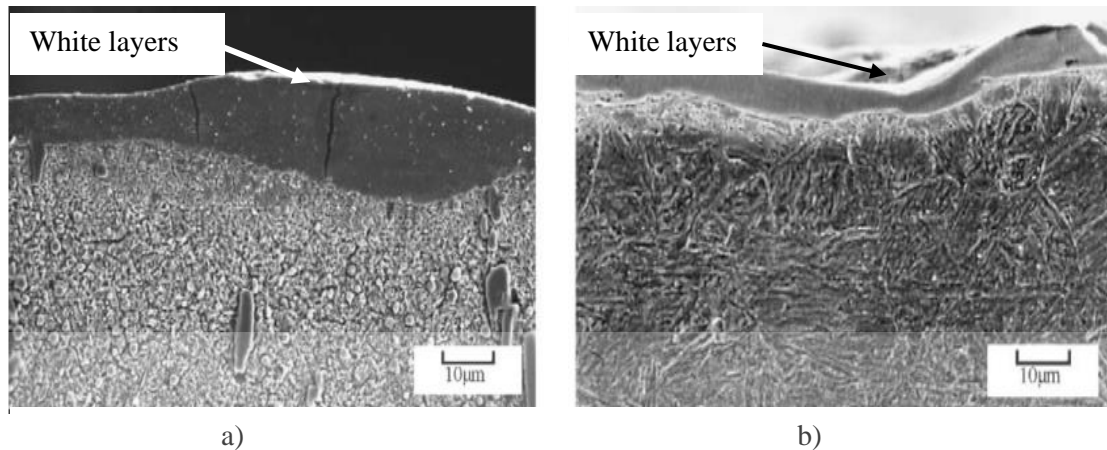


Figure 2.32 SEM photographs of (a) D2 white layer and (b) H13 white layer courtesy of Lee and Tai (2003)

2.3.3 Two-Level Factorial Design

Two-level factorial design is one of the tools in design of experiment (DOE) for analysing experimental data. It is a powerful tool that allows many factors to be examined at once. The simplest factorial design involves two factors at two levels (high level and low level). One of the problems encountered when using DOE, other than the factors to be chosen, is the degree to which it works in setting them up. The general rule is to set the level as far as possible so that the effect can be seen broadly and comprehensively; yet within the operation boundaries. Figure 2.33 shows the simplest example of two-by-two design layout compared to one-variable-at-a-time (OVAT) experiment. Factorial design offers statistically significant experimental results with minimum number of experiments but is capable of providing experimental results and comparisons. On the other hand, OVAT must replicate the run of experiment to provide comparative comparison results. The advantages of factorial design stand out as the number of factors used increases. For example, only 8 experiments are needed for three factors compared to 16 for OVAT experiment to investigate the same results (Anderson & Whitcomb, 2016).

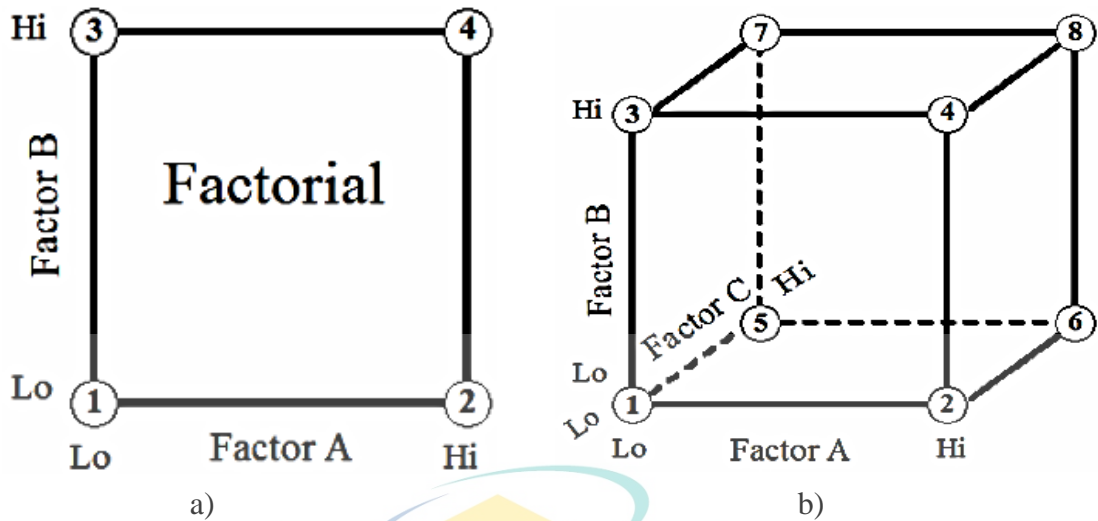


Figure 2.33 (a) One variable at a time (OVAT) versus (b) two-level factorial design
Source: Anderson and Whitcomb (2016)

Aghdeab and Mohammed (2013) states that statistical methods of factorial design help to improve operations by considering important factors and to determine the relative significant of these factors towards output response. Table 2.2 shows how EDM experiments to optimise electrode wear was designed for full factorial design on 3 level-2 level, where 9 experiments are suggested. This method also sets various combinations of factor settings to determine the best way to perform the experiments. While Table 2.3 shows the experimental design approach to study EDM parameter effects on MRR of Beryllium Copper (BeCu) using full factorial design from M. Ali et al. (2013). A two-level factorial approach was employed and the data was analysed using ANOVA to predict optimal parameter combination. The table shows that 18 experiments were required. Whilst, peak current is the most important factor affecting MRR; voltage is the least importance.

Table 2.2 Two-level factorial design by Aghdeab and Mohammed (2013)

Experiment No	Factor		Electrode Wear Weight (g)
	Current (A)	Machining Time (min)	
1	4	5	
2	4	7	
3	4	10	
4	6	7	
5	6	10	
6	6	5	
7	10	10	
8	10	5	
9	10	7	

Table 2.3 Two-level factorial design to investigate EDM on beryllium copper from M. Ali et al. (2013) experiment.

Run	Factor A Peak Current (A)	Factor B Machine Voltage (V)	Factor C Pulse on Time (µs)	Factor D Pulse off Time (µs)
1	17.5	27.5	102.5	155
2	5	10	200	10
3	30	10	5	10
4	17.5	27.5	102.5	155
5	5	10	5	10
6	30	10	5	300
7	5	10	200	300
8	30	45	200	300
9	30	45	200	10
10	30	10	200	300
11	30	45	5	300
12	5	45	200	10
13	30	45	5	10
14	30	10	200	10
15	5	45	5	300
16	5	10	5	300
17	5	45	5	10
18	5	45	200	300

2.4 Summary

The electric discharge machine has unique capabilities such as machinable hard material, high accuracy and good surface finish as well as no cutting forces involved. However, EDM has several limitations including limited process for electrical conductive materials, slow machining process for excellent surface finish and heat affected zone near the cutting edges. The introduction of magnetic field has important practical values for EDM enhancement. This discharge process has parameters that need to be set up properly. Nevertheless, the input depends on the EDM machine controller which may come from Mitsubishi, Soddiq or Agie Charmiles which makes the process is much broader to discover. The use of magnetic fields by manipulating EDM machining parameters such as peak current (I_p), pulse time, load voltage (V) and voltage servo reference (S_v) indicates that MFAEDM has positive effects and electrode material thermal conductivity should not be neglected. Apart from that, this magnetic field contributes to machining debris removal by extracting excess metal particles from the magnetic material. Application of magnetic field in EDM machine set up has purified the machining process and creates an intensely concentrated discharge spark. The benefits of MFAEDM can be justified from the calculation of MRR and EWR, analysis of discharge waveforms and micrograph observation of surface integrity. Material removal rates, electrode wear rate, surface roughness and surface integrity were analysed through MFAEDM modification. Nonetheless, no reports have been made regarding the effect of MFAEDM magnetic field polarity.

اونيورسيتي ملايسيا فھڻ

UNIVERSITI MALAYSIA PAHANG

CHAPTER 3

METHODOLOGY

3.1 Introduction

This chapter describes the research methodology focusing on electric discharge machining (EDM) equipment and experimental set up to conduct this study. The chapter describes the research approach, research process, methods of data collection, type of data analysis and research limitations of the study. Figure 3.1 shows the overall outline plan for the research methodology to achieve the objectives of the study. There are two divisions of experiment namely conventional EDM and MFAEDM where the results of both will be analysed to compare the output. Charmilles EDM die sinking machine is the main equipment used in this study to machine AISI 420 mod tool steel as the specimen material. Full factorial design experiment was employed in this research, a tool that allows simultaneous experiments on many factors. A series of data collections was collected from this experimental approach to justify the hypothesis and establish the discovery. Specific EDM machine parameters were set as shown in Table 3.1 to create applicable cutting condition for the experiment.

اونيورسيتي ملايسيا قهغ

UNIVERSITI MALAYSIA PAHANG

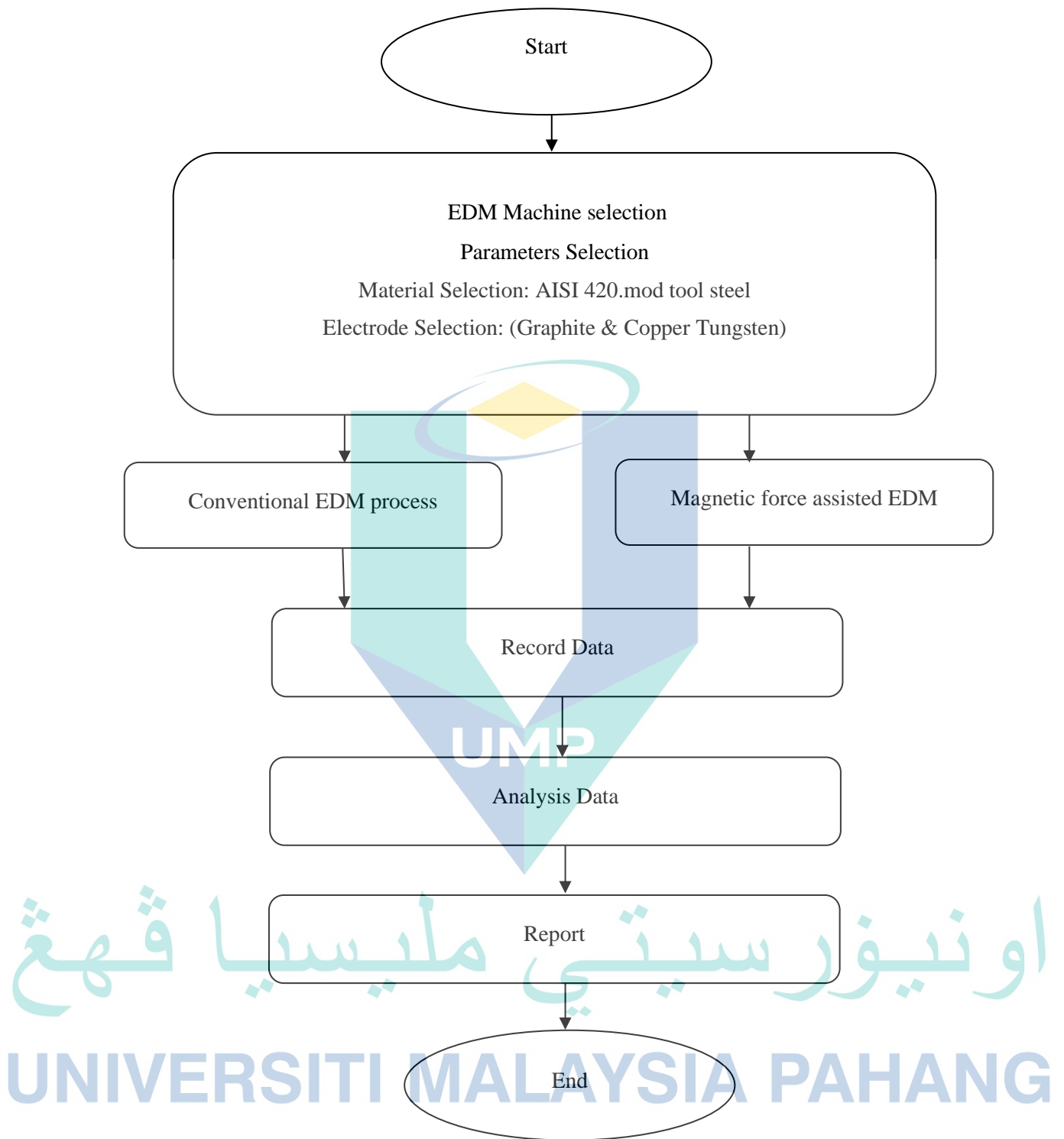


Figure 3.1 Overall research outline to achieve research objectives

Table 3.1 Experiment parameters set up

Working conditions	Descriptions
Work piece	AISI 420.mod (30 mm × 30 mm × 15 mm)
Electrode	Graphite, Copper tungsten (Ø 25 mm x 40 mm)
Magnet polarity combination	North-South, North-North
Magnetic flux density	0 T, 0.54 T
Peak current	8 A, 24 A
Pulse duration	50 µs, 100 µs
Dielectric fluid	Kerosene
Depth of cut	2 mm

3.2 Research Process and Equipment

One of the unique features of EDM is that the machining technique is not influenced by material hardness; but by electrode electrical conductivity and sample material. Therefore, the material removal process can be subjected to various types of metal that are electrically conductive materials such as metal, alloys, carbides, graphite or any other content regardless of their hardness. In general, the research methodology for this study is simplified as shown in Figure 3.2. There is a preliminary experiment in this study because to determine the range parameters that are appropriate to the research trend and the capabilities of the EDM machine used. As well as to choose the right type of electrode. Figure 3.3 shows the main equipment used in this study to remove material from the workpiece. This Charmilles Roboform22 is a high-precision die-sinking EDM for metal removal by thermal energy to erode the workpiece. Specification of the machine is shown in Table 3.2. Basically, in EDM, dielectric fluid is required in the container to help initiate the sparking process. Besides that, the dielectric fluid in the form of kerosene liquid serves as an insulator between the tool and the workpiece. It flushes away the metal particles to prevent shorting and acts as coolant. Graphite and copper tungsten electrodes which are electrically conductive material are utilized as shown in Figure 3.4. Cylindrical electrode of graphite and copper tungsten in dimension of 40 mm x Ø 25 mm was prepared because of its high melting point, good conductor and high machinability characteristics. Table 3.3 shows physical properties of the graphite and copper tungsten electrode. The preliminary experiment uses both electrodes, but for the main experiment only graphite

electrode is used to make the comparison of the machining effect between conventional EDM and MFAEDM.

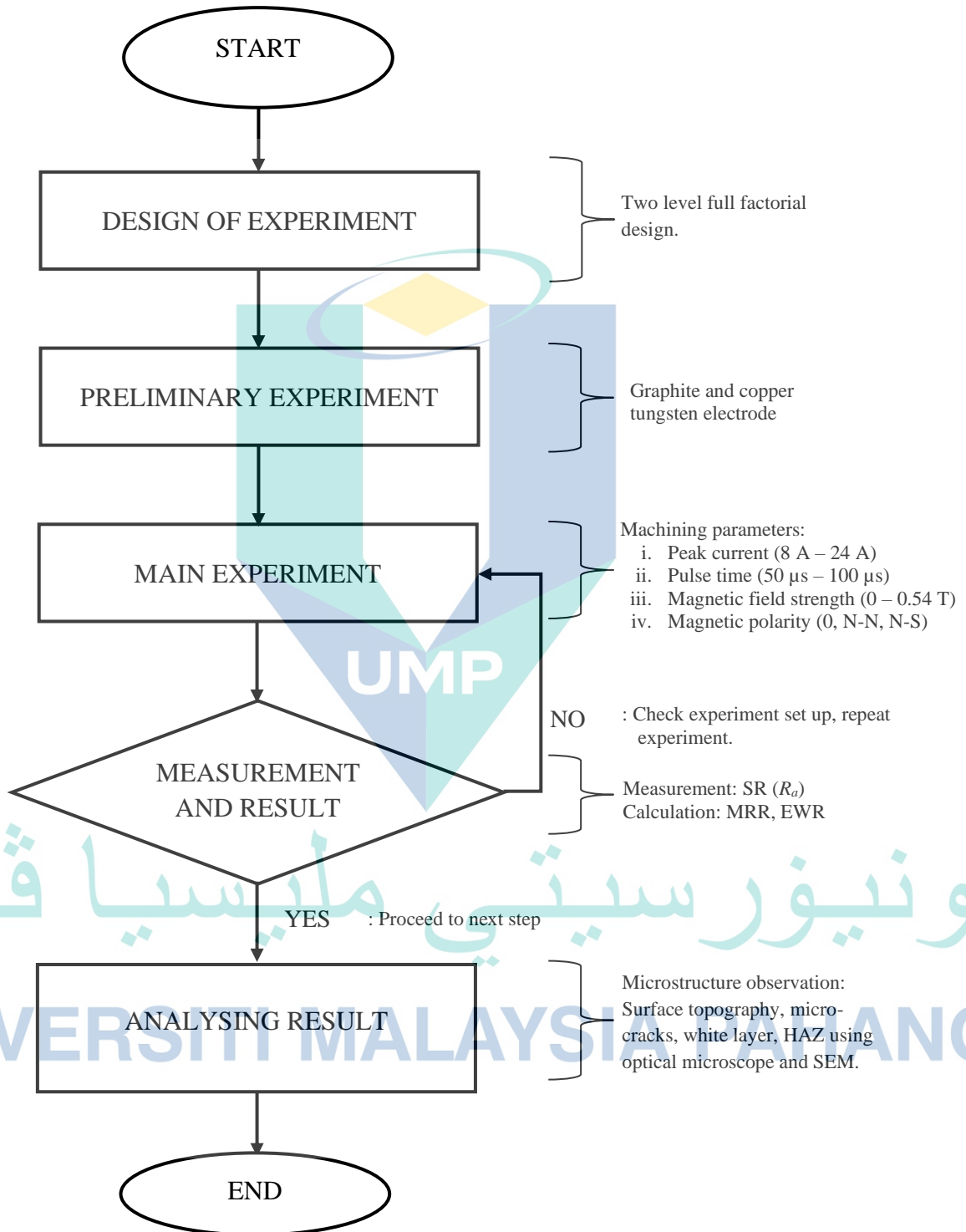


Figure 3.2 Flow chart of experiment methodology



Figure 3.3 Charmilles Roboform EDM

Table 3.2 Charmilles Roboform EDM specification

Element	Description
Max. distance table to sleeve	145/405 mm
Max . electrode weight	10 Kg
Working vessel length inside	760 mm
X-axis traverse	330 mm
Y-axis traverse	270 mm
Dielectric aggregate	H 500 mm × W 850 mm × D 1084 mm



Figure 3.4 a) Graphite electrode and b) copper tungsten electrode

Table 3.3 Properties of graphite and copper tungsten electrode

Physical properties	Graphite	Copper tungsten
Electrical resistivity ($\mu\Omega$ cm)	14	3.83
Thermal conductivity (W/mK)	160	238
Melting temperature ($^{\circ}\text{C}$)	3675	3410
Density (g/cm ³)	1.811	14.84
Coefficient of thermal expansion ($1/^{\circ}\text{C}$)	7.8×10^{-6}	10.2×10^{-6}

Source: Pavan and Sateesh (2020)

This study involves data analysis received from AISI 420.mod where machining time, specimen mass before and after the machining process are crucial for determining material removal rate analysis. The element properties of AISI 420.mod tool steel are summarized in Table 3.4. The collected measurements were utilized to compare the performance of conventional EDM process and magnetic field-assisted EDM. Apart from that, to achieve the novelty of this research, the machining process was repeated for both combinations of magnetic polarity (N-N and N-S). These raw specimens were machined into 30 mm (length) x 30 mm (width) x 15 mm (thickness) as illustrated in Figure 3.5. AISI 420.mod is a tool steel manufactured through metallurgical cold work powder. This tool steel is commonly used to produce durable and high-performance press tool because of its high wear resistance, corrosion resistance and excellent surface finish compared to standard AISI 420. Other than that, the material has dimensional stability after hardening and tempering which is much better than the other all known high-performance cold-work tool steels. This material was selected for the samples to prove the suggested technique is applicable for tool and die industry.

Table 3.4 Chemical composition of AISI 420.mod tool steel

Component Element Properties	Metric
Carbon, C	0.38%
Chromium, Cr	13.60%
Manganese, Mn	0.50%
Iron, Fe	85.22%
Vanadium, V	0.30%

Source: ASSAB Group (2020) *STAVAX ESR*. Retrieved from <https://www.assab.com/>

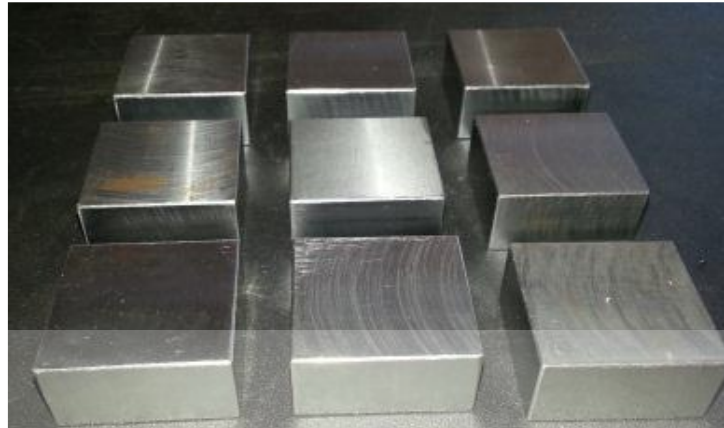


Figure 3.5 Stavax ESR specimens

A pair of permanent magnetic bars was placed into the machining area to create repulsive or attractive magnetic field line action during EDM machining as shown in Figure 3.6. This permanent magnet has 0.54 Tesla magnetic field strength. The specimen and these magnetic bars were clamped together with 2mm aluminium spacer between them using a fixture as illustrated in Figure 3.7 which was specially fabricated for this experiment. Firstly, the experiments were carried out in normal condition to produce the datum result, which was noted in conventional EDM. Other two EDM methods were run under magnetic field influence where the sparks were directed in between a pair of permanent magnets. In one condition, the permanent magnets were clamped in between Stavax ESR sample so that the same pole faced each other (N-N) to achieve repulsive magnetic field between both. Then, magnetic devices were arranged in different polarity (N-S) to create attractive magnetic field between them.



Figure 3.6 Permanent magnet (0.54 Tesla)



Figure 3.7 Fixture used for clamping specimen and magnetic bars

After the accomplishment of each sample machining, the workpiece was cleaned from dust and fluid using air gun to minimise experiment error. The work also required mathematical solution to be developed to gauge the EDM machining output such as machining time, electrode mass wear, metal removal rate and the average of surface roughness measurements. The result from the analysis determined if MFAEDM was the better technique for EDM process or vice versa.

3.3 Method of Data Collection

Apart from optical images observation as the evidence of machining output improvement, data obtained through EDM machining and specimen measurement were analysed using Design-Expert software. Table 3.5 below shows complete design of the experiment for conventional EDM and MFAEDM machining. The experiment was run thoroughly as suggested in the design experiment software. Full factorial of 2 level format used in this design experiment is enough to compliment the main objective to study the effect of magnetic polarity in magnetic field-assisted EDM. Two-level factorial designs are considered an excellent gear for screening factors because they are incredibly efficient and produce maximum information with minimum experiment as suggested by Anderson and Whitcomb (2016).

Before running the experiment, the electrode and workpiece were shaped according to the designated dimension. Whilst, lathe machine was used to machine the electrode; conventional milling machine was used to machine the materials. Permanent magnet was applied and placed around the electrode as well as workpiece to carry out the experiment. In MFAEDM experiments, permanent magnets were clamped side by side to AISI 420.mod workpiece so that the selected pole faced each other to yield either repulsive or attractive magnetic field between them. Then, MFAEDM operation was conducted in which the sparks occur in the spark gap within the magnetic field. MFAEDM set up is illustrated in Figure 3.8.

Table 3.5 Design of MFAEDM experiment

Run	Factor 1 Peak Current (A)	Factor 2 Pulse Time (μ s)	Factor 3 Magnetic Strength (T)	Factor 4 Magnet Polarity
1	8	100	0	N-N
2	24	50	0	N-N
3	24	100	0	N-N
4	8	50	0.54	N-N
5	8	100	0.54	N-S
6	8	100	0	N-S
7	8	100	0.54	N-N
8	24	100	0	N-S
9	24	100	0.54	N-S
10	24	100	0.54	N-N
11	24	50	0.54	N-S
12	8	50	0	N-N
13	24	50	0	N-S
14	24	50	0.54	N-N
15	8	50	0.54	N-S
16	8	50	0	N-S

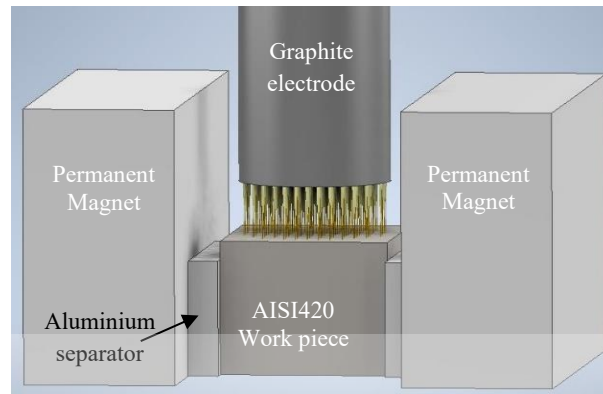


Figure 3.8 Illustration of magnetic field-assisted EDM arrangement

The machining time was collected by referring to recorded machining time on EDM machine screen panel. Then, the eroded electrode mass and machining time were used to analyse electrode wear rate (EWR). Meanwhile, the eroded sample mass per machining time was used to determine material removal rate (MRR). Figure 3.9 shows an example of machined specimen as to illustrate its surface condition after EDM machining (Run no.6).



Figure 3.9 AISI 420.mod tool steel sample after EDM machining

Precise electronic balance was utilized to measure the mass eroded from workpiece sample. The masses before and after machining were measured in gram using electronic balance YS Series Balance as shown in Figure 3.10. Similar procedure was employed to measure the mass from graphite electrode. Particular mass measurements were recorded accordingly and were divided by machining time to determine its MRR and EWR. Once the experiments were completed, sample surface roughness was measured by using surface roughness measuring device (SURFPAK) *SJ-301* which is stylus type surface roughness measuring system that has diverse high-precision function

feature for ease of operation. Surface roughness data was taken for four times and average data was calculated. Figure 3.11 shows the activities of surface roughness measurement.



Figure 3.10 Electronic balance device used to weigh the electrode and samples



Figure 3.11 Surface roughness measurement in progress

Surface topography of the samples was further examined using an optical microscope and related images were captured. Those samples then were sectioned and well polished as preparation for cross-section observation under the scanning electron microscope (SEM). Figure 3.12 shows the samples are ready for etching process before undergo for scanning electron microscope (SEM) observation. Figure 3.13 illustrates the equipment used for capturing sample images. The detail surface state and cross-sectional view were observed under SEM to justify the result of the surface roughness.

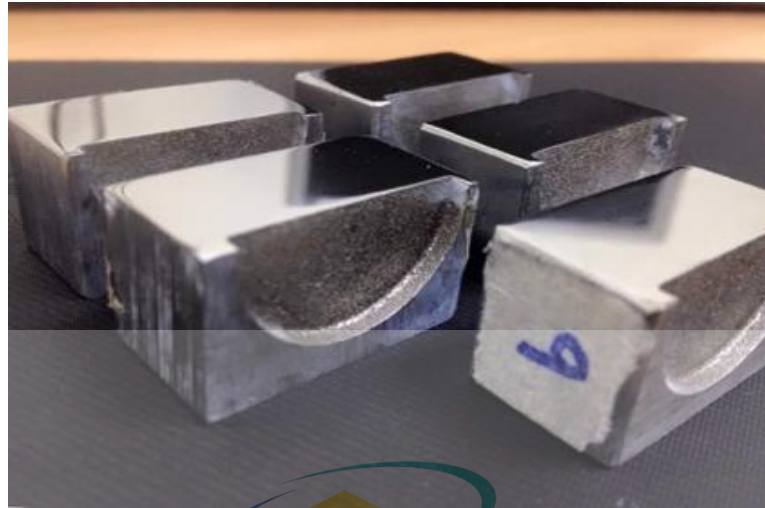
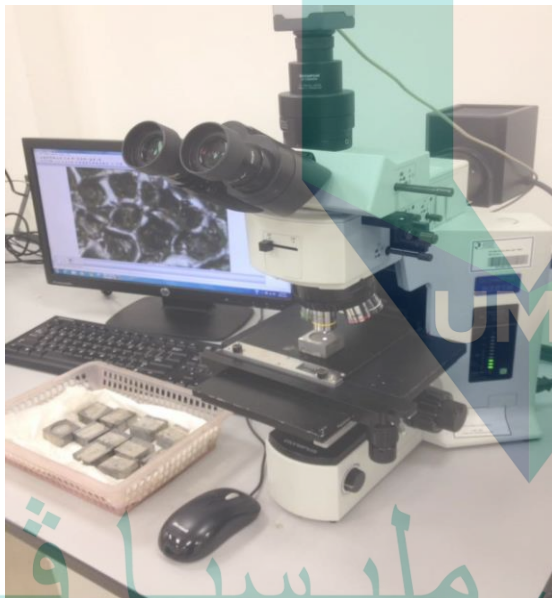
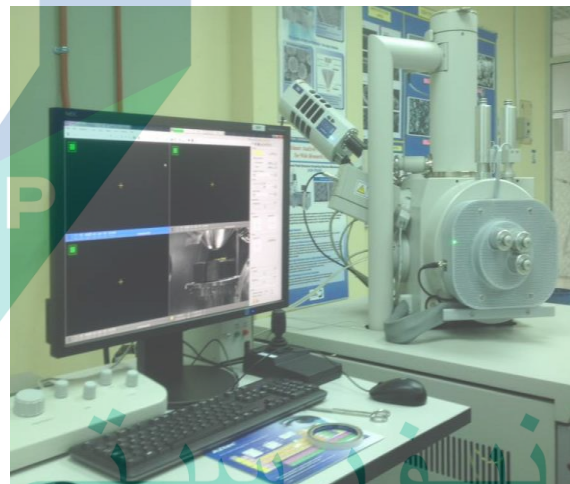


Figure 3.12 Sectioned and polished samples of AISI 420.mod



(a)



(b)

Figure 3.13 (a) Optical microscope and (b) scanning electron microscope

UNIVERSITI MALAYSIA PAHANG

3.4 Analysis of Machining Time

It is a term used when material removal process is performed to parent material using a particular machine by machinist. The time required to complete work order is closely related to material removal. In industrial production, machining time is vital in order to meet product demand within restricted time. In EDM process, low peak current

produces low spark intensity so it takes more time to complete the work. If higher peak current value is applied for sparking process, the completion time is reduced; but surface quality is certainly rougher. The machining time was recorded based on the time displayed on the EDM screen panel.

3.5 Analysis of Material Removal Rate (MRR)

One of the factors that can be employed to determine the effectiveness of machining process is MRR. When forecasting MRR, many factors need to be considered in machine operation to ensure the results produced are in good working order and has high productivity. An essential element in finding MRR is machining time. The selection of peak current used majorly contributes to the machining time; but it affects surface condition resultant. Moreover, the choice of tool material is also added to MRR valuation. Material removal rate (MRR) value for this study was calculated by using a formula shown in Equation 3.1.

$$\text{MRR} = \frac{\text{Mass of Material Removed from Part}}{\text{Time of Machining}} \quad (\text{g/min}) \quad 3.1$$

The cutting depth for the experiment was set at 2mm and the machining process was performed according to the parameters specified for each specimen. The mass of material was weighed before the EDM machining process began. Upon completion of machining, the specimen was weighed and material removal rate was calculated by comparing the weight of the workpiece before and after machining. The weight of the specimen was measured with the help of a digital weighing machine. The amount of weight that has been removed was divided by the recorded machining time.

3.6 Analysis of Electrode Wear Rate (EWR)

The electrode erosion can measure EDM machining efficiency. Improper material selection for the electrode used in EDM machining process reduces product accuracy due to the electrode wear features. Therefore, studying electrode wear rate (EWR) is useful to investigate ways to improve EDM productivity and process reliability. Ideal EWR on particular EDM process gives minimum EWR value which shows low volume of material

are disposed from the electrode for specific machining time. The formula to calculate EWR is shown in Equation 3.2.

$$\text{EWR} = \frac{\text{Mass of Material Removed from Electrode (g/min)}}{\text{Time of Machining}} \quad 3.2$$

The EWR value was determined by obtaining the electrode weight difference before and after EDM machining. Therefore, the mass of the electrode was weighed before the start of machining using digital weighing machine. This electrode was again weighed after the EDM machining was completed. The amount of corroded electrode mass was then divided by the time of machining to obtain the EWR value.

3.7 Analysis of Surface Roughness (R_a)

After the experiments were complete, it was necessary to observe and obtain surface information of each machining condition. This process can be performed using surface roughness gauge (SURFPACK SV-514). It is a stylus type of surface roughness measuring machine that has high precision features for easy and smooth measurement operation. It has an integrated drive unit that can achieve high degree straightness to check surface roughness texture. Information from surface irregularities in surface samples were used to evaluate the output of MFAEDM process. Four different positions were selected to examine surface roughness as illustrated in Figure 3.14.

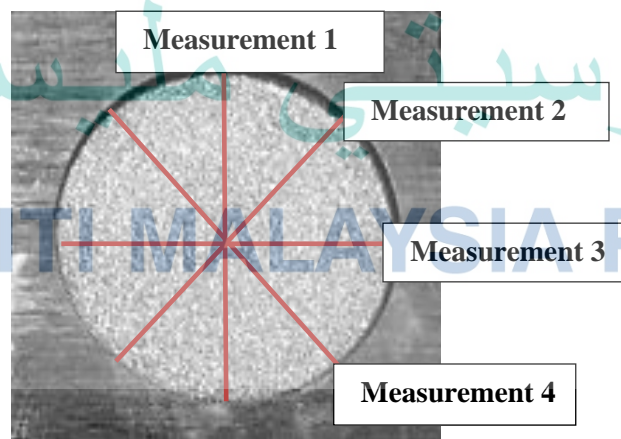
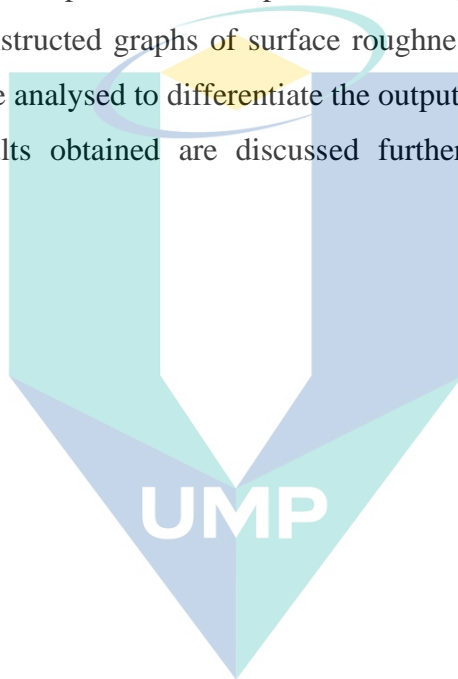


Figure 3.14 Surface roughness measurement methods

3.8 Summary

In conducting the experiments, machining consistency is vital to obtain acceptable results. Among the factors that must be emphasised in this test are machining parameters the constant size of graphite electrode. Conventional EDM experiments are aimed at obtaining datum results as the basis for comparing MFAEDM output at different polarity combination. Conventional EDM and MFAEDM experiments were performed under such experimental procedures. Afterwards, the machined samples were measured and observed under high magnification optical microscope and scanning electron microscopy (SEM). Subsequently, the constructed graphs of surface roughness (SR), MRR and EWR, and SEM observation were analysed to differentiate the outputs from conventional EDM and MFAEDM. The results obtained are discussed further in Chapter 4; Results and discussions.



اونيورسيتي ملايسيا قهغ

UNIVERSITI MALAYSIA PAHANG

CHAPTER 4

RESULTS AND DISCUSSION

4.1 Introduction

Chapter 4 generally discusses the results obtained throughout the experimental research activities. All data during EDM-machining was tabulated and analysis was carried out to demonstrate the necessary responses. Experiment outcomes such as material removal rate (MRR), electrode wear rate (EWR) and surface roughness (SR) were obtained so that responses from conventional EDM and magnetic field-assisted EDM were compared. In this experiment, mass of electrode and work piece material were weighed accordingly for further reflexion. Its material and machining time were recorded to determine material removal rate (MRR). The purpose is to determine electrode wear rate (EWR). Surface of EDM machined samples underwent surface roughness measurement and microscopic observation. Results from surface roughness measurement, image observation via scanning electron microscope and MRR as well as EWR calculations are essential for analysing the effect of different magnetic polarity on EDM spark.

4.2 Preliminary Experiment of MFAEDM

Even though, positive impacts of MFAEDM application are well discussed in the literature, experiments on the effects of magnetic polarity arrangement in MFAEDM study are still lacking. Therefore, the study was proposed and experiments were conducted to determine the effects. An initial set of experiments was performed to investigate appropriate parameter setting before the study was carried out. This action was taken to ensure that parameter range did not exceed machining boundaries and corresponds to EDM machine capacity. Two types of electrodes were tested to observe performance differences. Consequently, one of them was selected as the electrode for research purposes. DF3 tool steel (AISI O1) was employed as trail specimen because it

was a cheaper option. The outcomes of these preliminary experiments for MFAEDM using graphite and copper tungsten electrodes are shown in Table 4.1 and Table 4.2 respectively. Both results suggest that material removal rate (MRR) increases when peak current increases. It is important to note that MRR further increases when magnetic field (0.54 T) was introduced as shown in Figure 4.1 and Figure 4.2.

Table 4.1 Preliminary experiments of conventional EDM and MFAEDM using graphite electrode

Parameters	Conventional EDM			MFAEDM (N-N)		
	1	2	3	1	2	3
Peak current (I_p)(A)	6	9	12	6	9	12
Machining Time (min)	270.33	213.50	194.63	244.25	203.37	190.40
MRR (g/min)	0.020	0.025	0.028	0.022	0.026	0.029
Electrode Wear Rate (EW) (g/min)	-0.00009	-0.00013	-0.00014	-0.00005	-0.00007	-0.00006
Electrode Wear Ratio (EWR) (%)	-9.136	-10.135	-9.386	-4.425	-5.282	-4.354
Mean Surface roughness (R_a , μm)	2.39	3.03	3.73	2.26	2.82	3.41

Table 4.2 Preliminary experiments of conventional EDM and MFAEDM using copper tungsten electrode

Parameters	Conventional EDM			MFAEDM (N-N)		
	1	2	3	1	2	3
Peak current (I_p)(A)	6	9	12	6	9	12
Machining Time (min)	204.12	167.15	78.48	192.33	125.37	68.17
MRR (g/min)	0.020	0.024	0.052	0.021	0.032	0.059
Electrode Wear Rate (EW) (g/min)	0.00119	0.00139	0.00032	0.00092	0.00082	0.00023
Electrode Wear Ratio (EWR) (%)	6.020	5.988	0.616	4.383	2.541	0.383
Mean Surface roughness (R_a , μm)	4.18	5.23	5.56	3.87	4.7	4.76

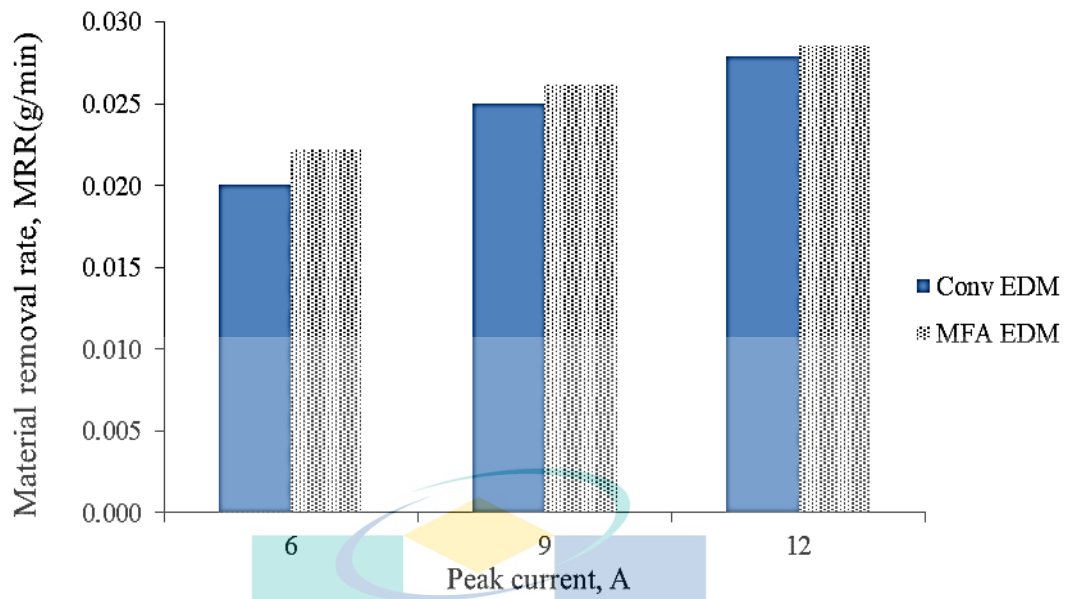


Figure 4.1 Comparison of MRR between conventional EDM and MFAEDM using graphite electrode

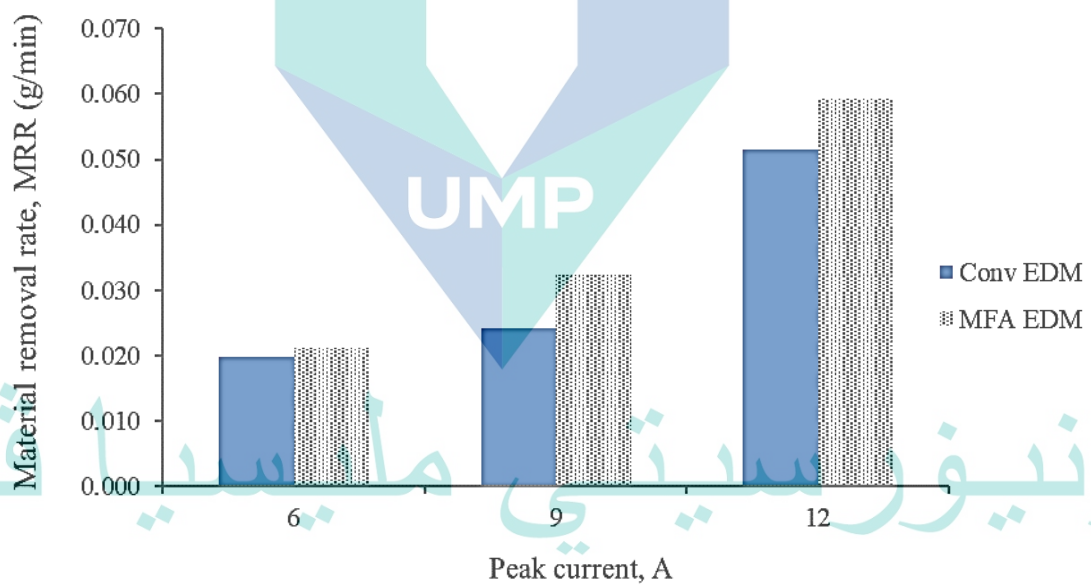


Figure 4.2 Comparison of MRR between conventional EDM and MFAEDM using copper tungsten electrode

Observations of surface roughness indicate that these two electrodes produced similar trends; whereby R_a increased as peak current value increased. The measured R_a values were even lower when MFAEDM was used in the EDM system as shown in

Figure 4.3 and Figure 4.4. However, the machining performance of graphite electrode provided lower R_a value than that produced by tungsten copper electrode. Thus, due to its lower surface roughness, lower material cost and negative EWR value, graphite electrode was more suitable to be employed in the study.

Beyond this encouraging effect of MFAEDM, another question was raised. What happens if magnetic polarity or magnetic field strength changes? So, another preliminary experiment for magnetic polarity effect on MFAEDM was conducted to investigate any possible significant effect and the result is illustrated in Figure 4.5. The figure compares MRR for different magnetic polarity in MFAEDM. Plot from the graph suggests that attractive magnetic field (N-S) formation has superior effect than repulsive magnetic field on EDM at 5.5 A which is interesting to explore in detail.

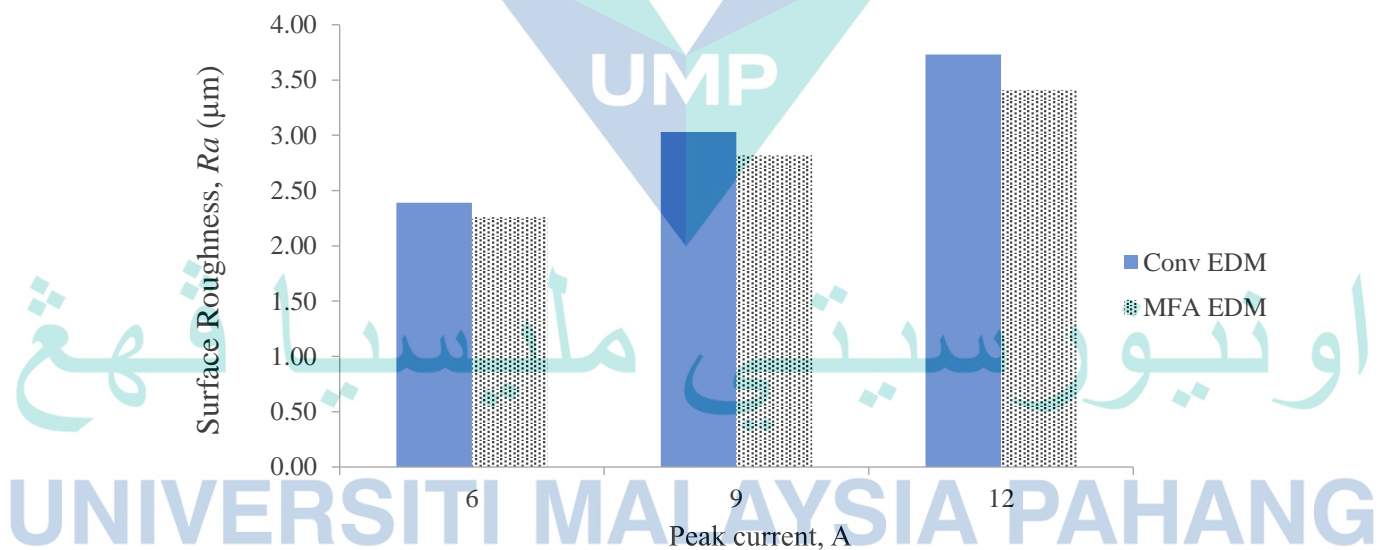


Figure 4.3 Illustration of SR between conventional EDM and MFAEDM at different peak current using graphite electrode

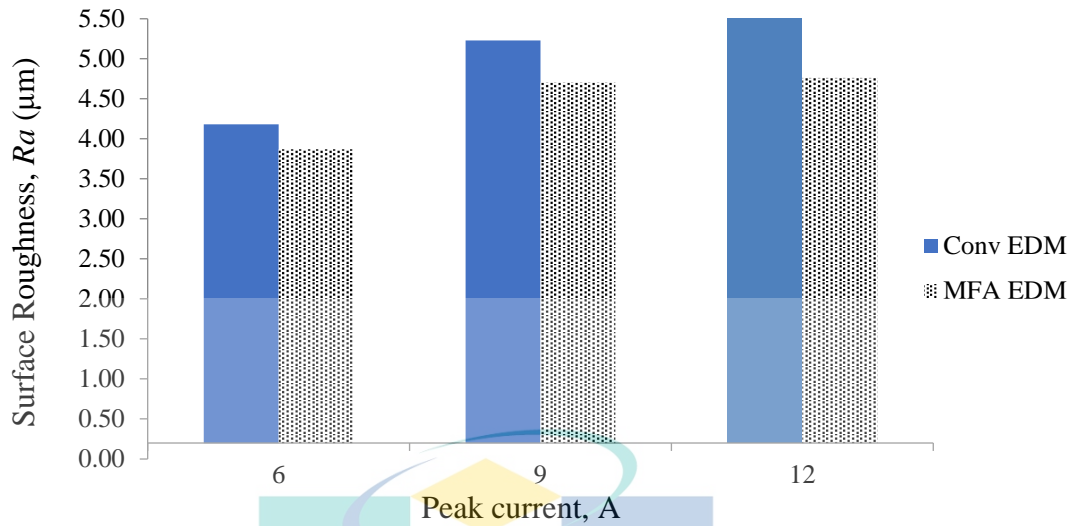


Figure 4.4 Illustration of SR between conventional EDM and MFAEDM at different peak current using copper tungsten electrode

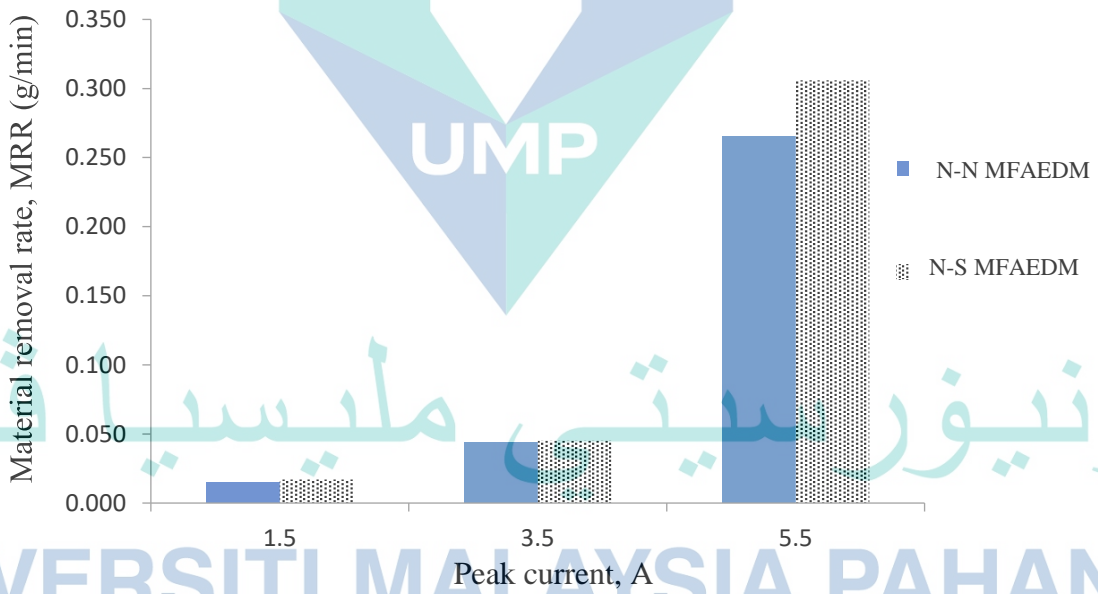


Figure 4.5 Effect of different polarity in MFAEDM on MRR

To optimise probable result, proper value of magnetic flux density and range of low level and high level peak current and pulse time should be selected. Lin and Lee (2008) partaked a good range of experiment parameters to investigate the effect of MFAEDM using magnetic flux density at 0.3 T. On the other hand, Gholipoor et al. (2016) used 0.38 T and 1.2 T in their investigation. Whilst Singh Bains et al. (2016) applied 12 A as the maximum peak current; Khan et al. (2013) applied 2.5 A to 6.5 A. From the literature review and these preliminary results, low-level peak current was decided to start at 8 A and upper-level at 24 A with 100 μ s pulse time to avoid electrodes and samples over burnt. In this experiment, raw data was collected for three different machining conditions. First, the experiments were carried out in normal condition to attain the datum result, which is noted in conventional EDM. The last two methods are MFAEDM operation in which the sparks conducted in between permanent magnet within the spark gap. In MFAEDM set up, permanent magnets of 0.54 T were clamped side by side to AISI 420 mod work piece so that the same pole faced each other (N-N) to obtain repulsive magnetism. Then, the magnetic devices were arranged in different magnetic polarity as (N-S) to create attractive magnetism which is the third method. Sixteen experiments were performed to investigate magnetic polarity effects on EDM machining.

4.3 Comparison between conventional EDM and MFAEDM

During EDM material removal process, a continuous cycle of discharge sparks was created through electrode towards workpiece to erode work material. The EDM machine produced an electric spark temperature in the range of 8000 °C to 12000 °C degrees Celsius which melted almost any conductive material. Theoretically, when EDM is in discharge progression, melting and vaporisation course in the machining area does not only remove the work piece materials but also erodes the electrode materials. Table 4.3 shows the overall result for EDM machining experiments using graphite electrode. First, MRR between conventional and MFAEDM are compared.

Table 4.3 Complete design of experiment table extracted from Design Expert

Run	Factor 1	Factor 2	Factor 3	Factor 4	Response1	Response2	Response3
	Peak Current (A)	Pulse Time (μ s)	Magnetic Strength (T)	Magnet Polarity	MRR (g/min)	EWR (g/min)	SR (R_a) (μ m)
1	8	100	0	-	0.065	-0.0009	6.152
2	24	50	0	-	0.386	-0.0060	7.557
3	24	100	0	-	0.484	-0.0075	9.294
4	8	50	0.54	N-N	0.042	-0.0006	4.947
5	8	100	0.54	N-S	0.091	-0.0014	5.158
6	8	100	0	-	0.069	-0.0010	6.169
7	8	100	0.54	N-N	0.094	-0.0014	5.499
8	24	100	0	-	0.482	-0.0073	9.285
9	24	100	0.54	N-S	0.551	-0.0084	7.487
10	24	100	0.54	N-N	0.551	-0.0084	8.485
11	24	50	0.54	N-S	0.483	-0.0074	5.456
12	8	50	0	-	0.041	-0.0006	5.265
13	24	50	0	-	0.386	-0.0058	7.583
14	24	50	0.54	N-N	0.454	-0.0069	6.309
15	8	50	0.54	N-S	0.050	-0.0008	4.751
16	8	50	0	-	0.040	-0.0006	5.437

اوديفور سديتي مليسييا فهاغ

UNIVERSITI MALAYSIA PAHANG

4.3.1 MRR

Material removal rate (MRR) figures were gained by calculating sample mass difference before EDM and after EDM machining against machining time. Throughout the investigation, data record shows that machining time reduced when peak current increased. The data also shows that machining time decreased even lower when MFAEDM was applied. When machining time was thoroughly reduced, MRR increased.

MRR for EDM experiments elevated when peak currents were increased from 8 A (0.041 g/min) to 24 A (0.386 g/min) for conventional EDM and 8 A (0.042 g/min) to 24 A (0.454 g/min) for MFAEDM as illustrated in Figure 4.6. The increment of MRR value produced higher current which led to superior spark and bigger implosion on sample surface (Kiyak & Cakır, 2007). Similar result trend was discovered when the experiments were repeated with higher pulse time value. It is evident in Figure 4.7 which illustrates MRR comparison between normal and MFAEDM with higher pulse time at 100 μ s. High pulse time also resulted in increment in MRR, 0.551 g/min at 100 μ s (24 A) compared to 0.438 g/min at 50 μ s (24 A). However, Arikatla et al. (2013) highlighted that at certain point, the increment of pulse time decreases in MRR.

The charts also reveal that MRR improved when magnetic field was applied in EDM machining area. Gap condition stability improved when magnets were attached in the EDM machining area by absorbing most debris particles from the spark gap. Machining improvement can be clearly visualized in both Figure 4.6 and Figure 4.7; whereby higher MRR values were recorded for N-N MFAEDM and N-S MFAEDM compared to conventional EDM. For example, at peak current of 24 A and 100 μ s pulse time combination, N-S MFAEDM recorded MRR at 0.551 g/min compared to 0.483 g/min for conventional EDM. MRR value increased if peak current and pulse time were increased. Additionally, it was noted that concentrated magnetic field also improved MRR for EDM machining.

The magnetic device used did not only enhance MRR but also facilitated debris settling at the magnet; thus, maximising service life of fluid tank filters. Lin et al. (2009) stated that magnetic field in EDM system does not only increase MRR but also flushes debris better from the spark gap. Hence, it improves sparking cycle which contributes for better EDM machining performance. Therefore, applying MFAEDM is an option for better machining efficiency in term of MRR.

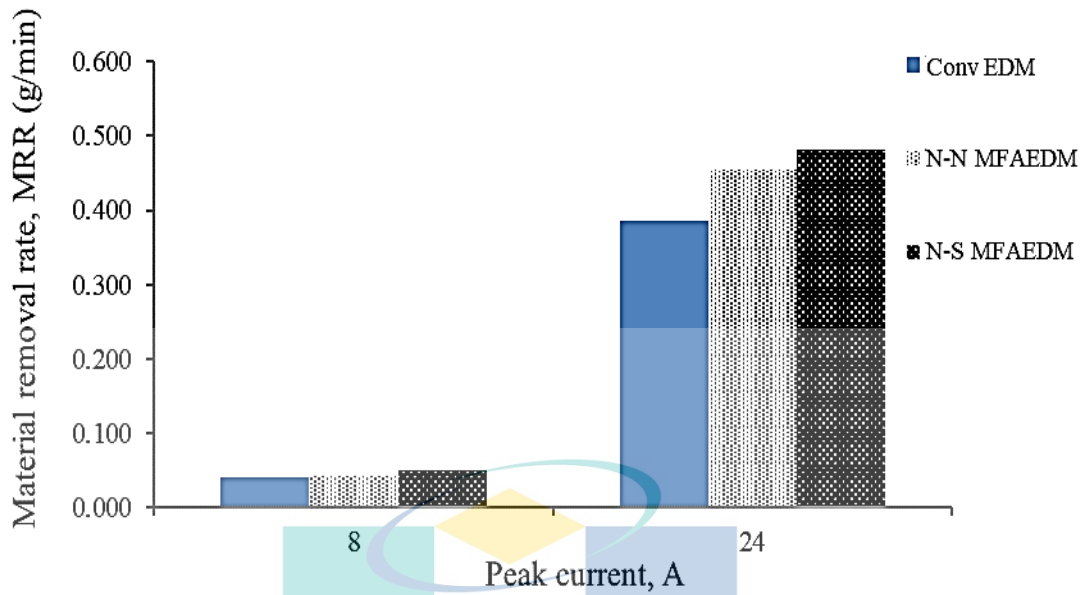


Figure 4.6 Comparison of MRR between conventional EDM and MFAEDM at 50 μs

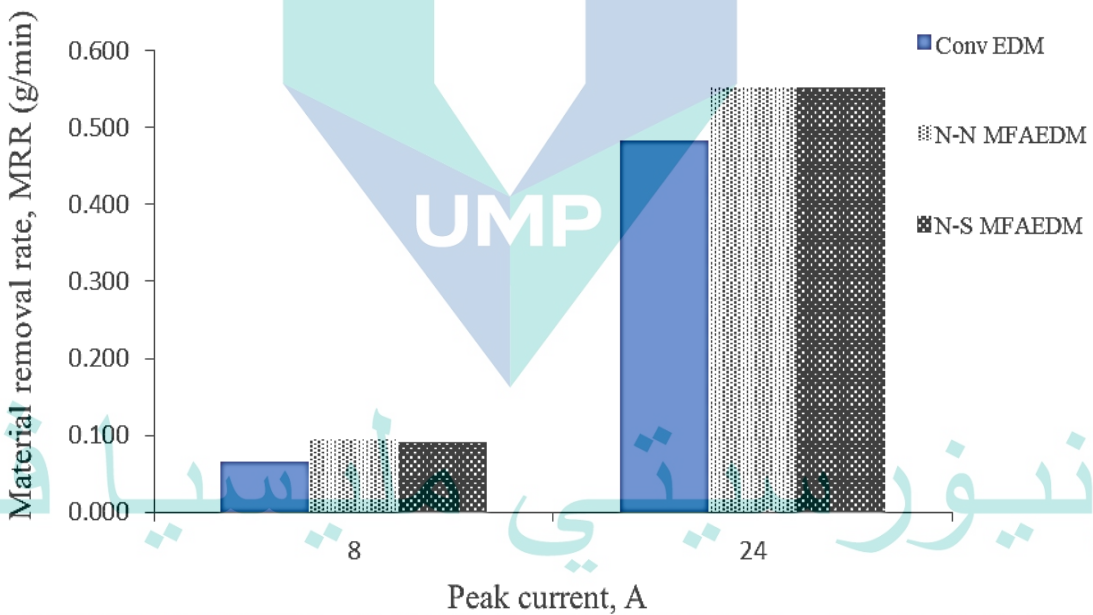


Figure 4.7 Effect of MRR between conventional EDM and MFAEDM at 100 μs pulse time

4.3.2 EWR

EWR results from EDM process mostly rely on machining parameters such as peak current, pulse time and machining time factors. As EDM cycle increases the temperature; the electrode starts to wear (Vishwakarma, Dvivedi, & Kumar, 2013). There is an inter-relationship between the volume of electrode wear and machining time in EDM known as electrode wear rate (EWR). Besides MRR, EWR is considered as a good tool to measure machining efficiency and to indicate cost-effective process. From the experiments performed, data obtained was calculated to determine EWR of graphite electrode for conventional EDM and MFAEDM comparison.

Figure 4.8 illustrates that EWR value for graphite electrode was negative for both conventional EDM and MFAEDM. The electrode wear rate for conventional EDM was -0.0006 g/min with peak current at I_p 8 A (50 μ s); whereas EWR value was -0.0058 g/min with peak current at 24 A (50 μ s). Supposedly, high peak current yields high EWR because high electric field strength energy causes greater electrode wear rate (V. Singh, Bhandari, & Yadav, 2017). However, it was the opposite with graphite electrode; whereby, as peak current increased EWR value decreased correspondingly (in negative number). This negative value trend in EWR of graphite has arisen due to a combination of peak current and pyrolytic carbon layers formation onto graphite electrode surface (Teimouri & Baseri, 2012). On the other hand, EWR value was higher (in negative value) for conventional EDM than MFAEDM. In N-S MFAEDM, EWR recorded at 24 A (50 μ s) was -0.0074 g/min which decreased as much as 0.0016 g/min compared to conventional EDM. Figure 4.9 shows similar EWR investigation but the experiment was conducted at higher pulse time (100 μ s). Both experiments suggest conventional EDM offers higher EWR than MFAEDM.

MFAEDM technique was acknowledged in improving the flushing system to remove residue debris in spark gap and minimize any abnormal discharge (Shabgard et al., 2016). Magnet devices improve debris flushing of which the debris attracted to magnets bar; hence, providing better path for next spark. When magnetic field removed the debris from spark gap to purify dielectric fluid, pyrolytic carbon deposited on the electrode surface was reduced. Thus, the amount of pyrolytic carbon deposited onto

electrode surface was minimized. Therefore, pyrolytic carbon thin layer was formed on graphite electrode surface in MFAEDM than that on conventional EDM.

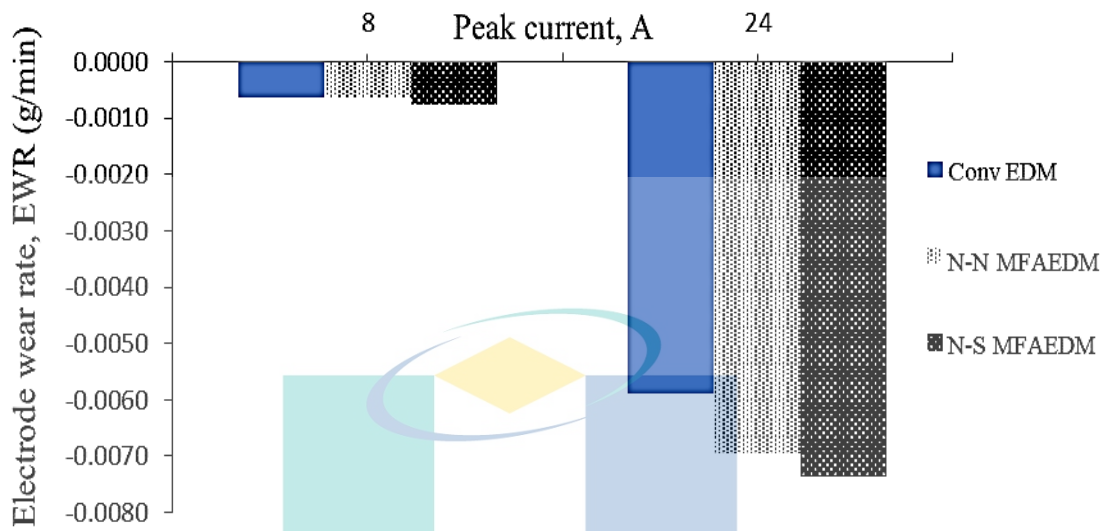


Figure 4.8 Comparison graph of EWR for conventional EDM and MFAEDM at 50 μ s

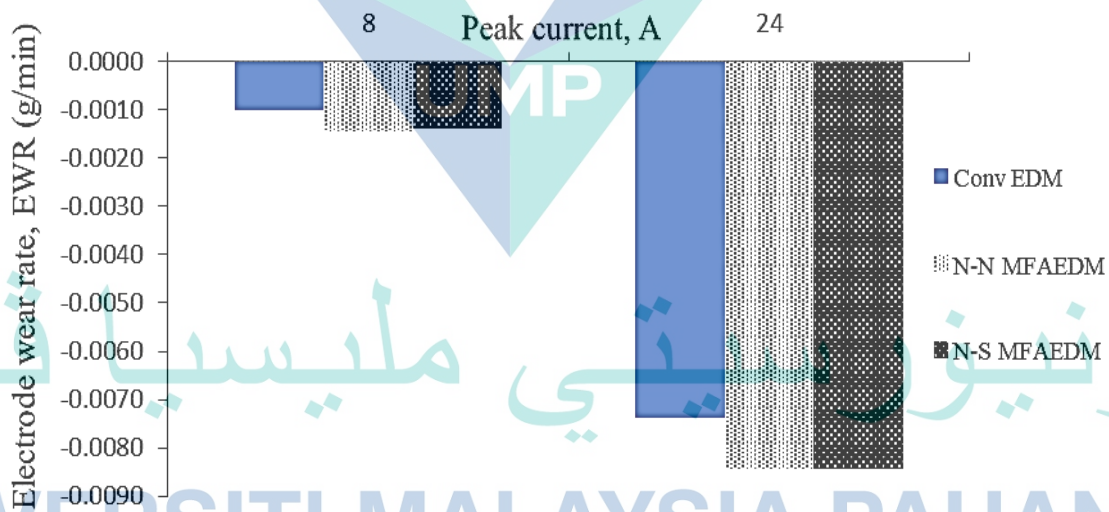


Figure 4.9 Comparison graph of EWR for conventional EDM and MFAEDM at 100 μ s

4.3.3 Surface Roughness

Surface roughness measurement normally represents surface finish texture state. If vertical deviations are large, it means the surface rough and vice versa. Good surface finish represents aesthetic appearance value but it has its own cost to put on. EDM machining parameters such as peak current and pulse-on time have prominent effect on sample's surface roughness. Peak current is the parameter that determines spark length and spark explosion magnitudes. Pulse time, which is time exposure (t_{on}) to spark and time for dielectric re-ionization (t_{off}), also corresponds to surface integrity in EDM (Sanjeev Kumar & Choudhury, 2007). Due to the significant characteristic, analysis of sample surface roughness were carried out for conventional EDM and MFAEDM.

Figure 4.10 and Figure 4.11 show comparison graphs of surface roughness between conventional EDM and MFAEDM at different peak currents at 50 μ s and 100 μ s, respectively. From both charts, R_a values increased when higher peak current applied. At higher current, spark intensity increased and higher heat energy created at the gap; hence, producing more micro-features on sample surface (Khan et al., 2013). This spark state created craters in the sample which in turn determined surface finish. In the case of conventional EDM at 0 Tesla (100 μ s), surface roughness value (R_a) increased from 6.152 μ m to 9.294 μ m for peak current of 8 A and 24 A respectively. When higher peak current applied, the crater is larger and deeper; as a result, the surface finish is coarse. Meanwhile, if low peak current employed; the craters are small so the surface finish is smoother and better.

As shown in the graphs, there is a significant effect of magnetic fields in EDM machining; whereby the technique delivers better surface roughness. At the presence of magnetic field, R_a is lower than the value obtained by conventional EDM. At peak current of 8A (50 μ s), the difference of R_a value between conventional EDM (5.437 μ m) and NS MFAEDM (4.751 μ m) was 0.686 μ m. Followed by peak current of 24A (50 μ s), R_a difference value between conventional EDM (7.583 μ m) and N-S MFAEDM (5.456 μ m) was 2.127 μ m. Therefore, surface roughness obtained by MFAEDM was lower than conventional EDM which was not only at low current but also at higher current practice. In MFAEDM, the spark produced was under higher pressure and squeeze so discharge

craters generated on machined surface was tiny and shallow which produced lower R_a number representing smaller average of absolute height profile value. Hence, EDM modification magnetic apparatus has good influence on surface finish which provides lower R_a value and more delicate surface finish.

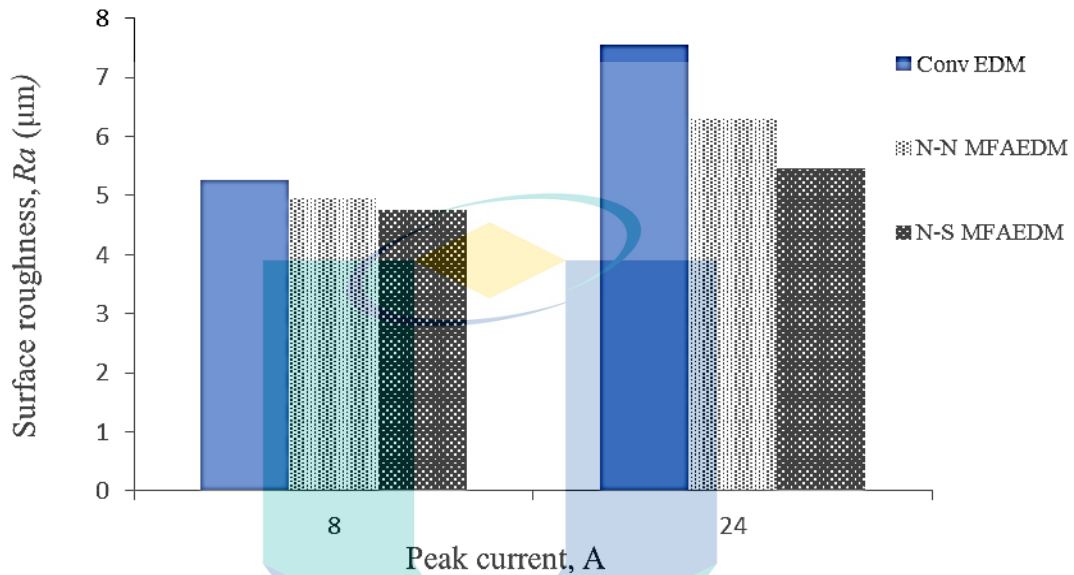


Figure 4.10 Surface roughness comparison of conventional EDM and MFAEDM at 50 μs

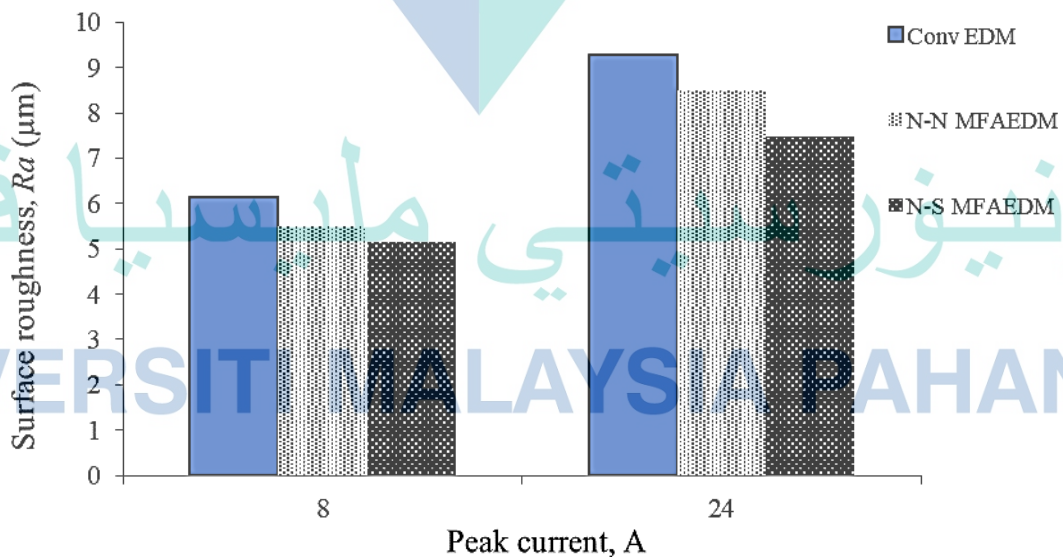


Figure 4.11 Surface roughness comparison of conventional EDM and MFAEDM at 100 μs

4.4 Effect of Magnetic Polarity in MFAEDM

Magnetic field drives magnetic lines according to the arrangement and combination of magnets. When magnet was attached to EDM machining area, machining debris was forced to expel from machining zone quickly and stick to the magnet bar. As it was well discussed in previous section, magnetic field restricted plasma spread; hence, energy at the machining area increased. Material removal mechanism augments the plasma density and pressure along the spark gap; consequently, enhancing EDM process. The introduction of magnetic field within EDM has improved surface integrity quality (Das, Kumar, Barman, & Sahoo, 2013; Efendee et al., 2018; Lin & Lee, 2008; Takezawa, Yokote, & Mohri, 2016). Even though positive impacts of magnetic field application in EDM were previously investigated, studies on magnetic polarity effects for MFAEDM are still lacking. Thus, the experiments were conducted to investigate the effects. First, MRR between N-N and N-S combination of MFAEDM are compared.

4.4.1 MRR

Figure 4.12 shows the effect of magnetic flux density and magnetic field line on material removal rate when it was arranged as north-north (N-N) and north-south (N-S) accordingly at 50 μ s pulse time. When 0.54 T of magnetic strength was applied at 8 A to MFAEDM machining, there was no major significant effect on magnetic polarity. However, there was a sign that N-S magnets combination produced superior result. On the other hand, the superiority of magnetic polarity effect can be observed at peak current of 24 A in N-S combination. This repulsive magnetic field demonstrated similar influence on EDM as in the preliminary experiments shown in Figure 4.5. The recorded MRR for N-N (0.454 g/min) was lower than MRR for N-S (0.483 g/min). This circumstance is related to magnetic field direction and magnetic field lines where the sparks are affected by the magnetic field (Takezawa et al., 2016). In N-S MFAEDM experimental setup, the magnetic field reacts perpendicularly to the electrode (Beeteson, 2001; Singh Bains et al., 2016). Then, resultant magnetic field recuperates and synchronises any disengage spinning electrons and ions from their core atom to increase ionisation processes (Gholipoor et al., 2016). The process increases plasma pressure and plasma density to exercise downward sparking force and melts the material.

In N-N MFAEDM, there is neutral spot in the magnetic field of which resultant magnetic field is zero (Serway & Jewett, 2013); hence, more chances of having free path ions. Meanwhile, in N-S MFAEDM the magnetic field acts tangential to the plasma channel. The state created in N-S MFAEDM decreases free path ions and increases ionization course. When N-S MFAEDM machining increases the ionization process, the plasma channel formation is accelerated within the spark gap. Hence, magnetic polarity of N-S MFAEDM combination maximises the ionisation for plasma channel creation and minimises the ignition delay time by purifying spark gap to improve MRR.

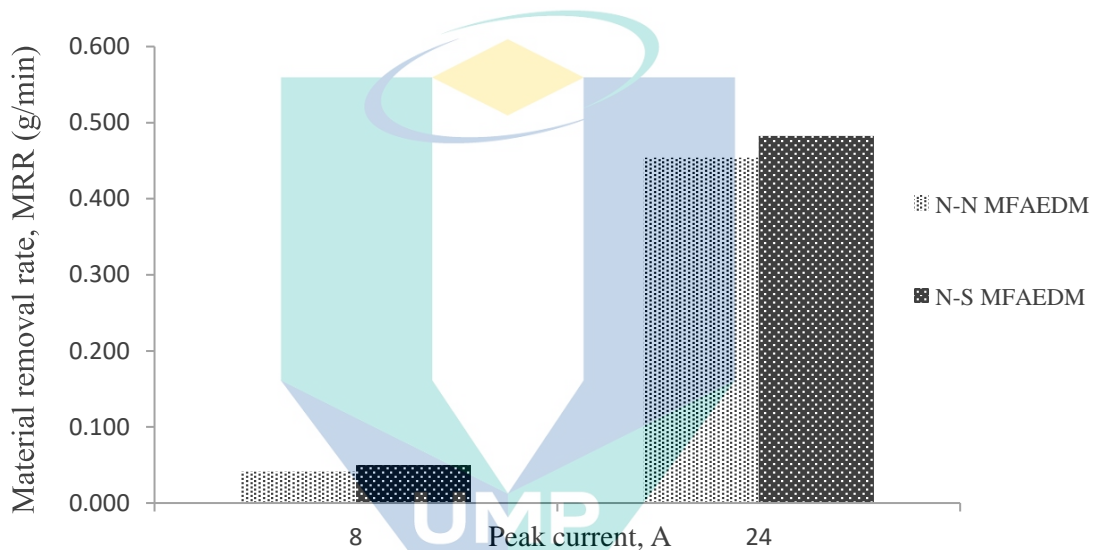


Figure 4.12 Effect of magnetic polarity in MFAEDM on MRR at 50 μ s pulse time

4.4.2 EWR

Electrode wear rate development in MFAEDM was high when high pulse current employed because large amount of electrode material eroded in short machining time. Significantly, high current contributed to high MRR; thus, high deposited debris quantity increased the possibility of pyrolytic carbon layer formation. Pyrolytic carbon immersed in kerosene could deposit on electrode surface to form protective layer. Additionally, there was no significant magnetic polarity effect in determining EWR. The EWR obtained by N-N MFAEDM and N-S MFAEDM is almost similar. At peak current of 8 A (50 μ s) the EWR for N-N MFAEDM was -0.0006 g/min and N-S MFAEDM was -0.0008 g/min; which the difference between the two methods was only 0.0002 g/min. Meanwhile, EWR values at 24 A (100 μ s) were the same for both MFAEDM methods (-0.0084 g/min).

Pyrolytic carbon deposited on electrode surface was in accordance with supply pattern of electrical discharge energy, machining polarity, and the mates of workpiece and electrode materials. Machining debris suspended within dielectric fluid would affect the possibility for pyrolytic carbon to deposit on electrode surface. Thick protective layer on electrode surface would be formed if pyrolytic carbon amount was large in the small gap width with long pulse duration as occurred to conventional EDM case. Even though MFAEDM recorded high EWR, it was caused by less amount of pyrolytic carbon deposited on electrode surface. Therefore, MFAEDM reduced the thickness of protective layer due to less pyrolytic carbon deposited on graphite electrode surface. In MFAEDM, the formation of pyrolytic carbon onto graphite electrode surface was lessened so EWR value recorded was slightly higher than conventional EDM (Lin & Lee, 2008). Thus, magnetic field-assisted EDM revealed the potential of debris expulsion, minimizing pyrolytic carbon deposited and improving machining efficiency.

4.4.3 Surface Roughness

As above topic is concerned, magnetic polarity effect on surface roughness can be observed in Figure 4.13. Surface roughness was reduced as much as 10.62 % at I_p :8 A and 8.62% at I_p 24 A when N-N MFAEDM was applied. When N-S MFAEDM was implemented, R_a value was reduced as much as 16.16% at 8 A and 19.38% at 24 A. Additionally, from this observation, N-S MFAEDM proposes better surface quality than N-N MFAEDM as was justified in Figure 4.14. These microstructures were obtained from a combination of 24 A peak current and 50 μ s pulse time EDM machining. As can be observed, melting and evaporation processes took place; subsequently, crater and recast layer were formed on the machined surface. Valley produced from the spark in conventional EDM (Figure 4.14(a)) was deeper and wider than N-N MFAEDM (Figure 4.14(b)). In fact, it was deeper and wider than N-S MFAEDM (Figure 4.14(c)). Thus, the comparison of crater depth and recast layer texture clearly shows that N-S MFAEDM has higher surface quality.

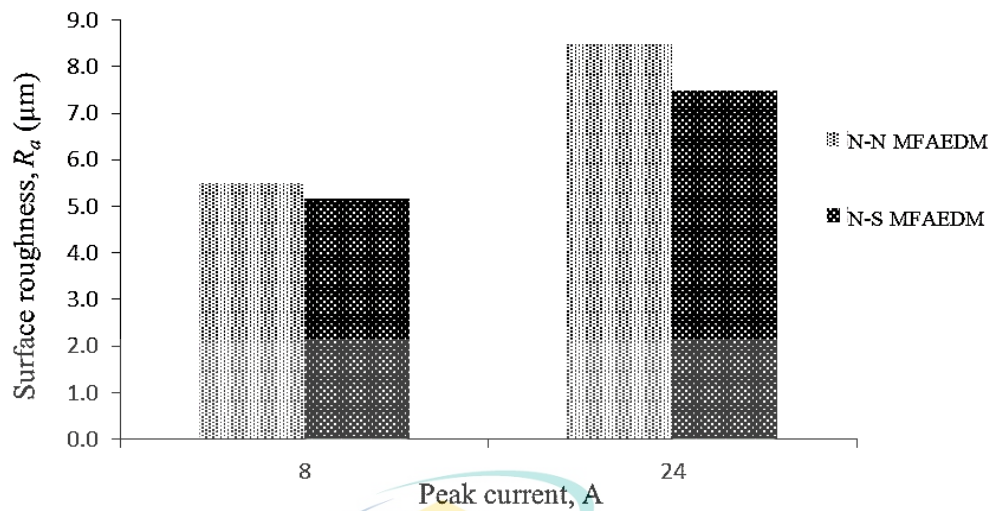


Figure 4.13 Effect of magnetic polarity in MFAEDM on surface roughness by using graphite electrode

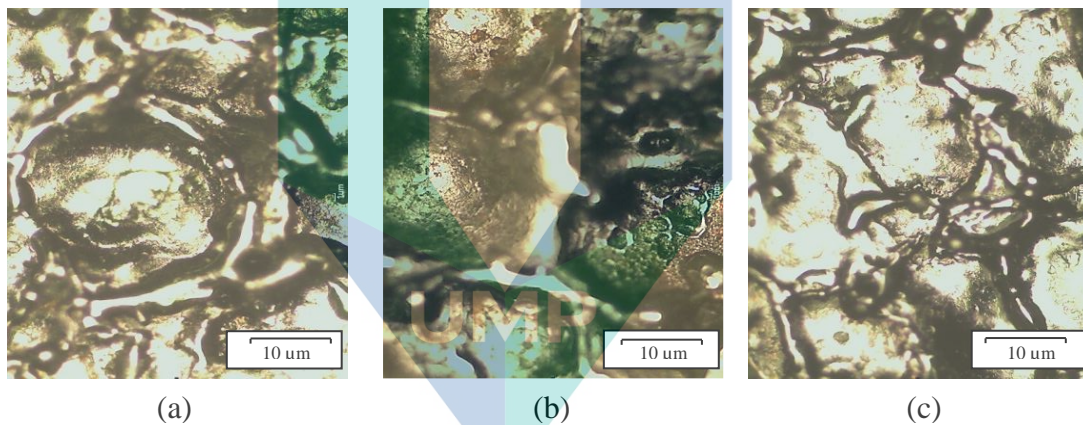


Figure 4.14 Surface microstructure of (a) conventional EDM, (b) N-N MFAEDM and (c) N-S MFAEDM at 200× magnification of optical microscope (24 A, 50 µs)

There was a neutral spot in the middle of magnetic field line pattern for N-N; which was in contrast with the magnetic field line of N-S combination. At the neutral point, resultant magnetic field is zero (Serway & Jewett, 2013). Therefore, plasma pressure for ionization process in N-N polarity was lower than N-S. Meanwhile, the magnetic field in N-S MFAEDM acts in tangential to the plasma channel accelerating the ionization process. In the meantime, the spark produced was squeezed and discharge craters generated on the surface was tiny and shallow. As a result, surface roughness was finer than N-N MFAEDM. Therefore, N-S magnetic polarity combination minimized the ignition delay time to increase MRR; and at the same time intensified the spark to refine surface quality of EDM samples.

4.5 The Effect of Magnetic Polarity on Surface Microstructure.

Figure 4.15 illustrates the structure of altered metal zone in EDM machining which consists of recast layer, heat affected zone and base material. The EDX analysis was carried out to fully understand the composition of different machined surface layers. It is understood that sample material compositions depend on diffusion of the substrate, electrode material and dissolved dielectric fluid (Hocheng, Guu, & Tai, 1998). Three different spots for elemental spectrums were acquired to constitute for three different machined surface layers which were recast layer, heat-affected zone and base metal as indicated in Figure 4.16.

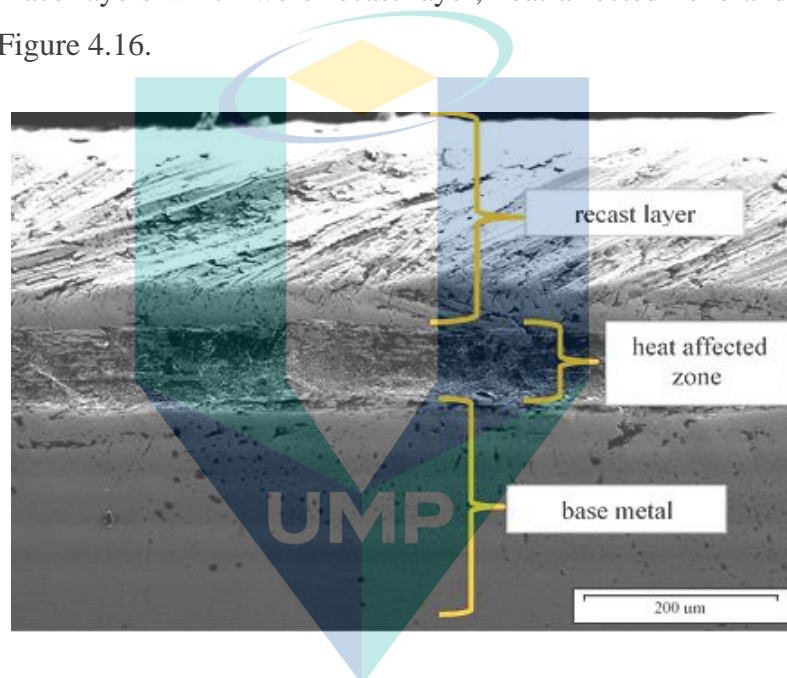


Figure 4.15 EDM surface layers (N-S MFAEDM, 24 A, 100 μs)

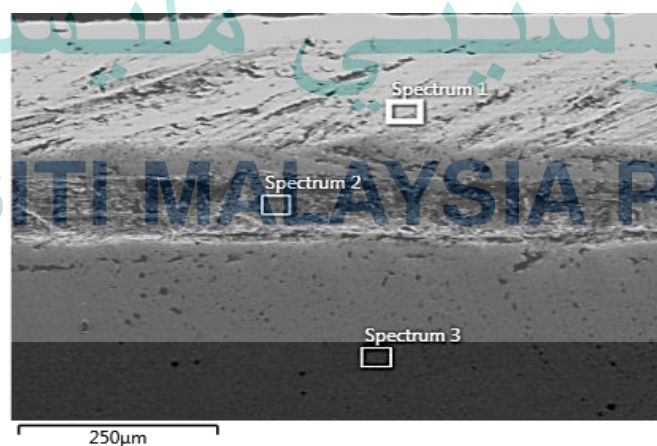


Figure 4.16 Spectrum spot on EDM sample surface (N-S MFAEDM, 24 A, 100 μs)

Table 4.4 shows quantitative element of the spectrum from EDX. The EDX analysis shows a significant uptake of C at the recast layer and heat-affected zone. This can be expected since graphite material was used as electrode. A portion of worn-out graphite electrode consists of carbon; whereby, C dissolved in kerosene during EDM process. Molten metal is then solidified together with carbon to form recast layer. As explained by Zinelis (2007), C uptake is a normal attribute to the decomposition of dielectric fluid due to extreme high temperature development. It can also be noticed for O and Al uptakes, especially at the heat-affected zone. This is probably due to oxidation of base metal; thus, forming Al_2O_3 at areas which are affected by extreme heat but without melting.

Table 4.4 Element of spectrums from EDX

Element	Spectrum 1		Spectrum 2		Spectrum 3	
	Apparent Concentration	Weight %	Apparent Concentration	Weight %	Apparent Concentration	Weight %
C	0.47	10.95	0.41	13.73	0.21	4.78
O	0.88	3.71	5.38	29.88	0.26	0.95
Al	0.53	4.76	3.61	32.92	0.22	1.90
Si	0.11	0.97	0.04	0.43	0.10	0.85
Cr	1.22	10.86	0.30	3.56	1.61	13.22
Fe	6.94	68.75	1.54	19.49	8.53	78.30

4.5.1 Surface Microstructure

It was observed that surface finish quality mostly depended on pulse current and pulse time selection. If higher surface quality was required, smaller peak current and pulse time should be applied to produce small spark size. Low crater depths were formed by electrical discharge spark. When high material removal rates were needed, high pulse current and pulse time should be selected. However, this selection produced poor surface finish with irregular topography due to deeper and wider craters on the machined surface (Arikatla et al., 2013; Lee & Tai, 2003). Surface topography comparison for conventional EDM, N-N MFAEDM and N-S MFAEDM by optical microscope can be observed in Figure 4.17, Figure 4.18 and Figure 4.19. The morphology sequences show the surfaces were blasted by discharge spark and the crater produced reflects the pattern caused by the spark. Examples of crater produced by low and high pulse time can be observed as in

Figure 4.17(a) and Figure 4.19(a) respectively. On the other hand, comparison of crater size formed by lower and higher peak currents can be observed based on Figure 4.17(a) and Figure 4.19(a).

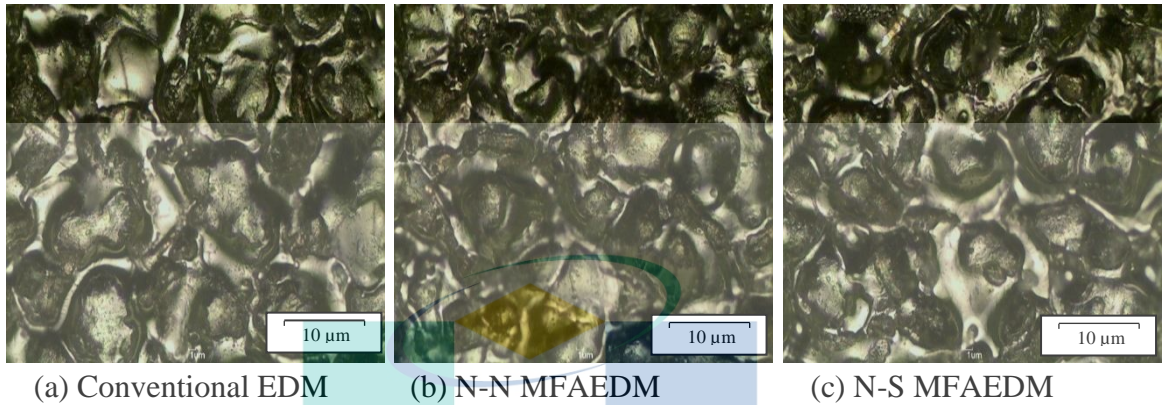


Figure 4.17 Surface of conventional EDM and MFAEDM at 8 A, 50 μ s (200 \times)

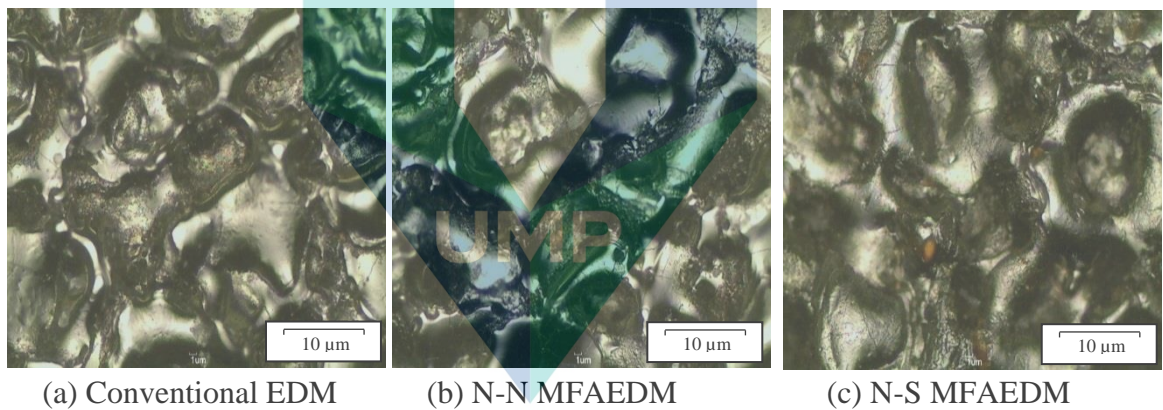


Figure 4.18 Surface of conventional EDM and MFAEDM at 8 A, 100 μ s (200 \times)

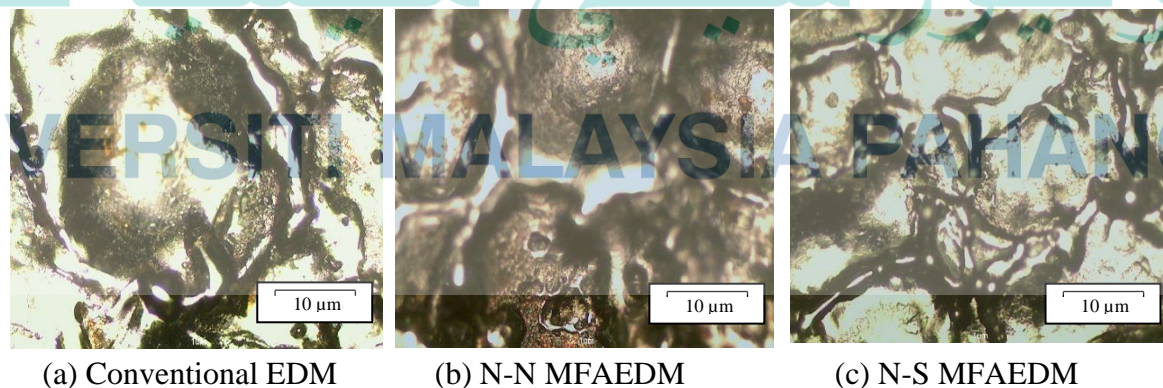


Figure 4.19 Surface of conventional EDM and MFAEDM at 24 A, 50 μ s (200 \times)

The morphology of EDM sample surface is caused by the amount of heat generated by the discharge process which involves melting and vaporisation of sample material followed by rapid cooling. Apart from the material surface deteriorated by discharge spark, white layer formation also contributed to surface roughness effect. As peak current and pulse time duration increased, amount of heat energy transferred to sample surface increased so more materials were melted. If this molten material is not swept away from the surface immediately, it solidifies and form white layer (Lee & Tai, 2003). The combination of discharge spark strength, magnetic field pattern and formation of white layer contributes to material surface roughness state. At low peak current, there was no big difference between conventional EDM and MFAEDM which can be observed in Figure 4.17. Whilst, conventional EDM crater shape produced was wider and deeper at 24 A, MFAEDM crater shape was narrower and thinner. Additionally, N-S MFAEDM crater surfaces were horizontally smoother as illustrated in Figure 4.19 and the difference of R_a value between conventional EDM ($5.437 \mu\text{m}$) and N-S MFAEDM ($4.751 \mu\text{m}$) was 28.1%. Pressure from N-S magnetic fields pattern refined the discharge spark quality by concentrating on the plasma channel and the spark itself. The comparison of images from SEM and 3D surface texture for N-N MFAEDM (Figure 4.20) and N-S MFAEDM (Figure 4.21) signifies that N-S MFAEDM has significant improvement on machined surface.

اونيورسيتي ملايسيا قهغ

UNIVERSITI MALAYSIA PAHANG

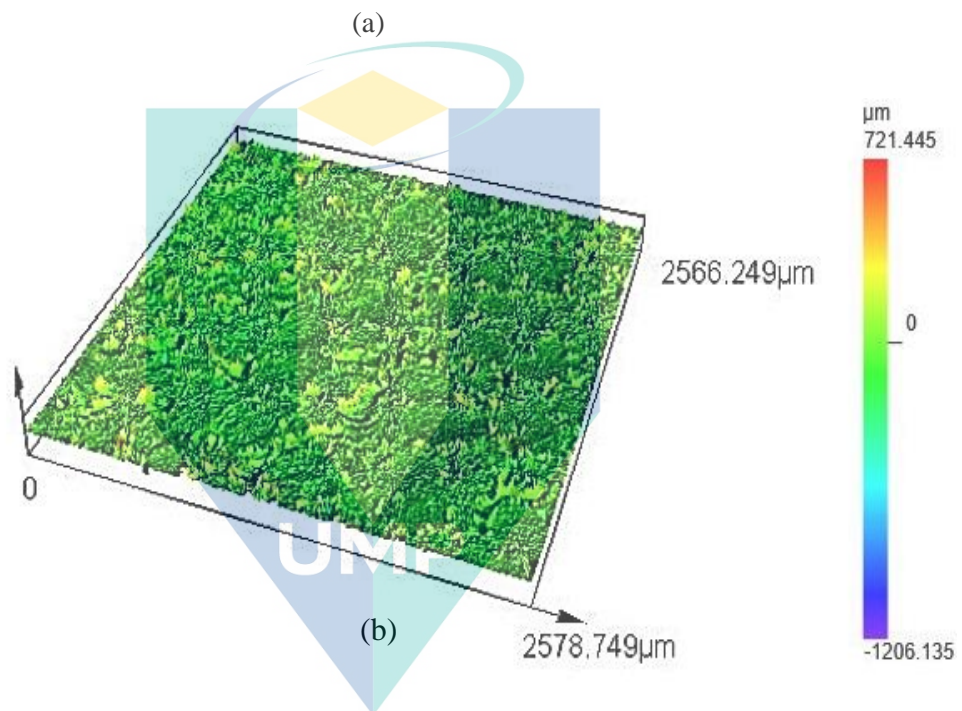
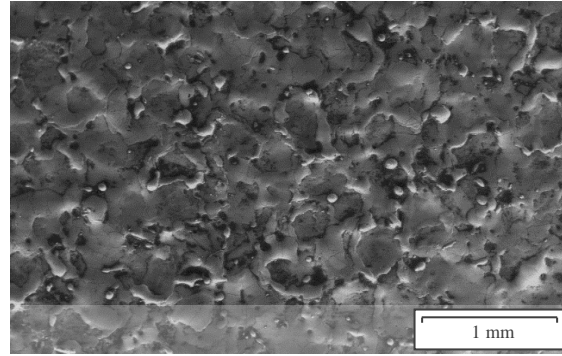


Figure 4.20 a) SEM (100×) and b) 3D surface texture (5×) of N-N MFAEDM at 24 A, 100 μs

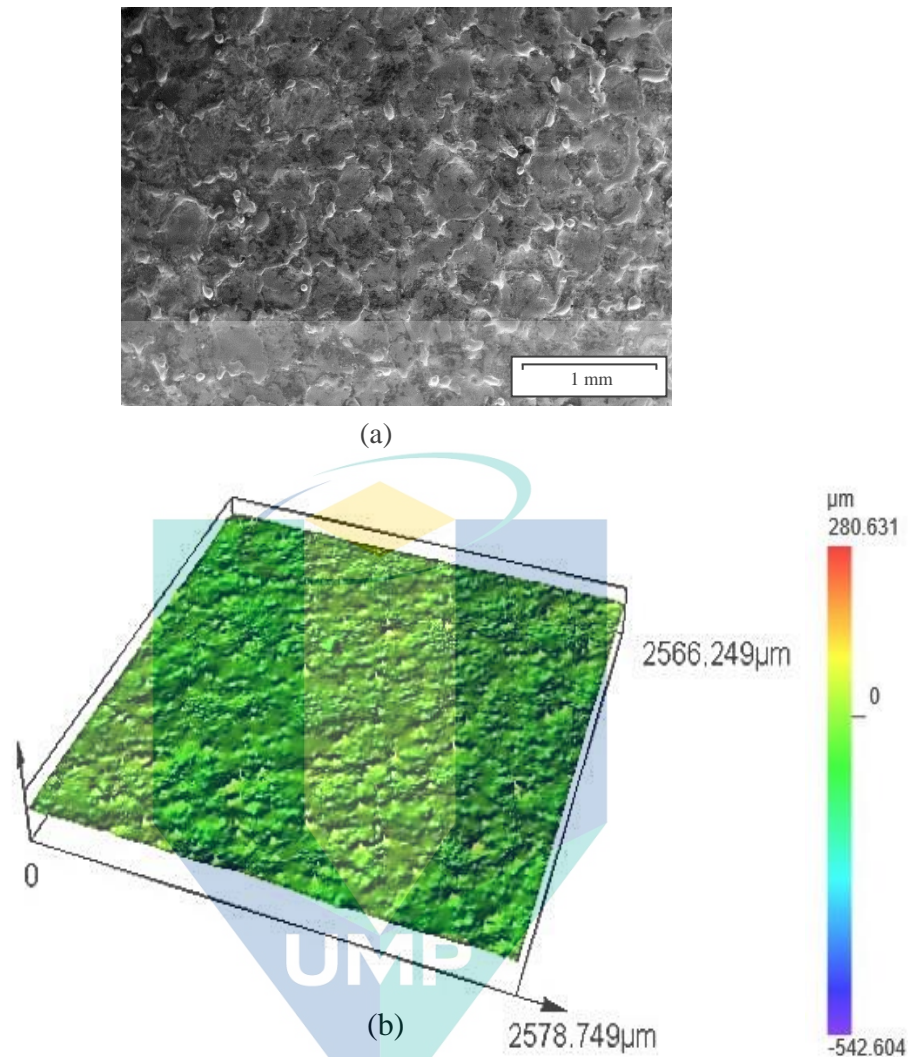


Figure 4.21 a) SEM (100 \times) and b) 3D surface texture (5 \times) of N-S MFAEDM at 24 A, 100 μ s

EDM crater surface observations via SEM images verified the comparison result of these EDM techniques; whereby N-S magnetic polarity combination provided superior surface integrity as witnessed in Figure 4.22. At 500 \times SEM magnification it was evident that N-S MFAEDM (Figure 4.22(c)) had a horizontally smoother surface, less bumpier and higher quality surface appearance than both N-N MFAEDM (Figure 4.22(b)) and conventional EDM (Figure 4.22(a)) due to spark alteration under magnetic field influence and magnetic-enhanced flushing system. The bumpier feature and several attributes on those surfaces can be observed using high magnification of SEM. Furthermore, under conventional machining condition, the surface shows high amount of tiny loose metal

particles which were initially melted due to spark discharges as shown in Figure 4.22(a). These small melted metals were unable to be thoroughly washed in dielectric fluid without magnetic field assistance. As a result, metal debris immediately solidified and formed many tiny particles over the machined surface.

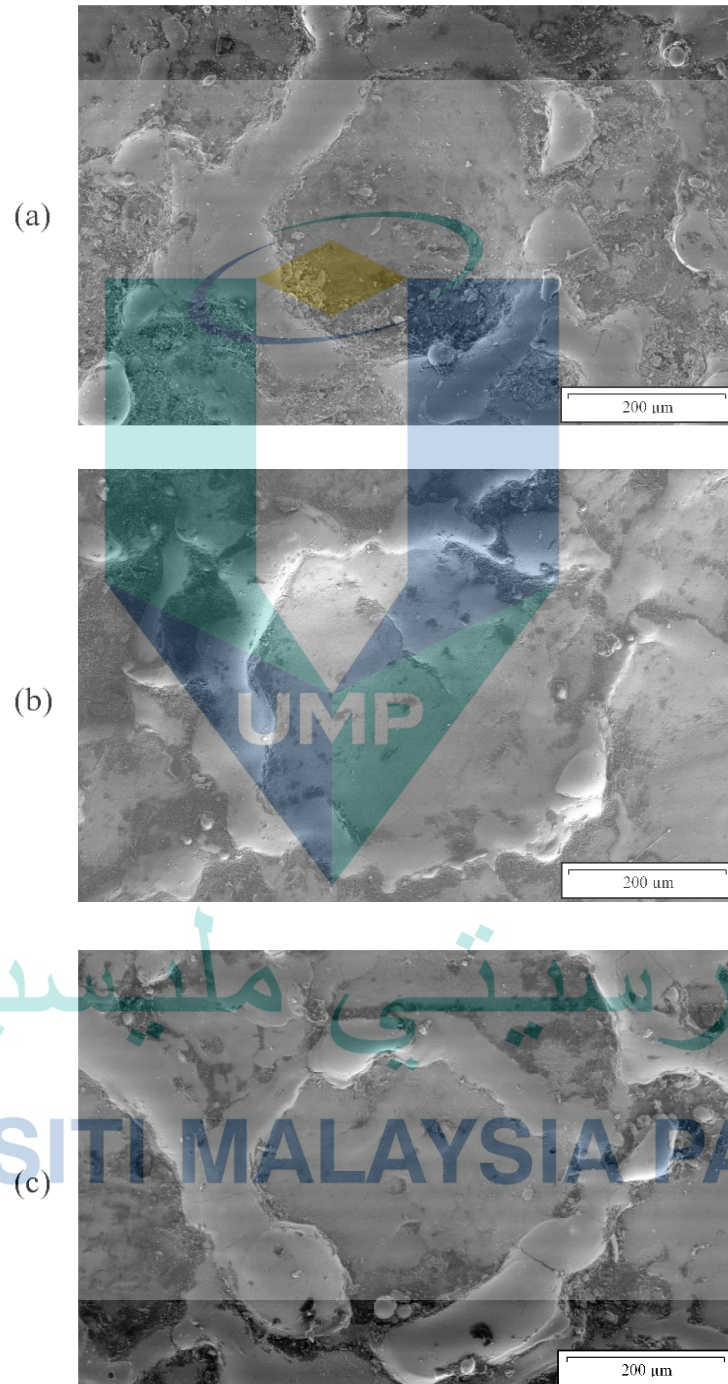


Figure 4.22 Crater surface comparison of (a) conventional EDM and (b) N-N MFAEDM (c) N-S MFAEDM at 24 A, 100 μ s (SEM 500 \times)

4.5.2 Recast Layer (White Layer) and Microcracks

Figure 4.23 shows example of microcracks possess on sample surface. The melted material was contracted more than the unaffected parent part during cooling process. The ingress of carbon and tensile stress was generated within the sample. When stress in the surface exceeds material's ultimate tensile strength, cracks are formed (Klocke, Hensgen, Klink, Ehle, & Schwedt, 2016). Due to rapid heating and cooling effects induced by machining process, it was found that the white layer was quite hard and non-etchable (Bormann, 1991) and material properties were lost because of high temperature (Kiyak & Cakır, 2007). This white layer was mainly composed of martensite and retained austenite, with some dissolved carbide.

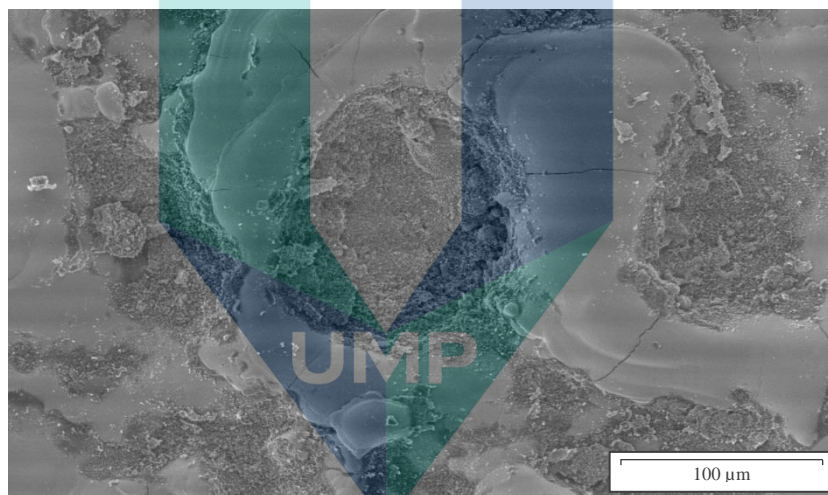


Figure 4.23 Microcracks on EDM surface at 8 A, 100 μ s (SEM 1000 \times)

Analysis of recast layer formation was completed by part-off specimen cross-sectional. Then, the specimen was polished with various grit sizes (P900-P2000) emery paper followed by diamond paste for high surface finish. SEM micrographs in Figure 4.24 and Figure 4.25 indicate the specimen obtained from conventional EDM (44.52 μ m) had thicker recast layer formation compared to N-S MFAEDM (40.20 μ m). Furthermore, the probability of surface cracks formation was proportionally lower during MFAEDM compared to conventional EDM machining as depicted in Figure 4.24 and Figure 4.25. It is accredited to proper debris removal so that the next discharge process may take place without obstruction from residue debris to form finer recast layer with fewer microcracks. Eventually, thicker recast layer formation on the surface was avoided in MFAEDM. The

finding was in line with (Singh Bains et al., 2016) where external magnetic field enhances flushing capability and reduces debris adhesion to the workpiece; hence, thinner recast layer is formed.

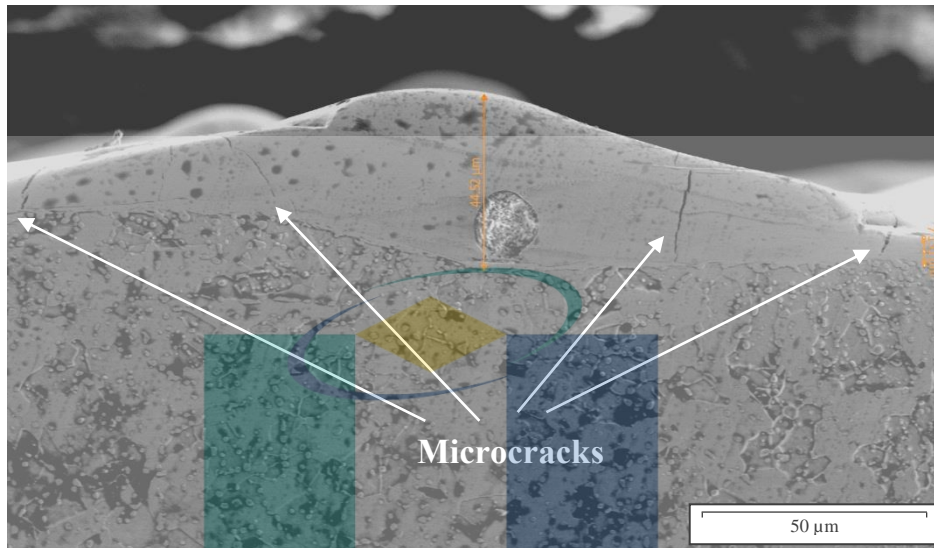


Figure 4.24 Cross sectional view of recast layer for conventional EDM (24 A, 100 μs, SEM 2000×)

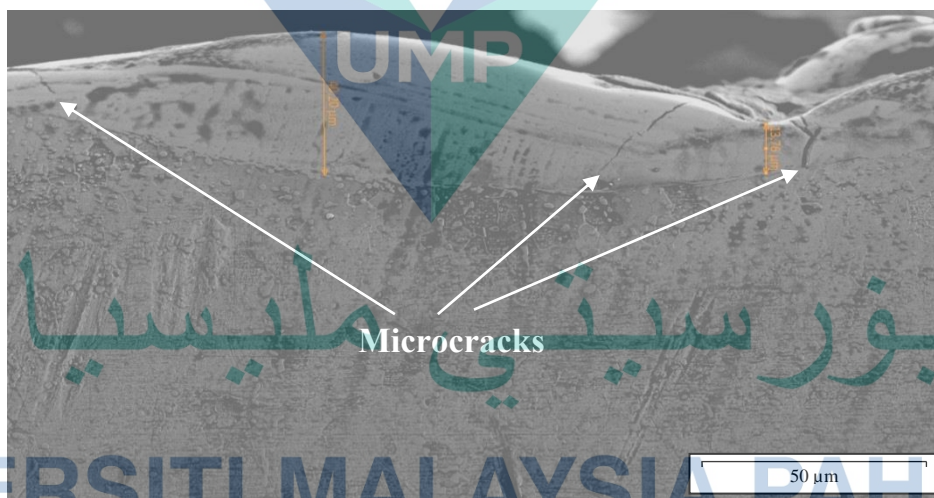
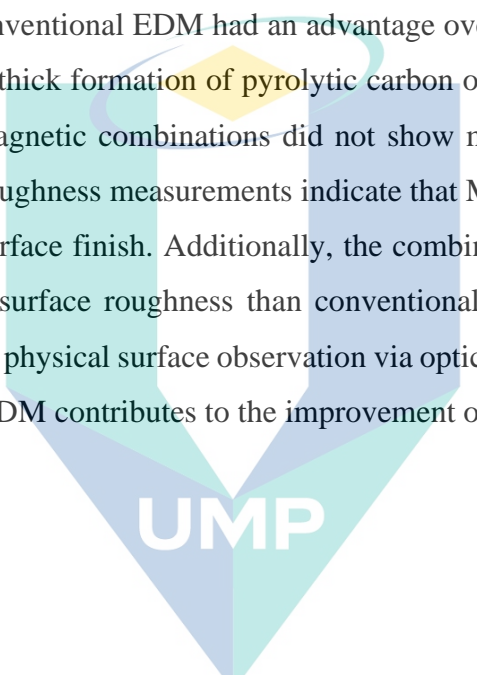


Figure 4.25 Cross sectional view of recast layer for N-S MFAEDM (24 A, 100 μs, SEM 2000×)

4.6 Summary

The effectiveness of MFAEDM method over conventional EDM can be evaluated based on MRR, EWR results, surface roughness measurements as well as direct observation of specimen surface by microscope and SEM. As a result of MRR comparison, there was an increase in MRR when MFAEDM method was used. Meanwhile, N-S magnet combination also had the potential to improve MRR. In terms of EWR calculations, conventional EDM had an advantage over MFAEDM. However, this advantage was due to thick formation of pyrolytic carbon on graphite electrode surface. The comparison of magnetic combinations did not show much difference in EWR for MFAEDM. Surface roughness measurements indicate that MFAEDM method is capable of improving EDM surface finish. Additionally, the combination of N-S magnetic field had better impact on surface roughness than conventional EDM and N-N MFAEDM methods. Results from physical surface observation via optical microscope and SEM also prove that N-S MFAEDM contributes to the improvement of surface roughness.

The logo of Universiti Malaysia Pahang (UMP) is a shield-shaped emblem. It features a yellow diamond at the top, a teal triangle on the left, and a blue triangle on the right. The letters 'UMP' are written in white across the bottom of the shield.

UMP

اونيورسيتي ملايسيا قهغ

UNIVERSITI MALAYSIA PAHANG

CHAPTER 5

CONCLUSION

5.1 Introduction

This chapter summarises the primary research points to conclude the data obtained from EDM investigation especially on the effect of magnetic polarity application in MFAEDM. The objective and scope of the study was successfully accomplished. Comparison of results obtained and statistical data analysis suggest that MFAEDM performance improves EDM operation for daily production. It was discovered that N-S combination is the best option for magnetic polarity application. The following conclusions are drawn based on the experiment results and observation of machined surface morphology.

5.2 Conclusion

MFAEDM clearly provides better MRR and surface quality but in terms of electrode wear rate it is quite difficult to determine which method gives better effect because there is pyrolytic carbon formed on the electrode. MFAEDM improves the debris flushing by attracting ferromagnetic material toward magnetic devices and away from machining area. It also highlights that discharge process erodes the workpiece without interruption from debris leftover. Thus, the time of machining was significantly reduced when MFAEDM was applied; thereby, increasing MRR compared to conventional EDM. The formation of a thicker restructuring layer was found in conventional EDM, while in MFAEDM a thinner restructuring layer is formed. In MFAEDM, the surface roughness (R_a) value was lower than conventional EDM because less residue debris leads to unsoiled recast layer formation and refined spark produced by magnetic flux density gives smoother surface finish. Surface topography from optical microscope and 3D profilometry show that conventional EDM has deeper, wider and irregular shape of the crater as compared to MFAEDM. The value of R_a and observations of the micro structure

from SEM confirm that the craters produced in MFAEDM were smaller and shallower than conventional EDM.

The research finding for N-N MFAEDM and N-S MFAEDM share the same advantage where both techniques improve the overall EDM process compared to conventional EDM. The only difference between N-N MFAEDM and N-S MFAEDM was the magnetic field line pattern created around the sparking area. In N-S MFAEDM the resultant magnetic flux line acts in tangential action to the electrode but for N-N MFAEDM, there is a neutral spot in magnetic flux line of which the resultant magnetic field is zero. Therefore, for better MRR N-S polarity combination should be applied. Plasma pressure for ionization process in N-S combination was higher than N-N. Therefore, high plasma pressure creates intense and shallower spark. As a result, crater produced on the machined surface is tiny and shallow. It is further noted that R_a value was decreased when N-S MFAEDM was applied. Hence, N-S magnetic polarity does not only increase MRR but also refine surface quality of EDM samples.

The surfaces were blasted by discharge spark and the crater produced reflects the pattern caused by the spark. Surface topography observation for conventional EDM, N-N MFAEDM and N-S MFAEDM via SEM images indicate N-S MFAEDM provided superior surface integrity. It was evident that conventional EDM and N-N MFAEDM had more tiny particles on the machined surface. Cross-sectional images captured from SEM prove that recast layer in N-S MFAEDM is thinner than in N-N MFAEDM. The bumpier feature, deeper valley attributes and more microcracks can be observed clearly for conventional EDM and N-N MFAEDM. Surface examination through 3D profilometry also shows that N-S MFAEDM had a higher quality surface appearance. The experiment results and microstructure observation verified that application of N-S MFAEDM has significant improvement on EDM machined surface.

5.3 Recommendation

These are several recommendations that should be considered for EDM machining. In this study, 2 mm cut depth is selected as experiment constraint. It is also feasible to put machining time as the constraint so that required time for completing all experiments can easily be forecasted.

Combination of EDM parameters should be selected suitably to the electrode and work sample properties capability. The reason is for the sparks to not halt the selected electrode or over burn the material. The limitation of the experiment is the need to optimise magnetic strength variation. It could only be achieved if succession of permanent magnet strength is available or eddy current system is developed to vary magnetic strength in the system. But the latter option would involve costly and quite challenging to retain the safety.

Overall view of the sample contour could be easily observed if 3D surface roughness is available. Standard roughness measurement procedures depend heavily on stylus instruments. Furthermore, it has limited range of length covered. However, this 3D surface roughness could configure sensitive characterization and complex engineering surfaces. This approach has the advantages of being non-contact and fast.

اونيورسيتي ملايسيا قهغ

UNIVERSITI MALAYSIA PAHANG

REFERENCES

- Abbas, N. M., Solomon, D. G., & Bahari, M. F. (2007). A review on current research trends in electrical discharge machining (EDM). *International Journal of Machine Tools and Manufacture*, 47(7), 1214-1228.
- Abdulkareem, S., Khan, A. A., & Konneh, M. (2009). Reducing electrode wear ratio using cryogenic cooling during electrical discharge machining. *The International Journal of Advanced Manufacturing Technology*, 45(11), 1146-1151.
- Aghdeab, S. H., & Mohammed, L. A. (2013). Experimental Investigations of Hole-EDM to Optimize Electrode Wear through Full Factorial of Design of Experiment. *Engineering and Technology Journal*, 31(13 Part (A) Engineering), 2572-2579.
- Ali, M., Amran, M., HUSSEIN, N. I. S., Mohd Rizal, S., Izamshah, R., Abdullah, R., . . . Sivarao, S. (2013). The effect of EDM die-sinking parameters on material removal rate of beryllium copper using full factorial method. *Middle-East Journal of Scientific Research*, 44-50.
- Ali, M. Y., Banu, A., Rahman, M. A., Al Hazza, M. H., & Chowdhury, A. G. K. (2020). *Micro Dry Wire EDM: Kerf Investigation using Response Surface Methodology*. Paper presented at the IOP Conference Series: Materials Science and Engineering.
- Anderson, M. J., & Whitcomb, P. J. (2016). *DOE simplified: practical tools for effective experimentation*: Productivity press.
- Arikatla, S. P., Mannan, K. T., & Krishnaiah, A. (2013). Influence of Pulse Current and Pulse on Time on Material Removal Rate and Surface Roughness in Electric Discharge Machining of AISI T1 High Speed Steel.
- Banu, A., Ali, M. Y., Rahman, M. A., & Konneh, M. (2020). Stability of micro dry wire EDM: OFAT and DOE method. *The International Journal of Advanced Manufacturing Technology*, 106(9), 4247-4261.
- Beeteson, J. S. (2001). *Visualising magnetic fields: numerical equation solvers in action* (Vol. 1): Academic Press.
- Bojorquez, B., Marloth, R., & Es-Said, O. (2002). Formation of a crater in the workpiece on an electrical discharge machine. *Engineering Failure Analysis*, 9(1), 93-97.
- Bormann, R. (1991). Getting those better EDM'd surfaces. *Modern Machine Shop*, 63(9), 56-66.
- Chakraborty, S., Mitra, S., & Bose, D. (2020). Experimental investigation on enhancing die corner accuracy during powder mixed wire EDM of Ti6Al4V. *Materials Today: Proceedings*.

- Chen, S., Yan, B., & Huang, F. (1999). Influence of kerosene and distilled water as dielectrics on the electric discharge machining characteristics of Ti-6Al-4V. *Journal of materials processing technology*, 87(1), 107-111.
- Choubey, M., Maity, K., & Sharma, A. (2020). Finite element modeling of material removal rate in micro-EDM process with and without ultrasonic vibration. *Grey Systems: Theory and Application*.
- Choudhary, R., Kumar, A., Yadav, G., Yadav, R., Kumar, V., & Akhtar, J. (2020). Analysis of cryogenic tool wear during electrical discharge machining of titanium alloy grade 5. *Materials Today: Proceedings*.
- Choudhary, S. K., & Jadoun, R. (2014). Current advanced research development of electric discharge machining (EDM): a review. *International Journal of Research in Advent Technology*, 2(3), 273-297.
- Das, M., Kumar, K., Barman, T., & Sahoo, P. (2013). Optimization of surface roughness and MRR in EDM using WPCA. *Procedia Engineering*, 64, 446-455.
- De Wolf, D., Cardon, L., & Balic, J. (2010). Parameter affecting quality of the electrical discharge machining process. *Adv Prod Eng Manag*, 5(4), 245-252.
- Efendee, A., Saifuldin, M., Gebremariam, M., & Azhari, A. (2018). *Effect of magnetic polarity on surface roughness during magnetic field assisted EDM of tool steel*. Paper presented at the IOP Conference Series: Materials Science and Engineering.
- Eubank, P. T., Patel, M. R., Barrufet, M. A., & Bozkurt, B. (1993). Theoretical models of the electrical discharge machining process. III. The variable mass, cylindrical plasma model. *Journal of applied physics*, 73(11), 7900-7909.
- Fan, Y., Bai, J., Li, Q., Li, C., Cao, Y., & Li, Z. (2016). Research on maintaining voltage of spark discharge in EDM. *Procedia CIRP*, 42, 28-33.
- George, J., Chandan, R., Manu, R., & Mathew, J. (2020). Experimental Investigation of Silicon Powder Mixed EDM Using Graphene and CNT Nano Particle Coated Electrodes. *Silicon*, 1-17.
- Gholipour, A., Baseri, H., Shakeri, M., & Shabgard, M. (2016). Investigation of the effects of magnetic field on near-dry electrical discharge machining performance. *Proceedings of the Institution of Mechanical Engineers, Part B: Journal of Engineering Manufacture*, 230(4), 744-751.
- Gholipour, A., Shabgard, M. R., Mohammadpourfard, M., & Abbasi, H. (2020). Comparative study of ultrasonic vibrations assisted EDM and magnetic field assisted EDM processes. *Iranian Journal of Mechanical Engineering Transactions of the ISME*, 21(1), 45-64.
- Giancoli, D. (2013). *Physics for Scientists & Engineers with Modern Physics: Pearson New International Edition*: Pearson Higher Ed.

- Goyal, R., Rohilla, V., Kumar, A., Goyal, A., & Mittal, S. (2020). Selection of range of pulse duration during cryogenically assisted electric discharge machining. *Materials Today: Proceedings*.
- Haron, C. C., Ghani, J., Burhanuddin, Y., Seong, Y., & Swee, C. (2008). Copper and graphite electrodes performance in electrical-discharge machining of XW42 tool steel. *Journal of materials processing technology*, 201(1-3), 570-573.
- Ho, K., & Newman, S. (2003). State of the art electrical discharge machining (EDM). *International Journal of Machine Tools and Manufacture*, 43(13), 1287-1300.
- Hocheng, H., Guu, Y., & Tai, N. (1998). The feasibility analysis of electrical-discharge machining of carbon-carbon composites. *MATERIAL AND MANUFACTURING PROCESS*, 13(1), 117-132.
- Jeavudeen, S., Jailani, H. S., & Murugan, M. (2020). Powder additives influence on dielectric strength of EDM fluid and material removal. *International Journal of Machining and Machinability of Materials*, 22(1), 47-61.
- Joshi, S., Govindan, P., Malshe, A., & Rajurkar, K. (2011). Experimental characterization of dry EDM performed in a pulsating magnetic field. *CIRP Annals-Manufacturing Technology*, 60(1), 239-242.
- Khan, A. A., Ndaliman, M. B., Mohammad, Y. A., Al-Falahi, M. D., Ibrahim, H. A., & Mustapa, M. S. (2013). The Effect of EDM with external magnetic field on surface roughness of stainless steel.
- Kiyak, M., & Cakır, O. (2007). Examination of machining parameters on surface roughness in EDM of tool steel. *Journal of materials processing technology*, 191(1), 141-144.
- Klocke, F., Hensgen, L., Klink, A., Ehle, L., & Schwedt, A. (2016). Structure and composition of the white layer in the wire-EDM process. *Procedia CIRP*, 42, 673-678.
- Klocke, F., Schwade, M., Klink, A., & Veselovac, D. (2013). Analysis of material removal rate and electrode wear in sinking EDM roughing strategies using different graphite grades. *Procedia CIRP*, 6, 163-167.
- Konig, W., & Klocke, F. (1997). *Fertigungsverfahren-3, Abtragen and Generieren*. Springer, Berlin.
- Kumar, A., Mandal, A., Dixit, A. R., & Mandal, D. K. (2020). Quantitative analysis of bubble size and electrodes gap at different dielectric conditions in powder mixed EDM process. *The International Journal of Advanced Manufacturing Technology*, 1-11.

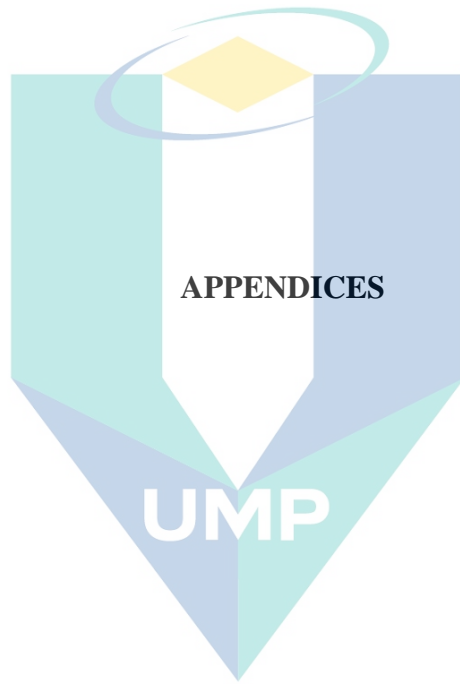
- Kumar, S., & Choudhury, S. (2007). Prediction of wear and surface roughness in electro-discharge diamond grinding. *Journal of materials processing technology*, 191(1), 206-209.
- Kumar, S., Goud, M., & Suri, N. M. (2020). An Investigation of Magnetic-field-assisted EDM by Silicon and Boron Based Dielectric of Inconel 706. *Silicon*, 1-9.
- Kumar, S., Srivastava, B., & Kumar, C. (2015). Study of MRR on AISI D3 Die Steel with Different EDM Parameters using Two Level Full Factorial Design. *IJIRST–International Journal for Innovative Research in Science & Technology*, 1(12), 380-387.
- Lee, H.-T., & Tai, T. Y. (2003). Relationship between EDM parameters and surface crack formation. *Journal of materials processing technology*, 142(3), 676-683.
- Li, L., Zhao, L., Li, Z., Feng, L., & Bai, X. (2017). Surface characteristics of Ti-6Al-4V by SiC abrasive-mixed EDM with magnetic stirring. *Materials and Manufacturing Processes*, 32(1), 83-86.
- Li, Y., Cui, C., Lin, B., & Li, L. (2020). *Machining Characteristics of IN718 by EDM with Cooled Electrode and Vibration of the Workpiece*. Paper presented at the Materials Science Forum.
- Lim, L., Lee, L., Wong, Y., & Lu, H. (1991). Solidification microstructure of electrodischarge machined surfaces of tool steels. *Materials Science and Technology*, 7(3), 239-248.
- Lin, Y.-C., Chen, Y.-F., Wang, D.-A., & Lee, H.-S. (2009). Optimization of machining parameters in magnetic force assisted EDM based on Taguchi method. *Journal of materials processing technology*, 209(7), 3374-3383.
- Lin, Y.-C., & Lee, H.-S. (2008). Machining characteristics of magnetic force-assisted EDM. *International Journal of Machine Tools and Manufacture*, 48(11), 1179-1186.
- Luo, Y., & Chen, C. (1990). Effect of a pulsed electromagnetic field on the surface roughness in superfinishing EDM. *Precision engineering*, 12(2), 97-100.
- Mahendran, S., Devarajan, R., Nagarajan, T., & Majdi, A. (2010). *A review of micro-EDM*. Paper presented at the Proceedings of the international multi conference of engineers and computer scientists.
- Mamalis, A., Vosniakos, G., Vaxevanidis, N., & Prohaszka, J. (1987). Macroscopic and microscopic phenomena of electro-discharge machined steel surfaces: an experimental investigation. *Journal of Mechanical Working Technology*, 15(3), 335-356.

- Mao, X., Yang, X., Zhang, M., Zhu, Z., & Huo, M. (2020). Development of Multi Micro Holes Synchronous Rotating and Vibration EDM Machine Tool. *MS&E*, 768(4), 042051.
- Marafona, J., & Chousal, J. (2006). A finite element model of EDM based on the Joule effect. *International Journal of Machine Tools and Manufacture*, 46(6), 595-602.
- Ming, W., Shen, F., Zhang, Z., Huang, H., Du, J., & Wu, J. (2020). A comparative investigation on magnetic field-assisted EDM of magnetic and non-magnetic materials. *The International Journal of Advanced Manufacturing Technology*, 109(3), 1103-1116.
- Murray, J., Sun, J., Patil, D., Wood, T., & Clare, A. (2016). Physical and electrical characteristics of EDM debris. *Journal of materials processing technology*, 229, 54-60.
- Newton, T. R., Melkote, S. N., Watkins, T. R., Trejo, R. M., & Reister, L. (2009). Investigation of the effect of process parameters on the formation and characteristics of recast layer in wire-EDM of Inconel 718. *Materials Science and Engineering: A*, 513, 208-215.
- Okada, A. (2004). Effect of Debris Accumulation on Machining Speed in EDM. *International Journal of Electrical Machining*, 9-14.
- Pandey, A., & Singh, S. (2010). Current research trends in variants of Electrical Discharge Machining: A review. *International Journal of Engineering Science and Technology*, 2(6), 2172-2191.
- Pavan, C., & Sateesh, N. (2020). Taguchi analysis on machinability of Inconel 600 using Copper, Brass, and Copper tungsten electrodes in EDM. *Materials Today: Proceedings*.
- Prakash, D., Tariq, M., Davis, R., Singh, A., & Debnath, K. (2020). Influence of cryogenic treatment on the performance of micro-EDM tool electrode in machining of magnesium alloy AZ31B. *Materials Today: Proceedings*.
- Puertas, I., & Luis, C. (2003). A study on the machining parameters optimisation of electrical discharge machining. *Journal of materials processing technology*, 143, 521-526.
- Qiang, H., Yong, H., & Wansheng, Z. (2002). Research of two-dimension EDM spark locations detection using electromagnetic method. *Measurement*, 31(2), 117-122.
- Rajabinasab, F., Abedini, V., Hadad, M., & Hajighorbani, R. (2020). Experimental investigation of the effect of tool material on the performance of AISI 4140 steel in the rotary near dry electrical discharge machining. *Proceedings of the Institution of Mechanical Engineers, Part E: Journal of Process Mechanical Engineering*, 0954408920922102.

- Rajkumar, G. M., Giridharan, A., Oyyaravelu, R., & Balan, A. (2020). Investigation on Magnetic Field-assisted Near-dry Electrical Discharge Machining of Inconel 600 *Advances in Unconventional Machining and Composites* (pp. 671-684): Springer.
- Rajurkar, K., & Pandit, S. (1988). RECENT PROGRESS IN ELECTRICAL DISCHARGE MACHINE TECHNOLOGY AND RESEARCH *Unknown Host Publication Title: ASME*.
- Rajurkar, K., & Yu, Z. (2000). 3d micro-edm using cad/cam. *CIRP Annals-Manufacturing Technology*, 49(1), 127-130.
- Ramasawmy, H., & Blunt, L. (2004). Effect of EDM process parameters on 3D surface topography. *Journal of materials processing technology*, 148(2), 155-164.
- Rao, P. N. (2013). *Manufacturing technology: metal cutting and machine tools* (Vol. 2): Tata McGraw-Hill Education.
- Renjith, R., & Paul, L. (2020). Machining characteristics of micro-magnetic field assisted EDM (μ -MFAEDM). *Materials Today: Proceedings*, 27, 2000-2004.
- Rouniyar, A. K., & Shandilya, P. (2020). Optimization of process parameters in magnetic field assisted powder mixed EDM of aluminium 6061 alloy. *Proceedings of the Institution of Mechanical Engineers, Part C: Journal of Mechanical Engineering Science*, 0954406220959108.
- Sahu, D. R., & Mandal, A. (2020). Critical analysis of surface integrity parameters and dimensional accuracy in powder-mixed EDM. *Materials and Manufacturing Processes*, 35(4), 430-441.
- Satynarayana, K., Rajkiran, K., & Chakradhar, D. (2020). *A Role of cryogenic in Wire cut EDM process*. Paper presented at the E3S Web of Conferences.
- Saxena, K. K., Agarwal, S., & Khare, S. K. (2016). Surface characterization, material removal mechanism and material migration study of micro EDM process on conductive SiC. *Procedia CIRP*, 42, 179-184.
- Serway, R., & Jewett, J. (2013). *Physics for scientists and engineers with modern physics*: Nelson Education.
- Seyedzavvar, M., & Shabgard, M. R. (2012). *Influence of tool material on the electrical discharge machining of AISI H13 tool steel*. Paper presented at the Advanced Materials Research.
- Shabgard, M. R., Gholipoor, A., & Baseri, H. (2016). A review on recent developments in machining methods based on electrical discharge phenomena. *The International Journal of Advanced Manufacturing Technology*, 87(5-8), 2081-2097.

- Shitara, T., Fujita, K., & Yan, J. (2020). Direct observation of discharging phenomena in vibration-assisted micro-electrical discharge machining. *The International Journal of Advanced Manufacturing Technology*, 1-14.
- Singh Bains, P., Sidhu, S. S., & Payal, H. (2016). Study of Magnetic Field-Assisted ED Machining of Metal Matrix Composites. *Materials and Manufacturing Processes*, 31(14), 1889-1894.
- Singh, G., Satsangi, P., & Prajapati, D. (2020). Effect of Rotating Magnetic Field and Ultrasonic Vibration on Micro-EDM Process. *Arabian Journal for Science and Engineering*, 45(2), 1059-1070.
- Singh, J., Singh, G., & Pandey, P. M. (2020). Electric discharge machining using rapid manufactured complex shape copper electrode with cryogenic cooling channel. *Proceedings of the Institution of Mechanical Engineers, Part B: Journal of Engineering Manufacture*, 0954405420949102.
- Singh, V., Bhandari, R., & Yadav, V. K. (2017). An experimental investigation on machining parameters of AISI D2 steel using WEDM. *The International Journal of Advanced Manufacturing Technology*, 93(1-4), 203-214.
- Sommer, C., & Sommer, S. (2005). *Complete EDM Handbook: Wire EDM, RAM EDM, Small Hole EDM; Practical Information for Designers, Engineers, Machinists, Tool and Die Makers, Mold Makers and Others in the Metal Machining Fields*: Advance Publ.
- Sundaram, M. M., Yildiz, Y., & Rajurkar, K. (2009). *Experimental study of the effect of cryogenic treatment on the performance of electro discharge machining*. Paper presented at the Proceedings of International Manufacturing Science and Engineering Conference.
- Sundriyal, S., Yadav, J., Walia, R., & Kumar, R. (2020). Thermophysical-Based Modeling of Material Removal in Powder Mixed Near-Dry Electric Discharge Machining. *Journal of Materials Engineering and Performance*, 1-20.
- Takezawa, H., Yokote, N., & Mohri, N. (2016). Influence of external magnetic field on permanent magnet by EDM. *The International Journal of Advanced Manufacturing Technology*, 87(1-4), 25-30.
- Teimouri, R., & Baseri, H. (2012). Study of tool wear and overcut in EDM process with rotary tool and magnetic field. *Advances in Tribology*, 2012.
- Thomson, P. (1989). Surface damage in electrodischarge machining. *Mater. Sci. Technol*, 5, 1153-1157.
- Tomura, S., & Kunieda, M. (2009). Analysis of electromagnetic force in wire-EDM. *Precision engineering*, 33(3), 255-262.

- Vishwakarma, U., Dvivedi, A., & Kumar, P. (2013). Finite element modeling of material removal rate in powder mixed electric discharge machining of Al-SiC metal matrix composites *Materials Processing Fundamentals* (pp. 151-158): Springer.
- Wong, Y., Lim, L., & Lee, L. (1995). Effects of flushing on electro-discharge machined surfaces. *Journal of materials processing technology*, 48(1-4), 299-305.
- Wu, K. L., Yan, B. H., Huang, F. Y., & Chen, S. C. (2005). Improvement of surface finish on SKD steel using electro-discharge machining with aluminum and surfactant added dielectric. *International Journal of Machine Tools and Manufacture*, 45(10), 1195-1201.
- Xu, M., Wu, Z., Gao, F., Liu, L., & Song, E. (2020). Error modeling and accuracy optimization of rotating ultrasonic vibration assisted EDM machine tool. *Journal of Mechanical Science and Technology*, 34(7), 2751-2760.
- Yadav, V. K., Kumar, P., & Dvivedi, A. (2020). Investigation on the Effect of Input Parameters on Surface Quality During Rotary Tool Near-Dry EDM *Recent Advances in Mechanical Infrastructure* (pp. 41-47): Springer.
- Yeo, S., Murali, M., & Cheah, H. (2004). Magnetic field assisted micro electro-discharge machining. *Journal of Micromechanics and Microengineering*, 14(11), 1526.
- Zhang, Q., Zhang, J., Deng, J., Qin, Y., & Niu, Z. (2002). Ultrasonic vibration electrical discharge machining in gas. *Journal of materials processing technology*, 129(1), 135-138.
- Zhang, S., Zhang, W., Liu, Y., Ma, F., Su, C., & Sha, Z. (2017). Study on the Gap Flow Simulation in EDM Small Hole Machining with Ti Alloy. *Advances in Materials Science and Engineering*, 2017.
- Zhang, X., & Uchiyama, K. (2017). *Improvement of EDM Machining Speed by Using Magnetic/Piezoelectric Hybrid Drive Actuator*. Paper presented at the MATEC Web of Conferences.
- Zinelis, S. (2007). Surface and elemental alterations of dental alloys induced by electro discharge machining (EDM). *Dental materials*, 23(5), 601-607.



اونيورسيتي ملايسيا قهغ

UNIVERSITI MALAYSIA PAHANG

STAVAX ESR

General

Stavax ESR is a premium grade stainless tool steel with the following properties:

- good corrosion resistance
- excellent polishability
- good wear resistance
- good machinability
- good dimensional stability during heat treatment

The combination of these properties provides a steel with outstanding production performance. The practical benefits of good corrosion resistance of a plastic mould can be summarised as follows:

- **Lower mould maintenance costs**
The surface of cavity impressions retain their original finish over an extended service life. Moulds stored or operated in humid conditions require no special protection.
- **Lower production costs**
Since cooling channels are less likely to be affected by corrosion (unlike conventional mould steels), heat transfer characteristics, and therefore cooling efficiency, are constant throughout the mould life, ensuring consistent cycle times.

These benefits, coupled with the high wear resistance of Stavax ESR, offer the moulder low-maintenance, long-life moulds for the greatest overall tooling economy.

Note: Stavax ESR is produced using the Electroslag Remelting (ESR) technique. The result is a mould steel with a very low inclusion level providing excellent polishability characteristics.

Typical analysis %	C 0.38	Si 0.9	Mn 0.5	Cr 13.6	V 0.3
Standard specification	AISI 420 modified, WNr: 1.2083 ESR, SUS 420J2				
Delivery condition	Soft annealed to approx. 200 HB				
Colour code	Black / Orange				



Stavax ESR core to make disposable polystyrene beakers. Millions of close tolerance mouldings with a very high surface finish have been produced.

Applications

Whilst Stavax ESR is recommended for all types of moulding tools, its special properties make it particularly suitable for moulds with the following demands:

- **Corrosion/staining resistance**
Moulding of corrosive plastics, e.g., PVC, acetates, and for moulds subjected to humid working/storage conditions.
- **Wear resistance**
Moulding abrasive/ filled materials, including injection moulded thermosetting grades. Stavax ESR is recommended for moulds with long production runs, e.g., disposable cutlery and containers.
- **High surface finish**
Production of optical parts, e.g., camera and sunglass lenses. Moulding of medical components, e.g., syringes and analysis vials.

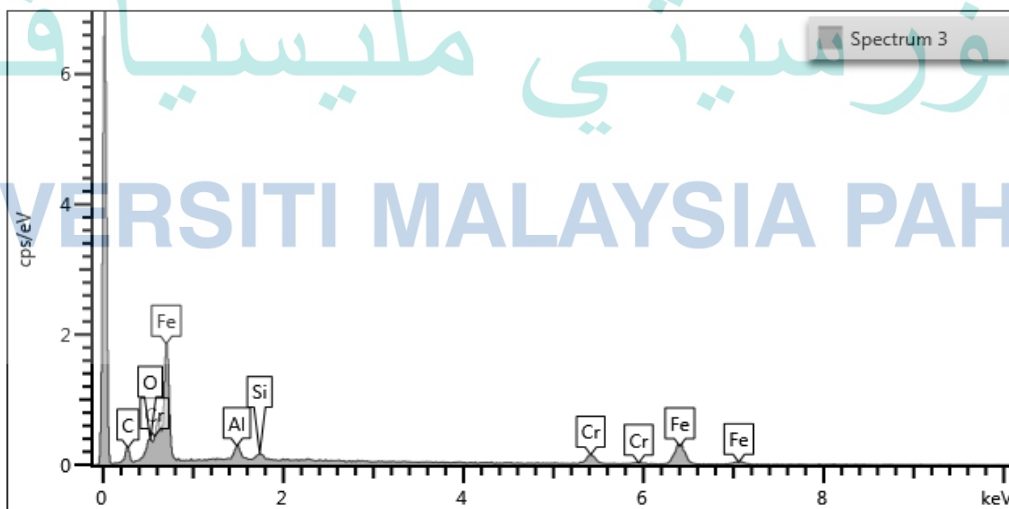
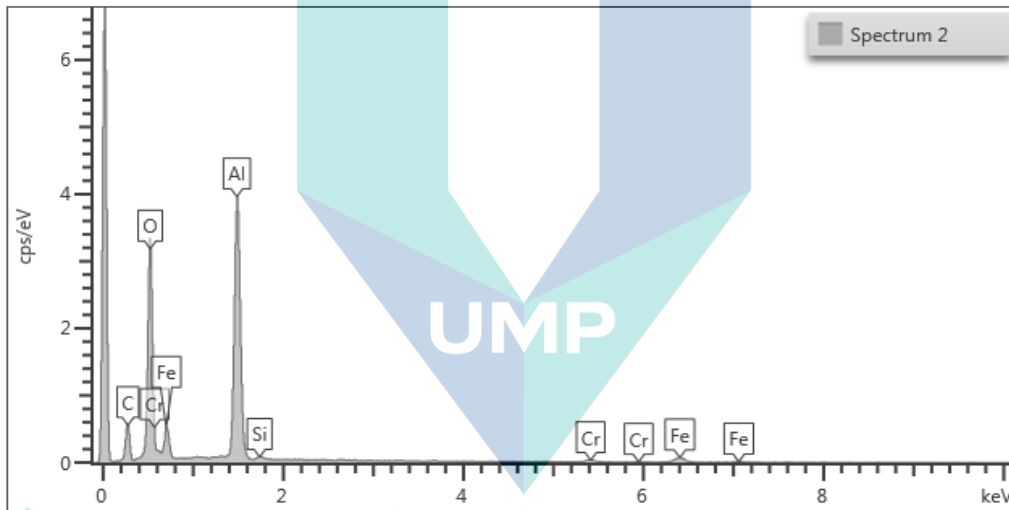
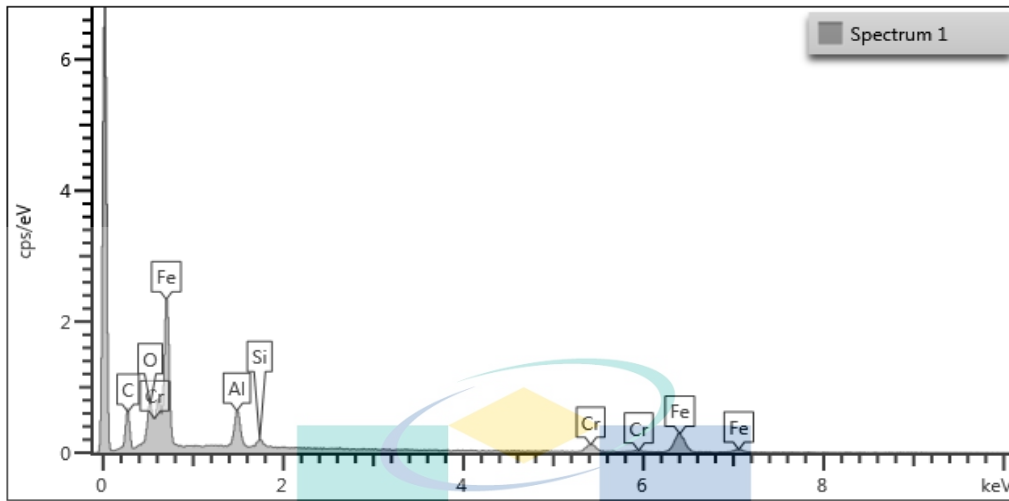


Stavax ESR is the right choice for lens mould with extreme demand on polishability.

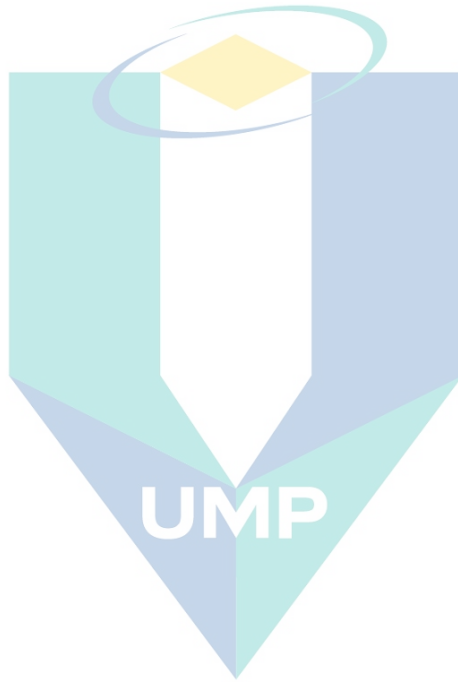
Type of mould	Recommended hardness HRC
Injection moulds for thermoplastics	45-52
Injection moulds for thermosetting plastics	45-52
Compression / transfer moulds	50-52
Blow moulds for PVC, PET etc.	45-52
Extrusion, pultrusion dies	45-52

UNIVERSITI MALAYSIA PAHANG

Appendix B: AISI 420.mod EDX spectrum composition



اونيورسيتي ملايسيا قهق
UNIVERSITI MALAYSIA PAHANG



اونيورسيتي ملايسيا قهغ

UNIVERSITI MALAYSIA PAHANG